Quantitative physiology of bacterial survival under carbon starvation and temperature stress

Elena Biselli

Munich 2019

Quantitative physiology of bacterial survival under carbon starvation and temperature stress

Elena Biselli

Doctoral thesis
presented to the Faculty of Physics
of the Ludwig–Maximilians–Universität
München

by
Elena Biselli
from Rome

Munich, 23.09.2019

Erstgutachter: Prof. Dr. Ulrich Gerland
Zweitgutachter: Prof. Dr. Joachim Rädler
Tag der mündlichen Prüfung: 29.11.2019

To my family,
for always supporting me in all my challenges.
Concussus, surgo.

Contents

List of Figures

List of Tables

Zusammenfassung

Eine große Anzahl der Bakterien auf der Erde lebt über große Zeiträume in einem Zustand mit sehr geringer Stoffwechselaktivität und nur geringem oder keinem Wachstum. Ein Grund dafür sind widrige Umwelteinflüsse und die damit einhergehenden Belastungen wie beispielsweise Ressourcenmangel. Innerhalb von Millionen von Jahren haben Bakterien diverse Strategien zur Anpassung an verschiedene Umgebungen, in denen sie überleben und sich weiterentwickeln, entwickelt, um ihre Fitness zu optimieren und bei günstigen Bedingungen schnelle Teilungszyklen zu durchlaufen. Viele dieser Überlebensstrategien sind jedoch immer noch ein Rätsel und es ist nur relativ wenig über die Mechanismen bekannt, die den dominanten Formen der bakteriellen Existenz zu Grunde liegen. Dies ist von besonderer Bedeutung, da die Phase unterdrückten Wachstums entscheidend ist, um den Beitrag von Mikroorganismen zur menschlichen Physiologie und Anfälligkeit für Krankheiten, sowie zur mikrobiellen Verträglichkeit und Antibiotikaresistenz zu verstehen.

Der Mangel an Informationen ist hauptsächlich auf die Schwierigkeiten bei der Definition, Reproduktion und Messung des Verhaltens von Bakterien in Zuständen des Wachstumsstillstands zurückzuführen, die oft unberechenbar und unvorhersehbar erscheinen, während die Zellphysiologie ähnlich vielfältig und oft spezifisch für die jeweiligen Umgebungsbedingungen ist. Daher ist es schwierig zu bestimmen, wie sich molekulare Mechanismen auf das Überleben auswirken. Dies erklärt, warum im letzten Jahrhundert Bakterien hauptsächlich während der exponentiellen Wachstumsphase untersucht wurden, die im Gegenteil ein genau definierter und reproduzierbarer Gleichgewichtszustand des konstanten Wachstums, der Genexpression und der molekularen Zusammensetzung ist. Infolgedessen hat eine zunehmende Kombination von Experimenten und Vorhersagemodellen, die sich auf diese Phase konzentrieren, ein tiefes Verständnis der bakteriellen Physiologie und Genregulation während des Wachstums geliefert. Ein ähnlicher quantitativer Ansatz, der sich auf die Phase der Stagnation konzentriert, fehlt weitgehend.

In dieser Doktorarbeit, tragen wir dazu bei, diese Lücke durch die Entwicklung neuer quantitativer Ansätze zur Untersuchung der bakteriellen Physiologie in ungünstigen Umgebungen zu füllen, in denen Stressfaktoren, wie beispielsweise Nährstoffmangel, auftreten und zusätzliche umweltbedingte Störungen, wie eine Temperaturerhöhung, die Zellen zwingen, Strategien zum Überleben zu aktivieren. Dazu arbeiten wir mit dem Bakterium *Escherichia coli* (*E. coli*), das unter den circa 10^{12} mikrobiellen Spezies, die auf unserem Planeten leben, wegen seiner Widerstandsfähigkeit, Vielseitigkeit und einfachen Handhabung eines der am besten untersuchten Bakterien darstellt.

In Kapitel 1, geben wir einen Überblick über die Physiologie des Lebenszyklus von *E. coli* und über die wichtigsten bisher verwendeten quantitativen Methoden, wobei wir uns auf das Verhalten während der Wachstumsphase konzentrieren.

In Kapitel 2, stellen wir den fehlenden quantitativen Ansatz zur Untersuchung der Physiologie von *E. coli* während der Sterbephase fest. Wir zeigen, dass bei Kohlenstoffmangel ein exponentieller Zerfall der Lebensfähigkeit als kollektives Phänomen auftritt, wobei lebensfähige Zellen Nährstoffe aus toten Zellen recyceln, um die Lebensfähigkeit aufrechtzuerhalten. Die

beobachtete kollektive Sterberate wird durch die Erhaltungsrate lebensfähiger Zellen und die Menge an Nährstoffen, die aus toten Zellen als Ertrag gewonnen werden, bestimmt. Unter Verwendung dieser Beziehung untersuchen wir die Kosten einer verschwenderischen Enzymaktivität während des Hungerns und den Nutzen des Sigma Faktors RpoS für die Stressreaktion. Während diese Aktivität die Instandhaltung und damit die Sterblichkeitsrate erhöht, verbessert RpoS das Recycling der Biomasse und senkt die Sterblichkeitsrate. Unser Ansatz ermöglicht daher quantitative Analysen darüber, wie sich zelluläre Komponenten auf das Überleben nicht wachsender Zellen auswirken.

In Kapitel 3, verwenden wir den im vorherigen Kapitel entwickelten quantitativen Ansatz, um zu untersuchen, wie das Überleben von *E. coli* bei Kohlenstoffmangel von den vorherigen Kulturbedingungen abhängt. Wir zeigen, dass Umgebungen, die nur langsames Wachstum unterstützen, aufgrund einer verringerten Erhaltungsrate zu einem längeren Überleben führen, was bedeutet, dass langsamer wachsende Zellen weniger Energie zum Überleben benötigen. Unsere Ergebnisse legen einen physiologischen Kompromiss zwischen der Fähigkeit, sich schnell zu vermehren, und der Fähigkeit, lange zu überleben, nahe, der Aufschluss darüber geben könnte, warum Bakterien außerhalb von Laborumgebungen nicht für schnelles Wachstum optimiert sind.

In Kapitel 4, untersuchen wir die Physiologie von *E. coli* unter dem kombinierten Stress von Kohlenstoffmangel und hohen Temperaturen und charakterisieren eine thermische Sicherung, die zu einer ruhenden und antibiotisch persistierenden Subpopulation führt. Diese Sicherung wird durch ein thermisch instabiles Enzym, MetA, im Methioninsyntheseweg implementiert. Die Kombination aus einer positiven Rückkopplung im Methioninsystem und einer doppelten Verwendung von Methionin für die Proteinsynthese und als Methyldonor führt dazu, dass sich die Bakterienpopulation bei erhöhten Temperaturen in zwei verschiedene Zustände aufspaltet, wobei jeweils eine Subpopulation wächst und die Andere schläft. Wir zeigen dann, dass diese ruhenden Bakterien nicht nur eine Antibiotikabehandlung, sondern auch Hitzeschocks überstehen, was darauf hindeutet, dass sich die thermische Sicherung ursprünglich als eine "bet-hedging" Strategie entwickelt hat, um das Überleben bei Hitzeschocks sicherzustellen.

Unsere Ergebnisse, die in Kapitel 5 zusammengefasst sind, ebnen den Weg für die Entwicklung eines neuen theoretischen Rahmens und experimentellen Ansatzes zum Verständnis der Bakterienphysiologie in der Phase des Wachstumsstopps, indem phänomenologische Modelle mit molekularen Mechanismen verknüpft werden.

Abstract

A large number of the bacteria on Earth live for long periods in states of very low metabolic activity and little or no growth due to starvation and other environmental stresses. Within millions of years, bacteria have developed several strategies to adapt to many different environments, where they survive and evolve to optimize their fitness and to undergo rapid division cycles when conditions become favourable. However, many of these survival strategies are still a puzzle and relatively little is known about the mechanisms that underpin the dominant modes of bacterial existence. This is particularly alarming, as the growth-arrest phase has become crucial to understand the contribution of microorganisms to human physiology and predisposition to disease as well as microbial tolerance and resistance to antibiotics.

The dearth of information is mainly due to the difficulties in defining, reproducing and measuring bacterial behaviours in growth-arrest states, which may often seem erratic and unpredictable, while cell physiology is similarly diverse and often specific to the particular environmental conditions. Thus, determining how molecular contributions affect survival is challenging. This explains why, in the last century, bacteria have been mainly studied during the exponential growth phase, which is, on the contrary, a well-defined and reproducible steady state of constant growth, gene expression and molecular compositions. As a result, an increasing combined use of experiments and predictive models focused on this phase has provided a deep understanding of bacterial physiology and gene regulation during growth. A similar quantitative approach that focuses on the growth-arrest phase is largely missing.

In this thesis, we contribute to fill this gap by developing new quantitative approaches to investigate bacterial physiology in hostile environments where stresses, such as lack of nutrients and additional environmental perturbations, like temperature increase, force the cells to activate strategies of survival. To do so, we choose to work with the bacterium *Escherichia coli* (*E. coli*) that, among the estimated 10^{12} microbial species living in our planet, is one of the most studied thanks to its hardiness, versatility and ease of handling.

In Chapter 1, we provide an overview of the physiology of *E. coli* life cycle and of the main quantitative methods so far used to study it, especially focusing on its behaviour during the growth-arrest phase.

In Chapter 2, we establish the missing quantitative approach to study *E. coli* physiology in the death phase. We show that in carbon starvation, an exponential decay of viability emerges as a collective phenomenon, with viable cells recycling nutrients from dead cells to maintain viability. The observed collective death rate is determined by the maintenance rate of viable cells and the amount of nutrients recovered from dead cells, the yield. Using this relation, we study the cost of a wasteful enzyme during starvation and the benefit of the stress response sigma factor RpoS. While the enzyme activity increases maintenance and thereby the death rate, RpoS improves biomass recycling, decreasing the death rate. Our approach thus enables quantitative analyses of how cellular components affect the survival of non-growing cells.

In Chapter 3, we use the quantitative approach developed in the previous chapter to study how survival of *E. coli* in carbon starvation depends on the previous culture conditions. We

show that environments that support only slow growth lead to longer survival in starvation because of a decrease of maintenance rate, meaning that slower growing cells need less energy to survive. Our results suggest a physiological trade-off between the ability to proliferate fast and the ability to survive long that could shed light on the long-standing question of why bacteria outside of laboratory environments are not optimized for fast growth.

In Chapter 4, we study *E. coli* physiology under the combined stresses of carbon starvation and high temperatures, characterizing a thermal fuse that leads to a dormant and antibiotic persistent sub-population. This fuse is implemented by a thermally unstable enzyme, MetA, in the methionine synthesis pathway. The combination of a positive feed-back in the methionine system and a dual-use of methionine for protein synthesis and as a methyl-donor results in the bacterial population splitting into two distinct states at elevated temperatures, growing and dormant. We then reveal that these dormant bacteria not only survive antibiotic treatment, but also heat shocks, suggesting that the thermal fuse has originally evolved as "bet-hedging" strategy to ensure survival in heat shocks.

Our findings, summarized in Chapter 5, pave the way for the development of a new theoretical framework and experimental approach to understand bacterial physiology in the growth-arrest phase, by linking phenomenological modeling to molecular mechanisms.

Chapter 1

E. coli physiology: growth, survival and death

1.1 Introduction

Bacteria have been studied intensively in the last century, as they are easily cultivable and their relatively simple genetics, composition and regulation make them ideal candidates to study general biological questions. When nutrients are plentiful, bacteria can sustain relatively fast growth rates. However, in the natural environment, they seldom encounter conditions that permit rapid division cycles and they rather starve and survive in growth arrest states for extremely long periods. While our understanding of bacterial physiology linked to gene regulation during the growth phase is deep, cell survival strategies in energy-limited and stressful environments are still a puzzle, due to several challenges in defining, reproducing and measuring these states. In this thesis, we solve some of these puzzles by working with the bacterium *Escherichia coli* (*E. coli*), the model organism par excellence in laboratory, which is also a protagonist in nature, for its diversity and genomic evolution as well as its role in the human microbiome and disease.

In this chapter, we first briefly introduce this bacterium and we describe its importance in nature, where it often faces stresses both in hosts and external environments, as a pathogenic or non-pathogenic microbe. Then, we provide an overview of the physiology of its life cycle and of the main quantitative methods so far used to study it. In particular, we focus on its behaviour in growth arrest states when facing starvation, high temperatures and antibiotics treatments, used in this thesis, highlighting how the complexity of these states has made them less attractive to investigate cell physiology and its molecular contributions.

1.2 *E. coli* natural history in a nutshell

E. coli is a Gram-negative chemo-organo-heterotrophic rod-shaped bacterium of the genus *Escherichia*, from the family *Enterobacteriaceae* (see Fig. 1.1A). It is a facultative aerobe, meaning that it can grow with or without oxygen, but it cannot grow at extremes of temperature or pH nor can it degrade dangerous pollutants or photosynthesize. It normally measures only about 1 μm long by 0.35 μm wide and it may have whip-like flagella, which it uses to move around in its environment, or hair-like pili, which allow it to attach to surfaces or to other cells (Fig. 1.1B). It is a common commensal inhabitant of the mammalian gut microbiome, but it is also found, albeit less commonly, in the gut microbiomes of birds, reptiles and fish, as well as in soil, water, plants and food [1, 2]. It can be a non-pathogenic and often helpful lodger in hosts as well as one

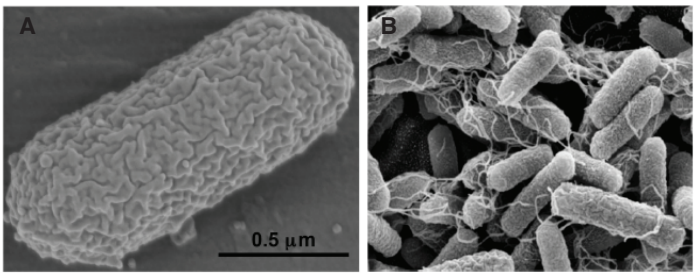

Figure 1.1: Scanning Electron Micrographs of *E. coli*. **(A)** *E. coli* B strain REL606, a laboratory strain with a typical rod-shaped morphology. **(B)** *E. coli* O119:HND strain A111, an enteropathogenic strain that produces hair-like pili. Images are taken from [4].

of the most important human pathogens (see Section 1.5). It was discovered in 1884 by the German microbiologist and pediatrician Theodor Escherich while he was studying gut microbes and their role in digestion and disease [3]. From that moment onwards, the *E. coli* non-pathogenic strains, which grow quickly on many different nutrients and can be isolated from virtually any human, were used in the first half of the 20th century by many scientists for groundbreaking studies on bacterial physiology, viruses and genetics and, in the 1950s, for the onset of molecular biology revolution [4]. Thus, many basic aspects of life, including the genetic code, transcription, translation and replication, were first worked out in *E. coli* [5–7] and, nowadays, this bacterium is prominently used in academic and commercial genetic engineering, biotechnology industry, pharmaceutical production and experimental microbial evolution.

1.3 *E. coli* in hosts

E. coli is typically the most common aerobe in the lower intestine of mammals, where it competes with other species for nutrients, which are often scarce. This happens because *E. coli* constitutes only 0.1-5% of the microbial community in the gut, which is primarily an anoxic environment dominated by obligate anaerobes, such as *Bacteroides* and *Firmicutes* ($\sim$ 90%) [4]. A small fraction of *E. coli* manages to occupy the mucus layer of the large intestine, where it grows very fast, as in laboratory cultures, with a doubling time between 30 and 80 minutes, it forms a complex, multi-species biofilm and it competes for nutrients, maintaining a population densities of $\approx 10^6 - 10^9$ cells per gram of fecal matter. Some of these cells move later to the lumen of the large intestine where they mainly starve, representing the majority of the population [8, 9]. This explains why the entire fecal matter in the large intestine of a human doubles in mass only about every 12 to 24 hours, unlike what happens in laboratories. *E. coli* diet varies a lot as it depends on the human oral food uptake, after which nutrients remain available for the cells only for a couple of hours [10]. This exerts an evolutionary pressure on the cells to adapt to fast growth and/or to improved or worsening nutrient conditions.

1.4 *E. coli* in the external environment

As any gut microbe, *E. coli* is regularly excreted into the harsher external world in fecal matter [4]. To cope with fluctuations of nutrition, temperature, oxygen, moisture, pH and to compete or cooperate with the surrounding microbial community, *E. coli* evolved in such a way that it can survive this hostility and variability long enough to make it back to a host [11]. The survival can last from several days to years [12, 13]. Among different strategies adopted in the external environment, *E. coli* ability to become dormant has recently attracted attention, as dormant

cells are usually also persister cells able to tolerate antibiotics (see Section 1.12). In Chapter 4, we will uncover one of the mechanisms that lead to *E. coli* persistence.

1.5 Pathogenic *E. coli*

Despite being often beneficial, *E. coli* is also a major cause of many diarrheal diseases, peritonitis, colitis, bacteremia, infant mortality and urinary tract infections that world-wide cost billions of dollars to treat and kill roughly 2 million humans each year [14–16]. Some strains may even cause cancer [17]. The transfection of pathogenic *E. coli* from the environment into the host is usually indirect: while trying to survive by facing starvation and other stresses in the external environment, they contaminate human food, faeces, water and inorganic surfaces thereby entering in the human food chain. Thus, understanding *E. coli* strategies of survival has also medical relevance.

1.6 Laboratory strain K-12 NCM3722

The model organism *E. coli* usually used in the laboratories is a non-pathogenic bacterium that, in the last century, has led to many advances in a variety of fields. In molecular biology, physiology and genetics, it was used to understand the genetic code [5], DNA replication [18], transcription [19], life cycle of bacterial viruses [20], gene regulation [21], the swarming motility behaviour [22] and antibiotic persistence [23]. In pharmacology, it helped for *in vivo* synthesis of recombinant therapeutic proteins such as insulin [24]. It is also the principal model organism in experimental evolution where, for example, was used to study the random nature of mutations [25] as well as long-term fitness [26] and predatory-prey interactions [27]. Finally, also many genetic engineering techniques and technologies, including molecular cloning and recombinant DNA [28], derive from *E. coli* studies.

Among the different laboratory strains available, *E. coli* K-12 was firstly isolated in 1922 in California from the stool of a diphteria patient. Ultraviolet light and acridine orange were then used to cure it of the temperate bacteriophage λ and F plasmid and stored at -80°C to avoid further mutations [29]. In this work, we use one of these cured strains, named NCM3722, first described by Sydney Kustu and colleagues in 2003 [30] and completely sequenced in 2015 [31]. The strain is derived from the more popular MG1655, but it grows 50% faster and it is incapable of colonizing the human intestine or survive outside the laboratory, thus allowing save handling and low safety standards.

1.7 Life cycle of a bacterium

The behaviour of a population of *E. coli* is determined by its environment. Under laboratory conditions, when cells are grown in liquid cultures in test tubes, we can accurately describe the environment by the chemical composition of the culture medium. To be able to grow, bacteria need hydrogen donors and acceptors, a carbon source, a nitrogen source, minerals (sulphur, phosphorus, magnesium, potassium) and growth factors (amino acids, purines, pyrimidines, vitamins) as well as trace elements (Fe^{3+}, Mn^{2+}) [32]. Additionally, several stresses such as pH, temperature and osmolarity changes need to be avoided. The exact composition of the media used in this work is provided in the Methods sections of the Appendices. When the environment sufficiently matches the conditions described, the bacterial population often shows a defined life cycle (see Fig. 1.2). After a lag phase, cell growth accelerates reaching a phase of exponential

growth, at the end of which growth rate slows down again (retardation phase) and cells enter a phase of growth arrest, usually divided in stationary phase and phase of decline [33]. While the actual bacterial life cycle can show more complexity, this schematic representation pinpoints to the fact that life for a bacterium is about more than just growth, as it includes periods of adaptation and survival. Indeed, as we mentioned at the beginning of this chapter, in the natural environment, bacteria seldom encounter conditions that permit periods of exponential growth. Rather, their life is characterized by long periods of nutritional deprivation punctuated by short periods that allow fast growth, a feature that is commonly referred to as the "feast-or-famine" lifestyle [34]. In the following sections, we will first describe *E. coli* behaviour in the "feast" phase, where it can grow exponentially, and we will introduce the main mathematical methods so far developed to describe its physiology in this state. These methods are important to understand, later, the quantitative approaches developed in this thesis to study the "famine" phase. Then, we will focus on the "famine" phase, which will be the central topic of this thesis, and we will highlight the main questions we want to answer in the next chapters.

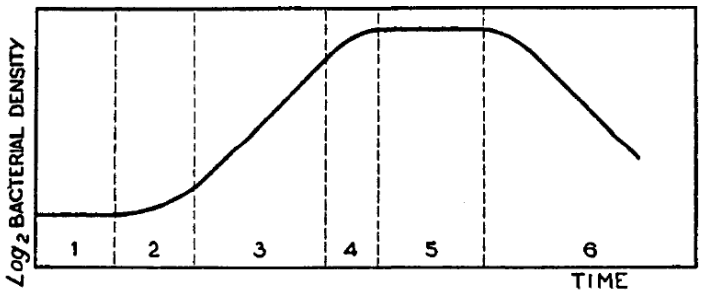

Figure 1.2: Bacterial life cycle. Schematic representation of possible bacterial population behaviours within a defined culture volume plotted versus time. The life cycle is divided in: lag phase (1), acceleration phase (2), exponential phase (3), retardation phase (4), stationary phase (5) and phase of decline (6). The image is taken from [33].

1.8 The growth phase

1.8.1 Exponential growth in batch culture and chemostat

In the absence of environmental changes, when placed in closed systems such as batch liquid cultures and provided with saturating concentrations of nutrients, bacteria eventually reach a state of balanced exponential growth, during which any constituent of the cell (DNA, RNA, proteome composition etc.) accumulates exponentially within the culture at the same growth rate μ and the average properties of the cells do not change [33, 35–37]. This state is mathematically described by the first phenomenological law in microbiology, postulated by Jacques Monod in 1949:

$$\frac{\mathrm{d}N(t)}{\mathrm{d}t} = \mu N(t) \tag{1.1}$$

where $N(t)$ is the bacterial density at time t, while the growth rate μ determines the ability of the bacteria to grow in the prescribed environment and can be accurately quantified by measuring the optical density of the culture [38]. The growth rate is described as a saturating function of the limiting substrate concentration S:

$$\mu = \mu_{\max} \frac{S}{S + K_S} \tag{1.2}$$

with $\mu_{\max}$ being the maximum growth rate and K_S the substrate saturation constant which supports a growth rate one half of the maximum [33]. By varying the quality of the nutrients used as substrates (for example, by changing the carbon source or adding a variety of amino acids), the growth rate can be modulated and cell doubling time can be easily varied from 20 min up to several hours.

As we will see in Chapter 3, the growth rate can be modulated also without changing the nutrient quality, if the cells grow in continuous cultures in chemostats, instead of batch cultures. In contrast to the latter, continuous culture is an open system with a continuous feed of influent solution that contains substrates and a continuous drain of effluent solution that contains cells, metabolites, waste products and any unused substrates. In this system, dilution rate and influent substrate concentration are the two parameters used to study microbial growth. The dilution rate controls the growth rate, while the influent substrate concentration controls the number of cells produced. Thus, growth rate and cell number can be controlled independently [39] and the change in bacterial density with time is

$$\frac{\mathrm{d}N(t)}{\mathrm{d}t} = \mu N(t) - DN(t) \tag{1.3}$$

where D is the dilution rate.

1.8.2 Proteome partitioning and flux balance growth models

The exponential growth law of bacteria represents the first example of "top down" approaches in quantitative biology and biophysics, where quantitative models are derived from phenomenological observations of bacterial physiology. We now summarize the main concepts of the new quantitative framework developed in the last decade to describe bacterial growth by linking molecular mechanisms to cell growth rate. A similar approach is missing in the growth arrest phase.

At the molecular level, cell growth requires protein synthesis: environmental nutrients are converted into amino acids by using metabolic proteins (nutrient influx); the aminoacids are then polymerized by ribosomes into polypeptide chains that make proteins (amino acid outflux).

Given the total cell proteome mass M, the mass fraction of a certain protein M_{i} is denoted as $\phi_{\mathrm{i}} = M_{\mathrm{i}}/M$, which is also a proxy for intracellular concentration [40], that in this work will be called c_{i} (see Chapter 4).

Based on empirical observations [41, 42], when bacterial growth rate is changed by modifying the nutrient composition of the medium, the mass fraction of ribosomal proteins ϕ_{R} varies linearly with the growth rate μ as

$$\phi_{\mathrm{R}} = \phi_{\mathrm{R}}^{\min} + \mu/\kappa_{\mathrm{t}}. \tag{1.4}$$

Second, when growth rate is changed by inhibiting protein synthesis, the mass fraction of ribosomal proteins ϕ_{R} changes linearly with growth rate as

$$\phi_{\mathrm{R}} = \phi_{\mathrm{R}}^{\max} - \mu/\kappa_{\mathrm{n}}. \tag{1.5}$$

The empirical parameters $\phi_{\mathrm{R}}^{\min}$ and $\phi_{\mathrm{R}}^{\max}$ are approximately growth medium independent and set the limits on the ribosomal protein fraction during exponential growth. The empirical

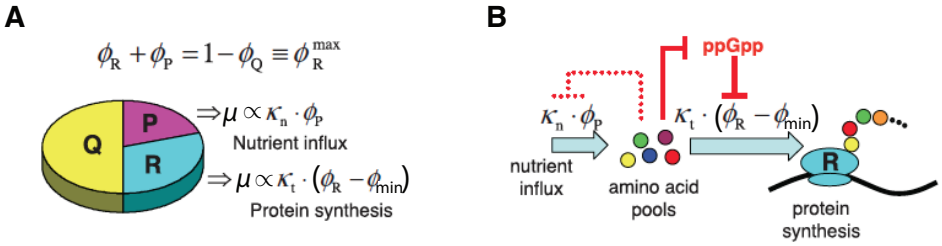

Figure 1.3: Phenomenological theory of bacterial growth. **(A)** Proteome partitioning. The growth theory comprises three key ingredients: (i) a three-component partition of the proteome, consisting of a fixed core sector (Q) and two adjustable sectors (R and P) whose fractions (ϕ_R and ϕ_P) must add up to a constant ($\phi_R^{max} = 1 - \phi_Q$); (ii) a ribosomal fraction ϕ_R containing all the ribosomal proteins and their affiliates and exerting a positive effect on growth (with growth rate $\mu \propto \phi_R - \phi_{min}$); (iii) a remaining fraction ϕ_P exerting a similarly positive effect on growth (with growth rate $\mu \propto \phi_P$) by providing an influx of nutrients. **(B)** Flux balance model. During steady-state exponential growth, efficient resource allocation requires that the nutrient influx ($\kappa_n \cdot \phi_P$) is flux-matched to the amino acid outflux $\kappa_t \cdot (\phi_R - \phi_{min})$. This can be coordinated by the alarmone ppGpp, which up-regulates ribosome synthesis and amino acid outflux in response to increase in the amino acid pools. It also has the opposite effect in response to decrease in the amino acid pools. Changes in ϕ_R also indirectly regulate nutrient influx through the constraint of $\phi_P = \phi_R^{max} - \phi_R$, in addition to direct regulatory mechanisms. Images are adapted from [41].

parameter κ_t is proportional to the *in vitro* protein translation rate and is a measure of the "translational efficiency" of the cell. The parameter κ_n correlates with the growth rate of the cell in a given medium in the absence of protein synthesis inhibition and is a measure of the "nutritional efficiency" of the cell [40].

To connect these phenomenological relations with the underlying regulatory mechanisms, as shown in Fig. 1.3A, we can divide the total proteome of a cell into a growth rate-independent fraction ϕ_Q, that may include negatively autoregulated housekeeping genes [43], and growth rate-dependent fractions, one for ribosomal and other translational proteins ϕ_R and one for metabolic proteins ϕ_P, including transporters and catabolic and anabolic enzymes [41] (see [43–46] for model extensions). The growth rate dependence of ribosome and metabolic proteins are constrained by the partitioning so that $\phi_R + \phi_P = \phi_R^{max}$ where $\phi_R^{max} = 1 - \phi_Q$. Thus, any increase in metabolic protein fraction to increase amino acid influx must necessarily decrease ribosomal protein fraction and thereby decrease the outflux of amino acids used for protein synthesis (see Fig. 1.3B) and viceversa.

We now show how these constraints of the proteome partitioning give rise to the empirical growth laws of Eq. (1.4) and Eq. (1.5).

Protein synthesis

As we said in Section 1.8.1, during exponential growth, the entire cellular content increases at the same rate, including the total proteome mass M. Neglecting protein turnover, exponential proteome mass accumulation is then written as $\mathrm{d}M/\mathrm{d}t = \mu M$, where μ is the exponential growth rate.

Proteome mass accumulation is maintained by a certain number of ribosomes. Thus, $M \propto N_R - N_R^{min}$, where N_R is the total number of ribosomes and N_R^{min} is the number of ribosomes not involved in protein synthesis. These ribosomes all translate at an averaged rate k per ribosome. Thus, the rate of proteome mass accumulation can be written in terms of the total number of

ribosomes N_{R} as

$$\mu M = k(N_{\mathrm{R}} - N_{\mathrm{R}}^{\mathrm{min}}). \tag{1.6}$$

The total mass of ribosomal proteins is denoted by $M_{\mathrm{R}} = N_{\mathrm{R}} m_{\mathrm{R}}$, where m_{R} is the mass per ribosome along with all the proteins co-regulated with ribosomal proteins. The mass fraction of ribosomal proteins can be denoted as $\phi_{\mathrm{R}} = M_{\mathrm{R}}/M$. Dividing Eq. (1.6) by total proteome mass M yields

$$\mu = \kappa_{\mathrm{t}}(\phi_{\mathrm{R}} - \phi_{\mathrm{R}}^{\mathrm{min}}), \tag{1.7}$$

which is the empirical growth law of Eq. (1.4), where $\phi_{\mathrm{R}}^{\mathrm{min}}$ is the fraction of ribosomal proteins not participating in protein synthesis and $\kappa_{\mathrm{t}} = k/m_{\mathrm{R}}$ is the "translational efficiency".

Amino acid flux

As shown in Fig. 1.3B, to maintain the protein biosynthesis required for growth, a steady influx of amino acids must be supplied to the ribosome. The dynamics of the free amino acid pool within the cell is determined by the amino acid influx rate on one hand and by their incorporation into proteins on the other hand. In media with amino acids supplied, influx is limited by the efficiency and the relative abundance of metabolic proteins involved in amino acid supply, such as transport proteins.

To describe this dynamics, we can assume that protein synthesis is limited by the influx of one of the amino acids (or a small group of amino acids) and denote the growth-limiting amino acid pool by a single coarse-grained entity of total mass M_a. Thus, the dynamics of the amino acid mass will be

$$\frac{\mathrm{d}M_a}{\mathrm{d}t} = J_a^{\mathrm{in}} - b\frac{\mathrm{d}M}{\mathrm{d}t} \tag{1.8}$$

where J_a^{in} is the amino acid influx rate and b is the fraction of translation events consuming the growth-limiting aminoacid used in proteins.

If we express the equation in terms of fraction of total protein mass M, we obtain that the dynamics of the mass fraction of the amino acid is:

$$\frac{\mathrm{d}a}{\mathrm{d}t} = \frac{J_a^{\mathrm{in}}}{M} - \frac{1}{M}\frac{\mathrm{d}M}{\mathrm{d}t}(b + a) \tag{1.9}$$

where $a = M_a/M$ is the mass fraction of the growth-limiting amino acid pool.

In steady state, there is no net change in the amino acid pool, $\mathrm{d}a/\mathrm{d}t = 0$, and the amino acid dynamics simplifies to the algebraic constraint

$$J_a^{\mathrm{in}}/bM = \mu \tag{1.10}$$

where $(a + b) \approx b$ [40]. In media with amino acids supplied, influx is limited by the fraction m_a of metabolic proteins that transport the amino acids. For a metabolic protein mass fraction ϕ_{P}, the flux can be written as

$$\frac{J_a^{\mathrm{in}}}{M} = k_a m_a \phi_{\mathrm{P}} \tag{1.11}$$

where k_a is a proportionality constant that characterizes the efficiency of the transporters. Thus, the rate of amino acid influx is proportional to the mass fraction of metabolic protein. Substituting equation Eq. (1.11) into equation Eq. (1.10) and considering the proteome partitioning constraint $\phi_{\mathrm{P}} + \phi_{\mathrm{R}} = \phi_{\mathrm{R}}^{\max}$, the amino acid flux equation becomes

$$\mu = \kappa_{\mathrm{n}}(\phi_{\mathrm{R}}^{\max} - \phi_{\mathrm{R}}), \tag{1.12}$$

which is the empirical growth law of Eq. (1.5), where $\kappa_{\mathrm{n}} = k_a m_a / b$ is a measure of "nutritional efficiency".

A similar result can be obtained in minimal media like the one used in this work, where there are no amino acids in the environment and bacteria are forced to produce amino acids on their own. In this case, aminoacids are synthesized from a pool of precursor metabolites driven by catabolic proteins, while the amino acid influx is given by the rate of amino acid biosynthesis driven by anabolic proteins [40].

In the last decade, this proteome partitioning framework coupled with the idea of balance of fluxes of resources supplied (influx) and consumed (outflux) has led to regulatory insights on the molecular level of bacteria. For example, it was used to identify the molecule cyclic adenosine monophosphate (cAMP) as a key regulator for proteomic resource allocation [44] and to show that the slow diffusion of the bulky tRNA complexes in the crowded cytoplasm imposes a physical limit on the speed of translation and cell growth [43]. In this work, the idea of balance of fluxes of resources supplied and consumed will be used to develop "top down" models of bacterial physiology under stresses such as starvation and high temperatures with the aim to reveal how cellular components affect cell survival and dormancy.

1.9 Fitness: costs and benefits of growing and surviving

Cell ability to survive and reproduce in a certain environment represents the fitness of the population. During exponential growth, one commonly employed method of quantifying microbial fitness is to calculate the maximum growth rate μ of the culture. Clonal populations of microbes are typically placed in a novel environment where they can grow. The growth rate of the population is then assessed periodically [47]. A genotype with higher growth rate will have a higher fitness, as it reproduces and thereby increases in frequency over time compared to a genotype with slower growth rate, which will be a less-fit competitor. Both the faster and the slower population can adapt to the environment over time, usually via substitution of new mutations. In doing so, as shown by R. E. Lenski et al. in the Long Term Evolution Experiment (LTEE) [47], their growth rate, thereby the fitness, typically rapidly increases during the first 1000 generations, with this increase decelerating over time, following a power law [48]. This suggests that the growth rate of the initial wild-type falls always short of the theoretical maximum, as subsequent mutations can easily increase it, regardless of the initial growth rate.

If we consider that nutrients can quickly be exhausted and bacteria need to be always ready for long periods of starvation, one hypothesis could be that they choose to do not grow at their maximum growth rate to facilitate adaptation when conditions become worse (see Chapter 3 for a more detailed discussion). It is, indeed, known that, also when nutrients are available, bacteria divert a substantive fraction of energy to functions other than growth, even if the environment would allow a faster growth rate [49, 50] (see also Section 1.10.4). Even if not well understood, this picture suggests that the fitness of a population cannot be defined just by its maximum

growth rate [51], but must be considered as the average proliferation across cycles of growth and death, where cell's ability to survive and cell's ability to grow fast can become competing objectives. Our findings of Chapter 2 and Chapter 3 suggest, indeed, that bacteria may not optimize growth rate at all costs. We will discuss how both death rate and growth rate are important when measuring fitness in environments where "feast" and "famine" alternate.

In every environment, cell fitness is determined by a balance of costs and benefits. Expressing proteins uses cellular resources and thus incurs fitness costs [52]. To balance these costs and generate a net fitness advantage, cells must couple protein expression and activity to beneficial processes. These cost/benefit tradeoffs [53] shape mechanisms that regulate protein expression and activity. Thus, in order to derive predictive models of the physiological consequences of protein expression and activity, the underlying sources of both cost and benefit must be identified and quantified. In the last 15 years, progress has been made in measuring costs and benefits during exponential microbial growth, linking protein expression to its effects on the fitness of the population. For example, in the *lac* system of *E. coli* growth, the cost is represented by the activity of the LacY proteins [52], while the LacZ proteins confer growth advantage when lactose is present [53]. In this case, the fitness function, given by the difference between the benefit and the cost, was shown to predict that for each lactose environment there exists an optimal LacZ expression level that maximizes growth rate. The fitness costs of protein expression have also been hypothesized to govern the speed at which proteins evolve [54, 55] and to influence the operation of regulatory circuits [41, 43]. However, except for few exceptions [56, 57], similar dissections of costs and benefits in non-growth states are rare in literature. We will contribute to fill this gap, dissecting costs and benefits that affect *E. coli* survival in carbon starvation in Chapter 2.

1.10 The growth arrest phase

When incubated in a closed, confined space, such as a test tube, bacteria eventually gradually stop to grow exponentially (see Fig. 1.2, phase (4)) and enter a stationary phase, during which the optical density of the culture remains constant (see Fig. 1.2, phase (5)) and cells need to respond to a wide range of stresses, depending on the specific conditions that have led to stationary phase. A phase of decline and death (see Fig. 1.2, phase (6)) usually follows the stationary phase.

As we remarked at the beginning of this chapter, also if predominant in nature, the study of growth arrested cells is far less studied in comparison to the exponential phase [58, 59]. The dearth of information is due, in part, to the challenges in defining, reproducing and measuring non-growing states of bacteria in the laboratory. The approaches that have been so far used to study bacterial cells in non-growing states are manifold and the resulting findings are diverse, not always reproducible and often specific to the particular experimental choices. A state that allows reproducibility and precise quantification of cellular physiology has not been defined so far and will be the central topic of Chapter 2.

The growth arrest of the population can be obtained in different ways. Here, we provide an overview of the main experimental conditions that cause growth arrest, later focusing on starvation, high temperature and persistence, which will be analysed in this thesis.

Starvation is perhaps the simplest and most intuitive approach to force the cells to enter stationary phase: bacteria are grown in a batch culture until carbon and/or nitrogen sources are depleted. At this point, many species exhibit a large decrease in viable cell counts. However,

for *E. coli*, in the absence of other stresses, the death of the entire population is usually never reached and a small fraction of the initial population can remain viable for years.

Growth arrest can be also caused by lack of oxygen. Also in this case, some cells survive anaerobic conditions for periods of at least several months [59]. On the other side, cell growth is prevented also when oxygen concentration surpasses the air saturation level. In this case, reactive oxygen species (ROS) accumulate as byproducts of aerobic metabolism and become toxic to the organisms since they are more reactive than molecular oxygen [60].

Also moderate changes in pH values can determine growth arrest, as they modify the ionization of amino-acid functional groups and disrupt hydrogen bonding, which, in turn, promotes protein unfolding and denaturation, destroying its activity. Moreover, high pH also impairs energy production, as it causes the neutralization of H^+ ions, whose concentration gradient across the plasma membrane of the cell allows the proton motive force to produce ATP in cellular respiration [32].

Growth arrest due to protein denaturation and unfolding is also caused by temperature increase respect to the optimal value for growth [32]. On the contrary, as temperature decreases, cell membrane becomes increasingly viscous with decreasing membrane fluidity and it eventually undergoes a phase change to a gel phase where biological function is lost [61].

Changes in osmotic pressure can also prevent cell growth and cause death: high osmotic pressure removes water from cell, causing shrinkage of cell membrane, while low osmotic pressure causes water to enter the cell and can determine cell lysis or burst if cell wall is weak and does not prevent excessive entry of water in the cell [32].

A different state in which cells remain growth arrested, despite an abundance of nutrients, is the persister state that is associated with antibiotic tolerance and can be triggered by several stresses such as starvation and high temperatures.

It remains possible that some cells that seem to lose viability during growth arrest states are actually entering a "viable-but-nonculturable" (VBNC) state, which is characterized by an inability to form colonies on rich media but the continued maintenance of the proton motive force. This state was first observed in *Vibrio cholerae* and *E. coli*, but subsequently also in phylogenetically diverse bacteria, and can often be induced by stresses that overlap with the initial stationary phase, such as prolonged starvation or high osmolarity.

1.10.1 Death and survival during starvation

When nutrients are depleted, cells enter a growth arrest phase due to starvation. The stationary phase at the beginning of starvation can last few hours in poor media such as minimal media (see Appendix A) or days in rich media such as LB (Luria Bertani). Then, unless able to form spores [62, 63], cells begin to lose viability and enter a death phase. The timing of entry into the death phase can vary from species to species (or even from strain to strain) in a given medium [13], as well as the population dynamics and the degree of loss of viability [13]. The triggers for the transition from stationary phase to death phase and the mechanisms of cell death are not well understood. Any of the stresses mentioned in Section 1.10 can contribute. Moreover, even when the death phase sets in, the mechanisms that allow some cells to survive longer than others are not clear. One hypothesis could be that living cells survive longer by catabolizing the detritus

of their dead siblings [13]. It was also hypothesized that nutrients released by dead cells could promote a regrowth of a subpopulation of cells ("cryptic growth", [64]). Alternatively, bacteria may choose apoptosis, a mechanism in which high-density cell cultures experience a form of programmed cell death [13]. After the death phase, bacteria can be maintained in batch culture for long periods of time without the addition of nutrients [65]. By regularly providing sterile distilled water to maintain volume and osmolarity, aerobically grown cultures can be maintained at densities of $\sim 10^6$ cells/ml for more than 5 years without the addition of nutrients. This period of long-term survival in starvation is characterized by several mutations.

The phenomenon of nutrient starvation has first been investigated extensively by Harrison in the 1960s [66], who reported about the decrease in bacterial viability in distilled water without additional nutrients. Still in the 1960s, Postgate and Hunter [67] presented an investigation of an exhaustive list of experimental conditions and their effect on bacterial survival during starvation using *Enterobacter aerogens*. In particular, they found an increase in death events for pH > 7, temperature and lack of buffer. In 1970s and 1980s, some mathematical approaches were developed with the aim to describe bacterial physiology during the death phase [68–70], but they did not explain the molecular mechanisms behind. From the 1980s to the 1990s, the field of starvation shifted from physiological studies to molecular biology [34, 71–78]. The work of Lange and Hengge-Aronis first identified the sigma factor σ^S or RpoS, a subunit of RNA polymerase that acts as the master regulator of the general stress response in *E. coli* [73]. Subsequently, the molecular effects of RpoS on gene regulation were investigated extensively. The widely regarded work of Zambrano et al. [78] reported that *rpoS* mutants of long-term starvation have a competitive advantage over their parent strain during starvation (GASP mutants). This discovery pushed the research of the last two decades back to phenomenological approaches, which try to understand general bacterial strategies. For example, the GASP activity helped to describe the long-term starvation phase as a phase of constant cell viability dominated by competing mutants [13], see Fig. 1.4A. More recent works, such as the publication by Gefen et al., examined the activity of synthetic promoters after entry into stationary phase and could explain cell survival with a regime of constant protein expression level in stationary phase (CASP, constant activity stationary phase) [56], shown in Fig. 1.4B.

1.10.2 RpoS general stress response during starvation

At the molecular level, *E. coli* starvation is dominated by RpoS activity (see Section 1.10.1). Genome-wide analyses of RpoS-dependent gene expression showed that up to 10% of the genes in *E. coli* are under direct or indirect control of RpoS [79, 80]. These genes are mainly involved in central metabolism and high-affinity uptake systems [81], nucleic acid synthesis, modification and turnover [82], DNA damage repair [83], proteactants of osmotic stress [84], cell size and envelope [81] and curli synthesis under oxidative stress conditions [85].

Importantly, bacteria use a combination of strategies to counteract potentially life threatening assaults. One strategy is to induce highly stress specific responses that can eliminate the stress agent (e.g., reactive oxygen species) and repair damage that has occurred at the DNA, proteins or membranes. The other strategy is to prevent the damage rather than repair it. Thus, expression of RpoS due to one kind of stress, in turn, leads to cross protection against other stresses, due to the global nature of the regulation, as RpoS itself is subject to complex regulation at all levels (transcription, translation, activity and protein degradation), thereby allowing integration of multiple stress signals in the cell [79]. Moreover, both *rpoS* gene

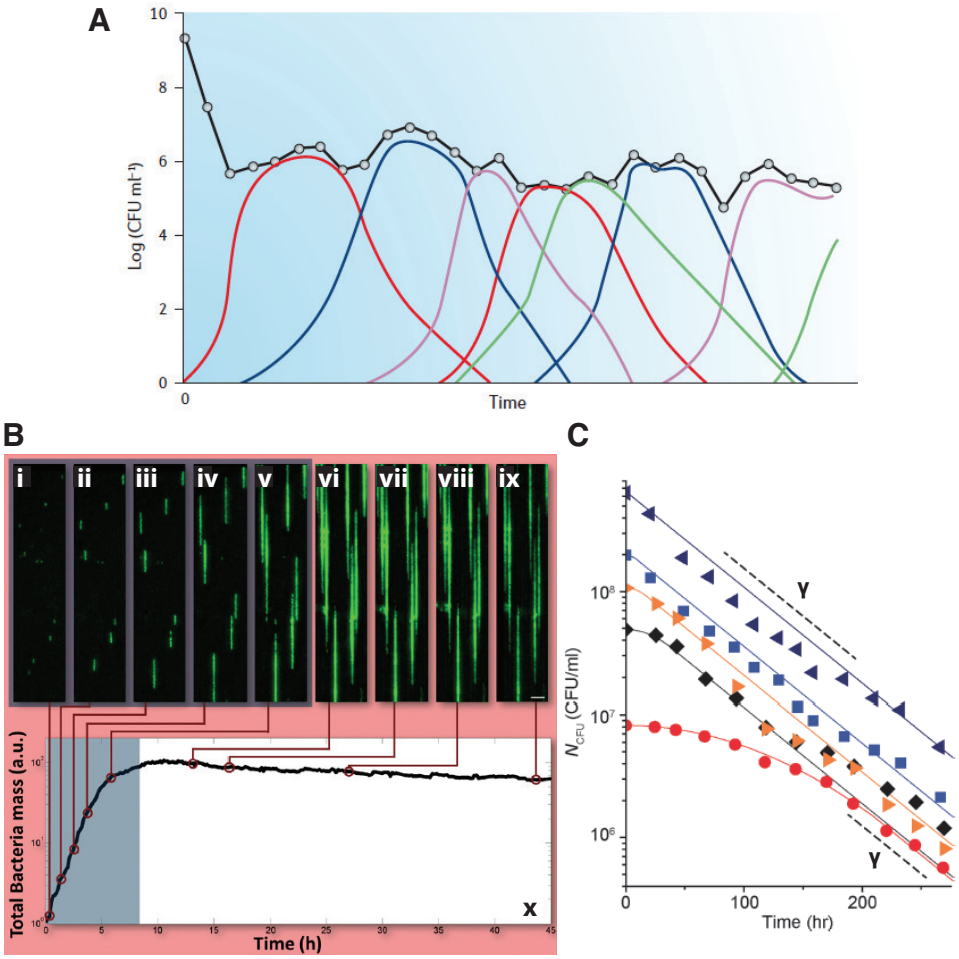

Figure 1.4: Bacterial physiology in different phases of growth arrest. **(A)** Population dynamics of long-term starvation-phase cultures in rich media. After growth, stationary and death phase (see Fig. 1.2) in LB rich medium, as cells continue to incubate under long-term starvation-phase conditions, the apparent number of living cells per ml (measured in colony-forming units, CFU per ml) remains relatively stable. However, these cultures are not static. There is a dynamic equilibrium between newly created growth advantage mutants (GASP) and less competitive cells. The birth rates and death rates within the population are balanced. Each coloured line represents a different GASP mutant that appears during long-term incubation. The black line represents the total population density. The image is taken from [13]. **(B)** Direct observation of single cells in stationary phase. Fluorescence imaging of the growth arrest of single cells, previously grown in minimal medium with amino acids in a microfluidic device. Constitutively GFP expressing bacteria trapped in the microfluidic device grow along the bacteria lines (i-v), and then enter stationary phase, where growth arrest can be directly visualized (vi-ix) and GFP expression indicates the constant promoter activity. Bar = 10 µm. (x) Growth curve in the microfluidic device. The total area of the bacteria in the microfluidic device is shown, as extracted from the total area of the fluorescence signal. The apparent decrease during more than 35 h of stationary phase is due to photo bleaching. The gray shaded area marks the exponential phase of growth. The image is adapted from [56]. **(C)** Exponential decay of viability in minimal medium. The number of living cells (measured in colony-forming-unit, N_{CFU}) of glycerol-depleted cultures is plotted over time in a semi-log graph. Different symbols indicate different cell densities at the onset of growth arrest. The lines have the slope of $\gamma = -0.018\ \mathrm{h}^{-1}$. For the cultures whose densities are above 10^8 cells/ml, N_{CFU} follows a single phase exponential decay. In the cultures with lower densities, however, we see biphasic kinetics. N_{CFU} decreases first gradually (the first phase) and then exponentially at the rate of γ (the second phase). The authors explain this phenomenon considering that, when carbon concentration decreases to low levels and the growth rate decreases, RpoS levels in the cells increase. Thus, they assume that RpoS increase forces biomass increase repression and induces the cells to save a small amount of carbon to survive longer. The image is adapted from [57].

and RpoS regulated genes are expressed in a such a way that their basal level during growth increases as the growth rate decreases, probably in preparation to harsh conditions [34, 79, 86–89].

1.10.3 Exponential decay of viability in the first phase of starvation

Despite the results and developments just mentioned, a large variety of very fundamental questions regarding bacterial survival during starvation remains open. In particular, as we show in Fig. 1.2, it is generally accepted in literature that, before the long-term starvation sets in and mutants take over, the initial survival of microbes after nutrient depletion follows a simple exponential decay. In literature, this decay was often reported and used to estimate cell dynamic behaviour [57, 66–70], even though the conditions that lead to this phenomenon were not well defined. The first rigorous test of the exponential decay was published in 2015 by Phaiboun et al. [57]. The authors show that, when depletion of carbon sources in minimal medium is complete, starved cells die exponentially, see Fig. 1.4C. However, the mechanism behind this phenomenon remains obscure and represents one of the major puzzles of microbiology. In Chapter 2, we will study the origin of the exponential decay revealing basic insights of bacterial physiology during starvation.

1.10.4 Maintenance energy

As we discussed in Section 1.9, cells often choose to do not maximize their growth rate at all costs. It is also known that the growth yield parameter Y_G, which gives theoretical estimates of the biomass yield during cell growth, is almost always lower than the theoretical maximum (in *E. coli*, Y_G is about one-third of the theoretical maximum), meaning that a substantive fraction of energy is diverted to functions other than growth [58]. Part of this energy is called "maintenance energy", the flux of energy needed to sustain a steady-state population of cells without net growth. Thus, it must be particularly important during starvation, when bacteria need to maintain basic cellular functions.

It is still unclear which are these functions. There exist eight different categories of non-growth functions to which energy can be diverted: shifts in metabolic pathways, energy spilling reactions, cell motility, changes in stored polymeric carbon, osmoregulation, extracellular losses of compounds not involved in osmoregulation, proofreading, synthesis and turnover of macromolecular compounds such as enzymes and RNA and defence against O_2 stress [90]. However, these functions vary in relative importance depending on the organism in question, its environment and its metabolic rate and they are not all requirements for maintenance energy.

One of the main challenges to solve this puzzle is the difficulty in measuring the contributors to "maintenance energy" [90]. To do so, in 1960s, Pirt described maintenance as "energy consumed for functions other than production of new cell material", providing an operational definition upon which to base observations [49]. Based on this definition, most empirical determinations of maintenance energy have been made in chemostats. As shown in Fig. 1.5, population sizes are measured across a range of dilution rates and maintenance energies are determined by extrapolating the results to a hypothetical zero-dilution (zero growth) condition. However, these methods measure the maintenance energy of the cells in physiological states of growth rather than growth arrest, thereby overestimating the minimum flux of energy required for simple survival. Moreover, they do not provide information about how the cells obtain this energy, which are the basic functions is needed for and if it can be modulated by bacteria to prolong their survival chances in starvation. We will focus on this topic in Chapter 2 and Chapter 3,

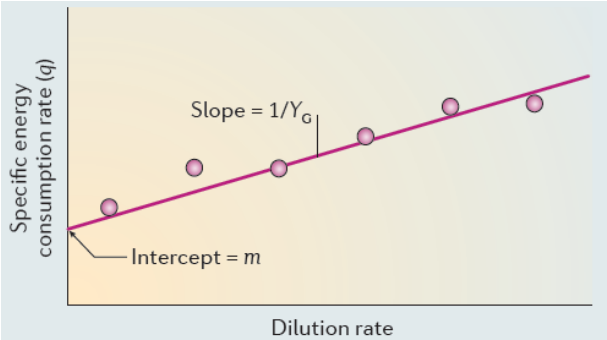

Figure 1.5: Estimation of maintenance energy. Exemplary plot for estimating the maintenance coefficient, β, based on the relationship $q = \mu/Y_G + \beta$. The growth rate μ is equal to the experimentally varied dilution rate and q, the specific energy consumption rate (in units of grams of substrates per biomass per time), is calculated from the observed rate of substrate depletion and the steady state biomass or population size. The slope of the plot gives the inverse of the growth yield, Y_G, and the intercept gives the maintenance coefficient, β. The image is taken from [58].

providing an alternative way of measuring maintenance costs in growth arrest states.

1.11 Death and survival at high temperatures

Another crucial source of stress for bacteria is temperature variation, whose effects will be studied in Chapter 4. Bacteria grow in a variety of environments from arctic oceans to hot springs, therefore the optimum growth temperatures vary considerably, affecting bacterial growth rate and survival. For *E. coli*, since it has evolved in the lower intestine of warm-blooded organisms, it is not surprising that its optimum temperature for growth is around 37°C. The dependence of the growth rate of *E. coli* on temperature shows usually different regimes, also depending on the nutrients available [91, 92]. However, generally, the growth rate increases up to 39-40°C. Above these temperatures, it starts to decrease until temperatures become growth prohibitive and cells cannot survive ($\approx$ 48°C for rich media [91] and $\approx$ 46°C for poor media [92]).

The growth rate decrease with temperature increase is generally due to proteins denaturation and unfolding, which eventually lead to a loss of protein function. A misfolded protein can find its way back to the native folded state, but in the majority of the cases denatured proteins expose hydrophobic groups thereby sticking together and forming aggregates of insoluble debris.

1.11.1 MetA and its relationship with temperature

Among the different aminoacids required for *E. coli* growth, methionine is essential for a number of important cellular functions, including protein synthesis, methylation of DNA and rRNA, biosynthesis of cysteine, phospholipids and polyamines, and can be directly synthesized by the cells [93]. However, the first enzyme of the methionine biosynthetic pathway, homoserine transsuccinylase (HTS or MetA), starts to degrade already at 25°C [94] because of ATP-dependent proteolysis [95] and is more heat-sensitive than any other essential enzyme in the cells [96, 97]. Its decay rate increases with temperature both in *in vitro* [94] and *in vivo* studies, where its half-life in minimal medium is 36 min at 37°C and only 25 min at 44°C [98]. At 46°C, the enzyme is completely inactive and aggregated. Thus, growth is no longer possible without the

addition of exogenous methionine.

The temperature sensitivity of MetA is not exclusive in *E. coli* and has been found in other mesophilic bacteria such as *Enterobacteriaceae* [99] and *Bacillus polymyxa* [100]. Therefore, it has been argued that this feature could be a regulation mechanism for growth at elevated temperatures and has been independently selected by evolution in many bacterial strains [96, 101]. The hypothesis is supported by the fact that, by simple random mutagenesis, *metA* mutants characterized by improved MetA thermostability and faster growth at high temperature can be obtained [92, 98], suggesting that *E. coli*, even if potentially able, may have on purpose not evolved to fix MetA thermostability. However, there has been so far no experimental evidence of any advantage due to MetA thermo-instability. Our results in Chapter 4, may show, for the first time, evidence of an advantage.

1.12 Bacterial antibiotic persistence

Temperature increase, namely fever, is typical of recurrent human infections characterized by persister bacteria, highly antibiotic-tolerant cells that constitute a small fraction of the population. They are transiently refractory to killing, without having acquired resistance through genetic modification [102]. Consequently, when the antibiotic pressure drops, the cells will give rise to a population that is as susceptible as the original one and that again possesses a similarly small proportion of persister cells. This discriminates persister cells from resistant mutants, which exhibit stable, inheritable drug insensitivity. However, as well as resistant cells, persisters cause antibiotic treatment failure and they have been shown to lead to the emergence of antibiotic resistance [103]. Therefore, they are a major public health concern of this century.

The presence of persisters within a population is usually revealed by viability measurements through colony forming units (CFU) on agar plates. Persisters exist when a killing biphasic pattern of the antibiotic used is observed: an initial fast decay of viability indicates that the majority of the population is susceptible to the drug and dies fast, while, beyond a certain threshold, the decay rate slows down approaching a plateau and only persister cells survive (see Fig. 1.6 and Chapter 4).

The existence of persisters was discovered by Joseph Bigger in 1944 when he could not sterilize a culture of *Staphilococcus aureus* with high doses of penicillin. He hypothesized that a minority of cells survived antibiotic treatment owing to their lack of growth rather than a heritable resistance mechanism [105]. However, this hypothesis was not confirmed for 60 years, until a study that used microfluidics and live imaging showed that the bacterial cells that survived antibiotic treatment were not growing (type I) or slowly growing (type II) before the addition of antibiotics [106]. In this way, cells inhibit growth of usual antibiotic targets normally involved in growth processes, making the antibiotic ineffective. Later, many studies have corroborated this observation, as reviewed in [107]. In addition to dormancy or slow growth, a decrease in metabolic activity is often associated with the persister phenotype [108].

1.12.1 Mechanisms and triggers of persistence

The formation of persister cells is usually triggered by environmental cues, most of which are various sources of cellular stress, such as starvation [106], temperature increase [109], extreme pH [110] and DNA damage [111]. In human infections, environments where biofilms proliferate have also been shown to be triggers of the persisters formation as they present the cellular

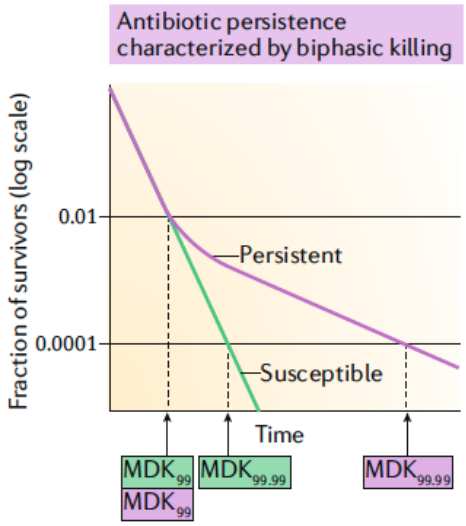

Figure 1.6: Antibiotic persistence. Biphasic antibiotic killing curve of a population of bacteria that, in addition to normal antibiotic susceptible cells (green), includes also persisters (purple). Persistence to antibiotic treatment leads to increased survival compared with susceptible cells, also if the minimum inhibitory concentration (MIC) and the initial killing of the bacterial population are similar to the ones of susceptible bacteria; however, the minimum duration for killing (MDK) for 99.99% of bacterial cells in the population ($MDK_{99.99}$) can be substantially higher owing to the survival of the persister cells. Note that pure exponential killing of the susceptible strain is rarely observed because most bacterial cultures have some level of persistence. Data shown are only illustrations from [104] and not actual measurements.

stresses described above [112]. Interestingly, even if the stress is applied to the entire population, only a fraction becomes persistent. The main reason of this splitting could be stochastic gene expression across the population: the flow of information from nucleic acids to proteins consists of a set of biochemical reactions that occur stochastically inside living cells due to the small copy numbers of molecules involved. Consequently, every cell can behave differently. However, the exact mechanisms of how these environmental cues induce the formation of persisters are still a matter of debate.

So far, the most studied mechanisms that appear to be responsible of some antibiotic persistence are toxin-antitoxin modules [113–115], which are involved in inhibition of cellular processes such as translation, DNA metabolism and decrease of the proton motive force [112]. Several global regulators are also considered important for the phenomenon [116]. An alternative model proposes that metabolic regulation is the main driver of persister formation and that toxin-antitoxin modules are only accessory to this control by locking the growth arrest [108]. Moreover, other studies show that cell-free spent medium induces persistence in *P. aeruginosa* strains, thereby suggesting the involvement of quorum sensing (QS) molecules released in the medium by the cells. Finally, it has been shown that the addition of exogenous methionine in *E. coli* cultures at high temperature reduces the fraction of persister cells within the populations and is correlated with high levels of MetA degradation [109], but the exact mechanism of persister formation is still unknown. In Chapter 4, we will shed light on this phenomenon.

1.12.2 Clinical relevance

Despite Bigger's discovery in the 1940s [105] and the identification of high persistence *hip* mutants [113], the clinical relevance of persisters was largely ignored until the early 2000s when Kim

Lewis proposed a possible role for persister cells in biofilm tolerance [117]. Subsequently, several independent studies showed links between the presence of persister cells and the chronic nature of different microbial infections. For example, remarkably higher persister levels were found in chronic infections of *Candida albicans* [118], cystis fybrosis from *Pseudomonas aeruginosa* [119] and *E. coli* urinary tract infections [120]. Moreover, independent *in vivo* experiments showed that, when antibiotic treatment stops, slow-growing *Salmonella Typhimurium* in murine cecum lymph nodes [121] and macrophages [110] appear, providing evidence for the ability of persisters to reinitiate infection when treatment stops.

More recently, it has been shown that persistence facilitates genetic resistance [103], either because of the shared mechanisms employed to overcome antibiotic killing [122–124] or because it accelerates mutagenesis and horizontal gene transfer [125].

Several methods and therapeutics are in use or under development to fight persistence. The first approach, suggested already by Bigger [105], is to apply intermittent antibiotic treatments that would allow the surviving persistent cells to resuscitate during the non-treatment period, after which they could be eliminated shortly afterwards during a subsequent treatment period. However, there are substantial evidence suggesting that sub-optimal antibiotic dosing regimens not only select for resistance development [126], but can also lead to increased levels of persistent cells, both *in vitro* [127] and *in vivo* [119]. Another strategy is the direct killing of persistent cells by using antibiotics that target cell processes crucial to maintain viability also during dormancy, such as membrane integrity activities, which, unlike growth processes, can never be switched off [128]. In alternative, as several antibiotics require active transport systems to enter the bacterial cell [129], stimulation of antibiotic influx was demonstrated to accommodate persister eradication [130]. Finally, as most antibiotics depend on active cell processes such as macromolecular synthesis to corrupt their targets, stimulation of the metabolism of quiescent persister cells is used to potentiate the activity of conventional antibiotics [131]. As we will see in Chapter 4, treatments with methionine may be successful in this context.

Chapter 2

Death rate of starved *E. coli* is set by maintenance cost and recycling yield

2.1 Introduction

Much of our systems-level understanding of bacteria is derived from the study of cells in the well-defined state of balanced exponential growth. As we said in Chapter 1, in this steady-state, the average properties of cells do not change [33, 35–37], enabling reproducible and precise quantitation of physiological characteristics. For instance, studies exploring the interdependence of gene expression and growth [41], the coordination of the proteome with metabolism [44], evolution [47] and the growth benefits and costs of enzymes [52, 53], all depend on measurements in steady-state exponential growth.

However, in nature, most bacteria spend the majority of their time in states of very low metabolic activity and little or no growth, in which nutrients are limited. Thus, non-growing states play an important role in the bacterial "feast-or-famine" life style [34] and our systems-level understanding of growth arrested bacteria lags behind that of growing bacteria [59].

Key to a quantitative analysis of bacteria facing starvation would be a well-defined reference state, ideally a steady-state analogous to balanced exponential growth, during which cellular physiology does not change. Yet defining such a state has proven challenging [59]. When cells are starved, several molecular processes occur inside the cells, such as a down-regulation of the metabolism [133] and the activation of the stress response system via the alternative sigma factor RpoS [73, 134]. At the population level, cannibalism phenomena may happen [135–137], as well as mutations [13], also leading to growing subpopulations of cells called "cryptic growths" [138–140], which can cause oscillatory decay patterns of viability [66, 67], but may also be not manifest [72, 140]. In complex media, the number of viable cells usually displays a non-monotonous time dependence with multiple periods of decrease, increase and stagnation [13]. Thus, albeit interesting, this scenarios cannot provide the needed reference state.

Interestingly, if bacteria are carefully starved of all energetic substrates (carbon starvation) at optimal temperature and pH, they show an exponential decay of viability for several orders of magnitude [57]. The simplicity of this phenomenon is crucial, since the entire dynamics can be described by one parameter: the death rate of the population, allowing quantitative analyses of survival curves [57]. Thus, the exponential decay of viability could be an excellent starting point for dissecting bacterial physiology of survival. In contrast to exponential growth, however, it has been so far not known why viability decreases exponentially during starvation. This miss-

ing knowledge prevented us from understanding how changes in death rate can arise from the plethora of genetic or environmental perturbations known in the literature [66, 67, 71–74, 140].

In this chapter, we fill this gap and uncover the origin of the exponential decay using a combination of quantitative starvation experiments and mathematical analysis. We show that in carbon starvation an exponential decay of viability emerges as a collective phenomenon, with viable cells recycling nutrients from dead cells for maintenance of viability. The observed collective death rate is determined by two physiological parameters: the average rate at which cells consume energy for the maintenance of viability and the efficiency at which viable cells recycle biomass from dead cells. This relation permits quantitative insights into how environments and genetic elements affect bacterial survival, as exemplified by a study of the cost of a wasteful enzyme and the benefit of the stress response sigma factor RpoS. While the enzyme increases the maintenance rate and thereby the death rate, RpoS improves biomass recycling, decreasing the death rate.

Our approach thus enables quantitative analyses of how cellular components affect survival of non-growing cells, their fitness and evolution, in a similar way to how exponential growth allows the quantitative analysis of bacterial physiology during growth, as mentioned in Chapter 1. Moreover, as exponential decay under nutrient deprivation seems to occur in a wide variety of organisms like yeast [141] or *Enterobacter aerogens* [67], our findings may be useful to investigate the behaviour of other microorganisms and could pave the way towards the understanding of starvation in more complex systems like multimicrobial communities.

This work is a project collaboration with Dr. Severin Josef Schink, Constantin Ammar and Prof. Dr. Ulrich Gerland. This chapter is adapted from Schink J. S.*, Biselli E.*, Ammar C. and Gerland U., *Death rate of E. coli during starvation is set by maintenance rate and biomass recycling*, Cell Systems 9, 1-10, 2019 (*co-first author).

2.2 Survival kinetics of *E. coli* after carbon starvation

To study the kinetics of the death phase, we induce carbon starvation in a wild-type strain of *E. coli* K-12 NCM3722 by growing cells until the carbon substrate, glycerol, is exhausted (see Fig. 2.1A and Appendix A). Complete carbon starvation is often an experimental challenge. Indeed, towards the end of carbon depletion, cells may adapt to the coming starvation, e.g. by storing nutrients [57, 142], if the carbon source is uptaken with low affinity. When cells are grown in casamino acids or more complex media with different carbon sources such as lysogenic broth (LB), some nutrients may remain in the medium, supporting prolonged survival of the cells [56]. Moreover, *E. coli* may excrete fermentation products such as acetate during growth (Crabtree effect) [143–146] and use them as nutrients to survive during starvation. However, acetate excreting is growth rate dependent and absent below a growth rate threshold of ≈ 0.76 h^{-1} [143]. Considering these issues, we study starvation with a single carbon substrate, glycerol, to which the cells have a high affinity [147] and do not excrete acetate, as their growth rate is ≈ 0.7 h^{-1}.

During the following period of starvation, we measure the time-dependent density of viable cells in the culture, $N(t)$, by plating and colony counting. The survival kinetics $N(t)$ displays a remarkably clean exponential decay on a timescale of days (Fig. 2.1B). The instantaneous death rate

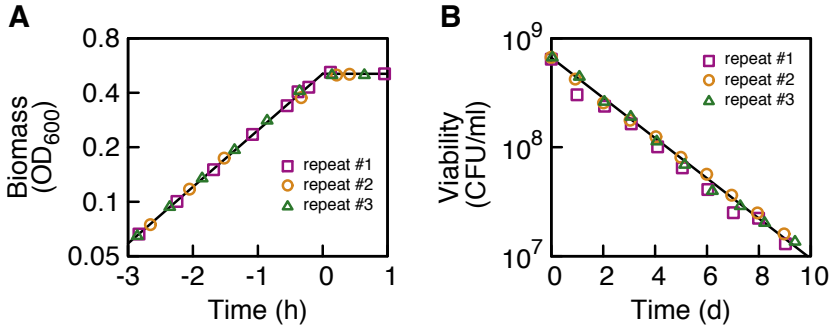

Figure 2.1: Growth and starvation dynamics. (A) Growth of *E. coli* K-12 NCM3722 in glycerol minimal medium, measured using optical density (OD_{600}). Exponential growth at growth rate $\mu = 0.70$ h^{-1} (slope of the exponential fit, black line) halts abruptly when glycerol is depleted at $t = 0$. Colors denote three biological repeats. **(B)** The starvation following glycerol depletion leads to an exponential decay of bacterial viability $N(t)$, measured in colony forming units (CFU) per ml. Colors correspond to the three experiments in panel A. The death rate $\gamma = (0.43 \pm 0.04)$ d^{-1} (slope of the black line, value reported with one standard deviation) is the average value of fits to 12 independent experiments, see Table A.1 for details.

$$\gamma(t) = -\frac{\mathrm{d}\ln N(t)}{\mathrm{d}t} \equiv -\frac{\dot{N}(t)}{N(t)} \tag{2.1}$$

reaches a value of $\gamma = 0.43$ d^{-1} after less than one day into starvation (Fig. 2.2A-C) and remains constant for over 2 orders of magnitude of viability decay.

The first day of adaptation refers to the so called "stationary phase", during which cells finish to divide and remain almost all viable, activating the stress response to starvation. This phase can last less than one day [57, 66, 67], as in our case, or several days [13, 56]. After this decay, mutants gradually dominate the behaviour and long-term survival can last several months to years [13, 137, 148], showing alternating phases of re-growth and decay, as described in Fig. 2.2D,E and in Section 1.10.1.

Cell size and shape change during growth, depending on the growth rate [35] and on the growth transitions [149]. In our case, after completing cell divisions within the first hour into starvation, the mean length and width of cells remain invariant throughout the exponential decay of viability (Fig. 2.3A). A comparison of cell width and length during growth and starvation, see Fig. 2.3B,C, reveals a substantial loss of elongated cells and gain of cells about half this size. This indicates that, during the first hour after starvation, long cells complete their division, while smaller cells do not manage to finish their division cycle.

Interestingly, when the exponential decay sets in, we do not detect any significant growing subpopulation, dismissing the hypothesis of cell turnover in the first days of cell starvation (Fig. 2.4A,B), and treatment with an antibiotic lethal to growing cells (ampicillin) does not alter the exponential decay of viability (Fig. 2.4C). Furthermore, protein synthesis is not significant, as the capacity for protein synthesis in a starved culture is low (Fig. 2.4D,E,F) and complete inhibition with chloramphenicol does not alter the death rate (Fig. 2.4C). Together, these findings suggest a relatively low activity of bacteria during the exponential decay of viability, contrasting it with other kinds of growth arrest states, such as the constant activity stationary phase, where viability is constant and protein synthesis is much more significant [56].

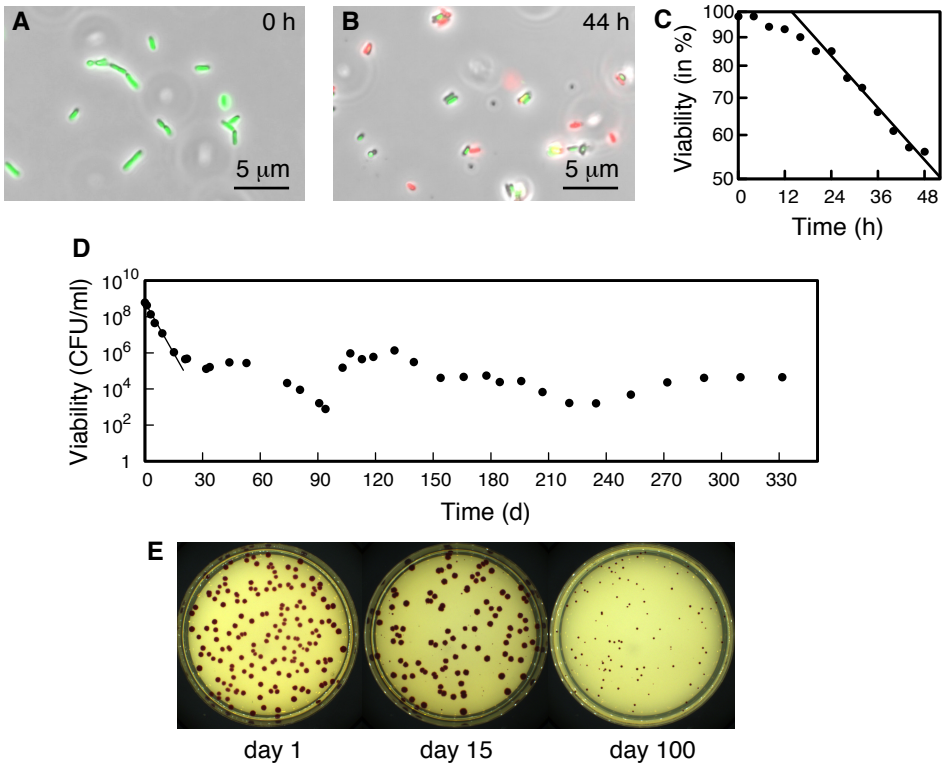

Figure 2.2: Short-term and long-term starvation dynamics. (A,B) Starved cells are stained using a Live/Dead stain that assays membrane integrity (see Appendix A) and counted manually using phase-contrast images. Green stained cells are counted as viable. Red-green stained and un-stained cells are counted as unviable. The first panel shows cells at the beginning of starvation ($t = 0$ h), while the second one shows cells after 44 h of starvation. **(C)** Kinetics of the transition into the exponential decay of viability, measured using the Live/Dead stain shown in panels A and B. Time point $t = 0$ marks glycerol exhaustion and entry into starvation. The black line marks the steady state death rate $\gamma = 0.43$ d^{-1} corresponding to the exponential decay of viability, as determined from viability assays on LB agar plates. **(D)** Long-term survival. After about 20 days of starvation, the exponential decrease of viability (black line) stops and cells enter a phase of long-term survival in starvation. Long-term survival can last at least several months to years and shows alternating phases of decay and regrowth [13, 137]. **(E)** During early starvation colony size and shape is homogenous. Late into the exponential decay, after 10-15 days of starvation, size and shape start to show heterogeneity with the appearance of tiny colonies, a sign for mutations [148]. Eventually after 100 days, colonies are all small. For size comparison, all three plates shown here were incubated for 1 day. For the experiment in panel D, at later time-points plates were incubated several days before counting, to ensure that all colonies have reached a visible size.

2.3 Recycling of nutrients from dead cells

With ongoing starvation, we observe that an increasing number of bacteria lose their membrane integrity, which is measured using propidium iodide staining (see Fig. 2.4A,B). Concurrently, the impaired integrity could lead to biomass leaking out of the cells and into the supernatant. There, these biomolecules pose a potential nutrient source for the viable population. We investigate the impact of the leaked nutrients for survival, by inoculating a small number of viable cells into supernatant of a starved culture. We perform this experiment by diluting starved cells 4.5-fold into their own supernatant. The kinetics following the dilution into supernatant is bi-phasic, see Fig. 2.5A, purple circles: cell death halts for 1.2 days and then the exponential decay of viability resumes at the original death rate of $\gamma = 0.43$ d^{-1}. In contrast, diluting cells 4.5-fold into fresh medium without carbon substrate (see black data in Fig. 2.5A) or into supernatant

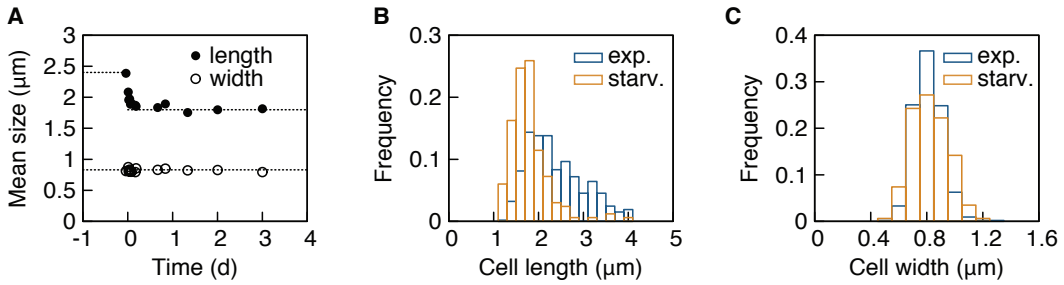

Figure 2.3: Cell size during exponential growth and starvation. (A) Mean cell length $< l >$ measured by phase contrast microscopy relaxes from the lengths during exponential growth, $< l >= 2.4$ µm, to the mean length during starvation 1.8 µm, in less than one hour. Cell width does not change significantly after entry into starvation. **(B,C)** Distributions of cell lengths and widths during exponential growth (blue) and after 2 days of starvation (yellow).

extracted prior to starvation, where dead cells are absent (see Fig. 2.5B,C), does not alter the survival kinetics.

2.4 Balance between biomass recycling and maintenance flux

That *E. coli* can survive on the nutrients leaked from dead cells suggests that we need to understand the population as a collective, rather than independent individuals, because the survival of some cells is coupled to the death of other cells in the population. To study this collective process, we introduce the quantitative model depicted in Fig. 2.6A. We are particularly interested in how the exponential decay arises and what determines the death rate. The model describes the system in terms of a supply flux J_s, which provides viable cells with nutrients from the biomass of dead cells (left arrow), and a demand flux J_d, which represents the consumption of nutrients for the maintenance of viability (right arrow). The demand flux is proportional to the number of viable cells, $J_\mathrm{d} = \beta N(t)$, with the proportionality constant β identified as the maintenance rate per cell. The supply flux, on the other hand, is proportional to the number of cell deaths per unit time, $J_\mathrm{s} = -\alpha \dot{N}(t)$. Here, the proportionality constant α quantifies the "yield" of a single dying cell, i.e. the amount of released nutrient that can be taken up by other cells, and is a measure of the efficiency of the biomass recycling. Whenever a supply-demand balance is achieved, we have

$$J_\mathrm{s} = -\alpha \dot{N}(t) = \beta N(t) = J_\mathrm{d}. \tag{2.2}$$

As time passes during starvation, fewer viable cells are left and fewer die. However, the fluxes can still remain precisely balanced. This happens at the specific value of the death rate that corresponds to the ratio of the maintenance rate to the yield,

$$\gamma = \frac{\beta}{\alpha}. \tag{2.3}$$

As long as the population stays in this balanced state, the death rate is constant and thus the viability will display an exponential decay,

$$N(t) = N(0)e^{-\gamma t} \tag{2.4}$$

consistent with the observation of Fig. 2.1B.

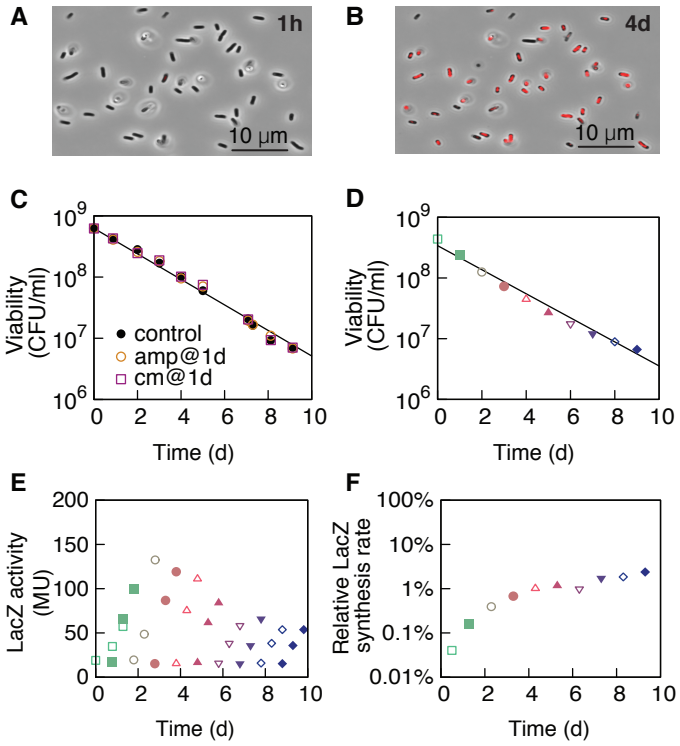

Figure 2.4: Absence of cryptic growth and not significant protein synthesis during starvation. **(A,B)** Two snap-shots of a time-lapse of a starved culture. Cells are extracted from batch culture, stained with propidium iodide (red) to detect loss of membrane integrity and starved in a µ-Slide (see Appendix A). After one hour of starvation almost no cells are stained red, i.e. lost their integrity. After four days, the majority of the cells have lost their integrity ($\approx 90\%$), consistent with viability counting by plating. During these time-lapse videos, no cryptic growth can be detected. **(C)** Antibiotic treatment of an exponentially decaying culture in batch with ampicillin (amp, 100 µg/ml) or chloramphenicol (cm, 35 µg/ml). After 1 day of starvation, a fraction of a control culture (black circles) is inoculated in a new sample and supplemented with ampicillin (amp, yellow circles) or chloramphenicol (cm, purple squares). The viability is recorded by plating. Treatment with ampicillin, administered freshly every day, does not alter the exponential decay of viability. Considering that ampicillin leads to lysis of growing cells, the absence of a change in the survival curve shows that no significant cryptic growth occurs during exponential decay. Also the treatment with chloramphenicol, a protein synthesis inhibitor, does not alter the exponential decay, indicating that the protein synthesis observed in panel D is not essential for survival. In order to test chloramphenicol effectiveness, after 7 days of starvation, both cultures are supplemented with 1 mM IPTG and LacZ activity is assayed using the Miller Assay [150] for 3 days. The culture with chloramphenicol does not show an increase of LacZ activity compared to the control culture indicating that the antibiotic is still inhibiting protein synthesis (data not shown). **(D-E)** A large culture of cells is starved (125 ml) and subcultures (5 ml) split off daily. After splitting, each subculture is supplemented with 1 mM IPTG to induce the *lac* operon and LacZ activity is assayed using the Miller Assay [150] every 12 h. In Fig. 2.9 it is shown that import of IPTG via LacY induces an energetic cost that increases death rate. Generally, however, during starvation the expression level is small, compared to expression levels achieved during growth (110 MU in panel C of this figure corresponds to 1% of the maximal expression in Fig. 2.9D). Thus, when IPTG is added during starvation, the effect of IPTG transport on the death rate is negligible. **(D)** Viability at the extraction points of ten different cultures (symbols). Every symbol/color corresponds to one subculture. After extraction, viability of the subcultures follows the main culture (data not shown). **(E)** Total LacZ expression (see Appendix A) of each of the ten subcultures is recorded for two days. **(F)** LacZ expression level per viability, normalized to the value during exponential growth prior to starvation, $2.6 \cdot 10^5$ MU/(d $\cdot 10^9$CFU). After about two days of starvation, LacZ expression levels increase to a constant rate of about 1% of the pre-starvation level.

How is the supply-demand balance of Eq. (2.2) achieved? The survival kinetics of Fig. 2.5A suggests that the starved culture is self-balancing, automatically returning to an exponential decay after perturbations to supply-demand balance. Eq. (2.3) would then define a stable steady-

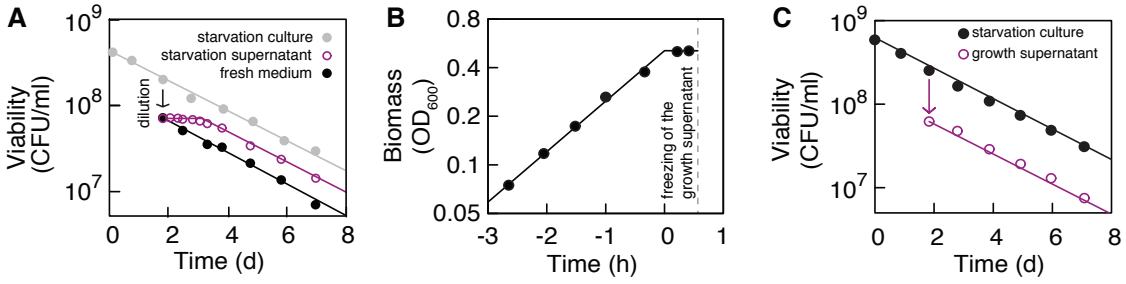

Figure 2.5: Cell survival on supernatant. (A) After 44 h of starvation, cells from an exponentially decaying culture ($2.6 \cdot 10^8$ CFU/ml, starvation culture, grey circles) are diluted 4.5-fold ($6.2 \cdot 10^7$ CFU/ml) into supernatant of the same starvation culture (purple open circles) and into fresh carbon free medium (black filled circles). While cells into fresh medium keep on dying exponentially with the death rate $\gamma = 0.43$ d^{-1} (slope of the black line), in the culture with addition of supernatant (purple open circles) cells survive for a lag time $T = 1.2$ d before dying again exponentially with the death rate $\gamma = 0.43$ d^{-1} (slope of the purple line). **(B)** A sample of the supernatant of a control culture (black circles) is extracted and frozen at the end of exponential growth (growth supernatant) when all the cells in the culture are still viable and there isn't any dead cell in the supernatant (see Appendix A). **(C)** After 2 days of starvation of the control culture, the frozen supernatant is defrosted and $6 \cdot 10^7$ CFU/ml starved viable cells of the control culture are diluted into it (purple arrow). The cells keep on dying exponentially and no lag time is observed (purple circles), confirming that, in the absence of dead cells in the supernatant, nutrients are not released in the culture and viable cells cannot use them to survive longer.

state. To see how this can arise, we consider a model that describes the average metabolic state of viable cells by a single coarse-grained state variable ϵ, subsuming the intracellular concentrations of nutrients and energy-rich molecules, the proton motive force and other contributions. We refer to ϵ as the "energetic state" and assume that it determines the death rate $\gamma(\epsilon)$ of the remaining viable cells. An increase of the energetic state, e.g. because the bacteria take up new nutrients, will lower the death rate. If the bacteria run out of internal energy storage, the energetic state will decrease and bacteria will die at a higher rate. With this step we implicitly assume that all bacteria are in a similar energetic state. The energetic state changes according to the difference between the supply and demand flux per viable cell,

$$\frac{\mathrm{d}\epsilon}{\mathrm{d}t} = \frac{J_\mathrm{s} - J_\mathrm{d}}{N} = \alpha\gamma(\epsilon) - \beta. \tag{2.5}$$

Due to the dependence of death rate γ on the energetic state ϵ, the system contains a negative feedback loop: a faster death rate leads to more nutrients becoming available. Viable cells take up these nutrients and improve their energetic state, which in turn slows the death rate again. As a result, cells reach a steady-state in the energetic state ϵ^* at $\mathrm{d}\epsilon/\mathrm{d}t = 0$, where fluxes are balanced and the death rate is given by Eq. (2.3). The stability of the exponential decay means that the system is self-balancing and any fluctuations in the supply or demand will be corrected by the population. Supply and demand are thus not fine-tuned to match each other, but rather for all supply and demand rates, the system will settle into an exponential decay with the death rate given by Eq. (2.3), see Fig. 2.6B for an illustration. A change of maintenance rate or recycling yield, as depicted in Fig. 2.6C,D, will be met with a change of death rate such that supply and demand will again be in balance.

While the model rationalizes the observed exponential decay of viability, we additionally seek an independent way to test it. To this end, we use the model to predict how long cells can survive, if a fraction of the population is killed. The sudden availability of nutrients should halt death until the nutrients are fully consumed, analogous to the experiment of Fig. 2.5A. We perform such an experiment by splitting a starved culture into two parts, killing one part with

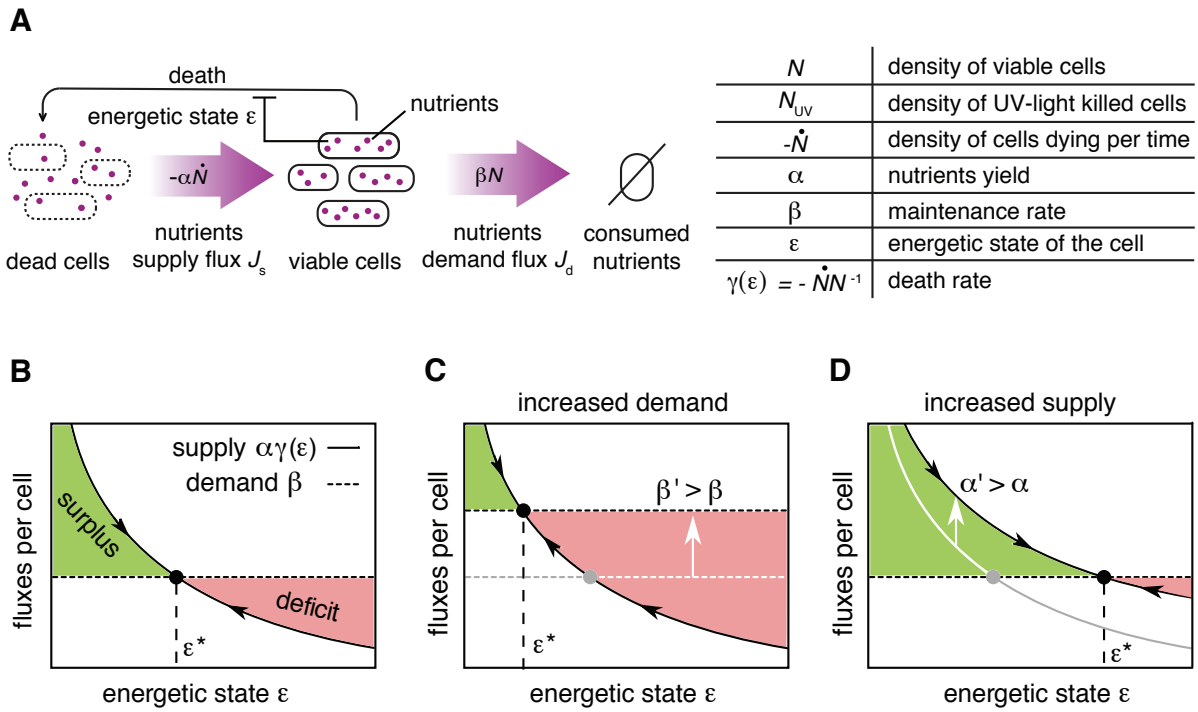

Figure 2.6: Supply and demand model: recycling of nutrients from dead cells. (A) Viable cells N take up biomolecules (nutrients, purple dots) leaked out from dead cells (supply flux of nutrients, $J_s = -\alpha\dot{N}$, where α is the nutrients yield) and metabolize them to maintain their viability (demand flux of nutrients, $J_d = \beta N$, where β is the maintenance rate). A disparity between the supply and demand fluxes will increase or decrease the energetic state ϵ of the cell, see (2.5); cell death (black arrow) is halted by an increase of the energetic state of the cells (repression arrow), which thus decreases the death rate of the population, $\gamma(\epsilon) = -\dot{N}/N$ and the supply flux, see Eq. (2.5). **(B-D)** Dynamics of the energetic state of the cell. **(B)** Nutrient fluxes per cell (supply per cell: $-\alpha\dot{N}/N = \alpha\gamma(\epsilon)$, solid line, where $\gamma(\epsilon)$ is assumed to be a monotonically decreasing function of ϵ; demand per cell: $\beta N/N = \beta$, dashed line) plotted against the energetic state during starvation. If the energetic state of the cells is low, many cells die and supply is higher than demand, leading to a surplus of nutrients (green), which increases the energetic state. Vice-versa, a high energetic state leads to less cell death, a nutrient deficit (red) and a decrease of the energetic state. Both surplus and deficit push the cells into a stable steady state (black circle) where supply balances demand. **(C)** An increase of demand due to a higher maintenance rate β (dashed line moves up), or **(D)** an increase of supply due to a higher yield α (solid line moves up) lead to a new steady state (black dot), that is lower or higher, respectively, than the original steady state (grey dot). Vice-versa, decrease of demand or decrease of supply leads to opposite effects than shown.

UV light, and then rejoining the two parts (see Fig. 2.7A, Fig. A.1, Appendix A). By varying the splitting ratio, we vary the fraction of killed cells. For example, in Fig. 2.7B,C we observe that when viable cells are mixed 50:50 and 30:70 with UV-killed cells, they show a bi-phasic survival, where the exponential decay sets in after a lag time of 2.3 d and 1.2 d, respectively.

Using our model, we can predict the lag time T produced by added nutrients: cell death is halted until an added amount E_0 of nutrient is consumed by the maintenance demand flux J_d, yielding a lag time

$$T = \frac{E_0}{J_d} = \frac{E_0}{\beta N}. \tag{2.6}$$

If the additional nutrient is supplied in the form of UV-killed cells with density N_{UV}, we have $E_0 = \alpha N_{UV}$. We can then use (2.3) to replace β/α with γ, such that the expression for the lag time becomes $T = \gamma^{-1} N_{UV} N^{-1}$. This theoretical prediction depends only on the death

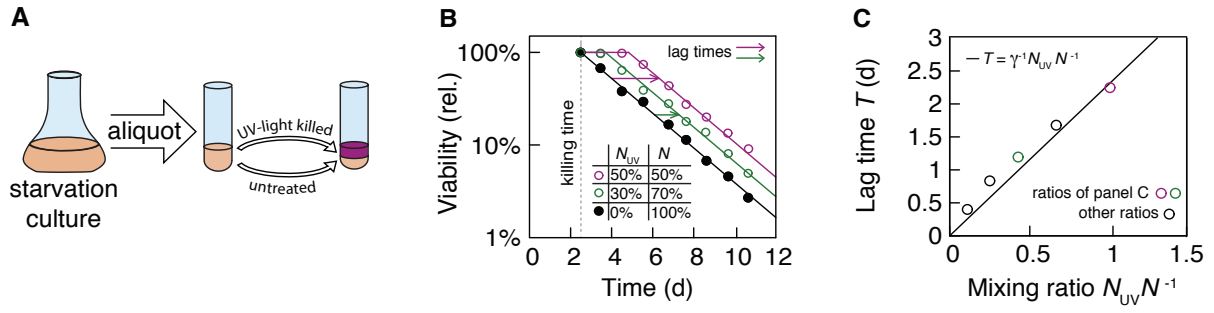

Figure 2.7: Survival on UV-killed cells. (A) Cartoon of the experiment. A sample of a large-volume starved culture (starvation culture in the flask) with N viable cells is extracted and inoculated in a different tube. A fraction of such sample is then exposed to UV light that lyses the cells (see Fig. A.1). After UV exposure, the UV sterilized culture (purple, N_{UV}) is mixed again with the untreated viable cells of the sample (salmon, N). The viability of the culture is then measured every day and compared with the viability of the starvation culture. The experiment is repeated using different mixing ratios of UV-sterilized N_{UV} and untreated culture N (see panel B). **(B)** The viability of two cultures of a) 50% UV-killed and 50% untreated viable cells (purple open circles), b) 30% UV-killed and 70% untreated viable cells (green open circles), both extracted after 2.5 days of starvation, is compared to the viability of a starvation culture of 100% untreated cells (black filled squares), see Appendix A for details. Both curves are normalized to the number of viable cells in the starvation culture (100%) after 2.5 days of starvation. The presence of UV-killed cells prolongs survival in the mixed culture for a lag time of about: a) 2 days (purple arrow), b) 1.2 days (green arrow). **(C)** Experimental lag time T increases linearly with the ratio of UV-killed cells to untreated cells, N_{UV}/N. The purple and green circles represent the lag times extracted from panel B, where $N_{\mathrm{UV}}/N = (50\%)/(50\%) = 1$ (purple circle) and $N_{\mathrm{UV}}/N = (30\%)/(70\%) = 0.43$ (green circle), respectively. The black line is the theoretical prediction derived in the main text.

rate γ, which is measured independently, and the mixing ratio of killed to viable cells, N_{UV}/N, which is controlled experimentally (see Fig. 2.7B,C). Using $\gamma = 0.43$ d^{-1} as the inverse slope of the black line in Fig. 2.7C, we find an excellent quantitative agreement between the model prediction and the lag time data.

2.5 Quantifying the maintenance rate for survival of a cell

The lag time calculated in Eq. (2.6) also provides a means to measure the maintenance rate β for the survival of a cell, by supplying defined amounts of nutrient E_0 and determining the resulting lag T, see Fig. 2.8A for a sketch of the experiment and Fig. 2.8B for an exemplary lag-time characterization. Analogous to Fig. 2.7C, increasing the amount of glycerol added to the culture increases the lag time, see Fig. 2.8C. All concentrations in Fig. 2.8C are chosen such that the amount of glycerol is too small to support growth (see Appendix A). We extract the maintenance rate as the slope of the data in Fig. 2.8C (and in Fig. A.2 for other time-points). We find that maintenance rate remains constant at $\beta = 0.49 \pm 0.04$ fmol/(CFU $\cdot$ d) in units of glycerol per viable cell per day throughout the starvation, see Fig. 2.8D, consistent with our interpretation of the cells being in a steady state. Given that growth of 10^9 cells/ml requires 10 mM glycerol as carbon source, this measurement reveals that a cell can survive for about 20 days with the amount of glycerol required for one cell doubling. Assuming that one molecule of glycerol yields 15 ATP [150], this maintenance rate corresponds to about $5.2 \cdot 10^4$ ATP/s per cell, which can be converted to a free energy dissipation rate of about $1.0 \cdot 10^6$ k_BT/s, where k_BT denotes the thermal energy unit and the hydrolysis of one ATP releases about 20 k_BT [59].

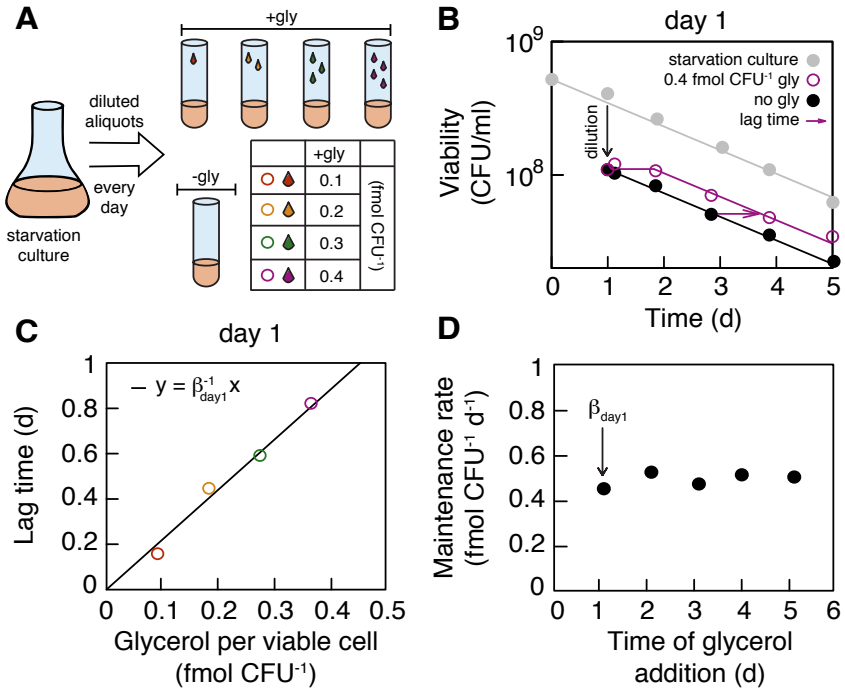

Figure 2.8: Maintenance rate measured by survival after glycerol addition. (A) Graphical synopsis of the experiment: a large-volume starved culture (flask, original culture) is split into small cultures supplemented with different small amounts of glycerol reported in the legend of the panel ("+gly", from 0.1 to 0.4 fmol/CFU) or no glycerol ("-gly") (see Appendix A). **(B)** A starved culture (starvation culture, flask) with a viability of $4.07 \cdot 10^8$ CFU/ml after 1 day of starvation is diluted to 10^8 CFU/ml (black arrow) in fresh medium supplemented with 40 µM of glycerol (purple open circles). Per viable cell, the glycerol addition in this experiment is 0.4 fmol/CFU. Glycerol addition leads to prolonged survival for a lag time $T = 0.825$ d (purple arrow) compared to a diluted control (black circles) without additional glycerol. After glycerol exhaustion, cell's viability decreases again exponentially with a death rate $\gamma = 0.43$ d^{-1}, as the diluted controls (exponential fits, purple and black lines). **(C)** Lag time of a culture treated as described in panels A and B after 1 day of starvation plotted versus different concentrations of additional glycerol, denoted by the colors defined in the legend of panel A. The purple circle refers to the lag time of panel B. Lag increases linearly with glycerol concentration, maintenance rate β is the inverse slope of the linear fit, see Eq. (2.6). **(D)** First black dot: maintenance rate of panel C measured after one day. Other dots: same measurement, performed during days two to five. Time average of the maintenance rate $\beta = (0.49 \pm 0.04)$ fmol/(CFU $\cdot$ d).

2.6 Maintenance cost incurred by a wasteful enzyme

The supply and demand model predicts that increasing the demand flux will stabilize the bacterial population at a larger death rate. We test this by forcing cells to dissipate additional energy, by exploiting the well-characterized futile transport of the non-metabolizable lactose-analog isopropyl-β-D-thiogalactopyranoside (IPTG) by the lactose permease LacY [52], see Fig. 2.9A and Appendix A. The additional demand due to IPTG transport should increase the maintenance rate β without contributing to the cell survival, thus increasing the death rate. We pre-express LacY during the growth phase (see Fig. 2.9B-D) and then observe that, during starvation, the death rate increases linearly with the LacY level (reported by co-expressed LacZ), see Fig. 2.9E,F, as predicted by Eq. (2.3). In contrast, the death rate does not significantly increase when LacY is expressed in the absence of IPTG, by deleting the lac repressor (Fig. 2.9F, black cross). Thus, the wasteful transport of IPTG, rather than gene expression, changes death rate. The cost incurred by the activity of a wasteful enzyme can be substantial in starvation. A fully active LacY transporter at wild-type expression level doubles the death rate of *E. coli*.

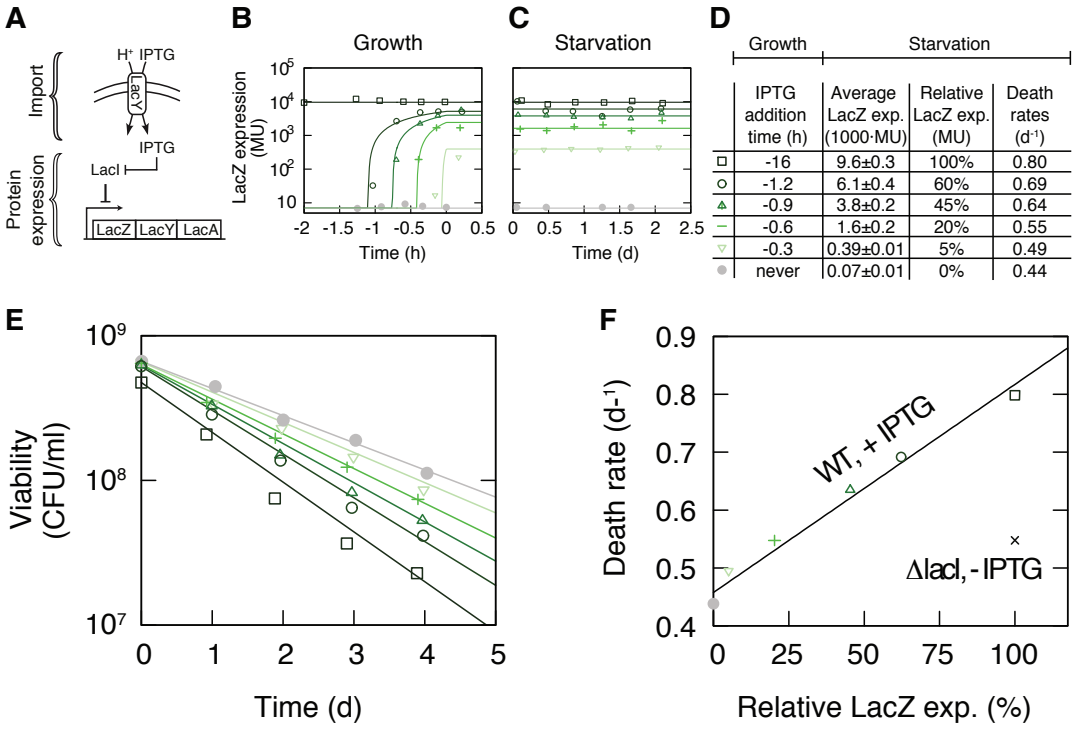

Figure 2.9: Increased demand leads to faster death rates. (A) Lac operon expression induced by IPTG. LacI: *lac* repressor inhibiting operon expression. LacZ: β-galactosidase. LacY: lactose/proton symporter; LacA: transacetylase. The artificial inducer IPTG is imported by LacY in a known energetically costly process [52], but is not metabolized by the cell. **(B)** Induction of the Lac operon with saturation amounts (1 mM) of IPTG at different times during exponential growth. Colors denote different experiments (see table in panel D). Data points: LacZ expression in Miller Units (MU), see Appendix A. Lines: logistic fits. **(C)** Data points: LacZ expression in starvation following the experiment of panel B remain constant. Lines: time averages. **(D)** Summary of IPTG addition time-points and the resulting average LacZ expression and death rate. **(E)** Viability over time during starvation of the cultures of panel B (same colors and symbols). The higher is the LacZ expression level in the culture the faster the cells die respect to the control culture without IPTG (grey circles). Lines are exponential fits, with death rates summarized in panel D. **(F)** Death rate of the cultures in panel C (same symbols and colors) plotted against LacZ expression (normalized to the highest expression value, see panel D). The black filled circles refers to other experiments with different IPTG addition times not shown in the previous panels. The black line is a linear fit. In comparison, *lacI* knock-out mutants, grown in the absence of IPTG (black star), show only a slight increase of death rate, despite full LacY expression.

Additionally, the finding that deleting the *lac* repressor leads to no significant increase of the death rate (Fig. 2.9F, black cross) shows that the cost of inducing gene expression in starvation is low. For LacY, we could attribute the death rate change to an increase in the maintenance rate based on a prior study [52]. Generally, however, the death rate is set by both yield and maintenance rate. Given an observed change of death rate, it is thus necessary to disentangle these two contributions. Towards this end, we next devise an assay to quantify changes of the yield.

2.7 Quantifying the yield of biomass recycling

To measure the yield of nutrients released from dead cells, we employ an assay independent of the maintenance rate β, using UV-killed cells as nutrient source instead of glycerol (see Fig. 2.10A and Appendix A). Interestingly, UV-killed cells can also support growth of viable cells, rather

than just survival, if provided in large quantity. This is in contrast to starvation, where bacteria do not grow, see Fig. 2.4A,B. We leverage this behaviour to determine the yield by measuring the growth of viable cells on dead cells: at different times during starvation, we aliquot a sample of a starved culture, UV-kill all cells in the sample and then mix it in a 99:1 ratio with the original culture (Fig. 2.10A). We then measure regrowth by plating.

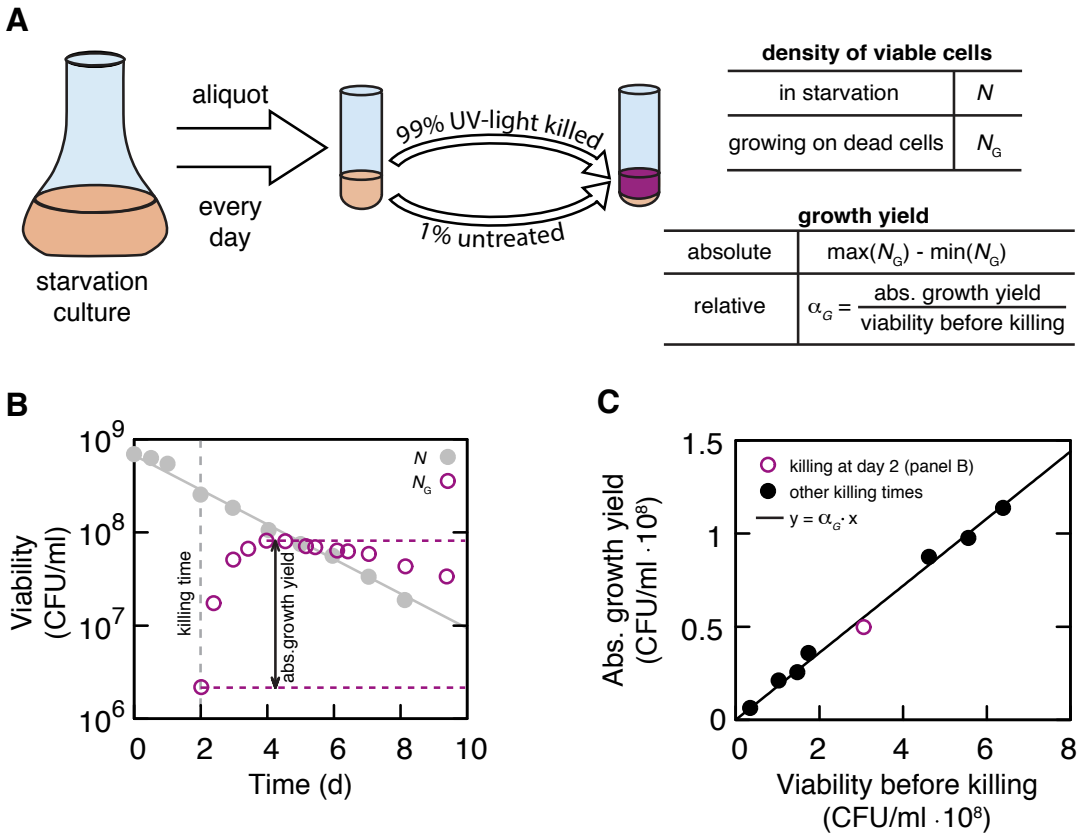

Figure 2.10: Yield measured by regrowth on nutrients released from dead cells. (A) Graphical synopsis of the experiment to measure the yield of the culture (see also Appendix A): at different times during starvation, a sample of a starved culture (starvation culture, flask) is aliquoted and 99% of the population is UV-killed. Thus, only 1% of the cells remain untreated and still viable. These viable cells grow on the UV-sterilized culture as described in panel B. **(B)** Grey data show the viability of a starvation culture over time. After 2 days of starvation, a sample is extracted from the starvation culture and 99% of the population is UV-killed (grey dashed line), while only 1% of the aliquot remains viable. Cells grow on the UV-sterilized culture (growth curve N_G): The population of the culture increases from a minimum value, $\min(N_G)$, to a maximum value, $\max(N_G)$, in less than 2 days after UV-sterilization. The absolute growth yield of the culture is defined as $\max(N_G) - \min(N_G)$. **(C)** The absolute growth yield (see panels A, B and Appendix A) is plotted against the viability of the starvation culture at the killing time. The absolute growth yield is directly proportional to the viability, meaning that during starvation nutrients are consumed, rather than accumulated. The (relative) growth yield α_G, a measure for the yield α, is the ratio of the absolute growth yield on UV-killed cells to the viability in the starvation culture at the killing time ($\alpha \propto \alpha_G = 0.18 \pm 0.02$) and is indicated as a black line.

Fig. 2.10B shows one exemplary measurement where the sample from the starving culture (grey dots) is taken after two days. The regrowth curve (purple circles) starts from a viability $\min(N_G)$ and reaches a maximum value $\max(N_G)$, such that the absolute growth yield is $\max(N_G)$-$\min(N_G)$. This absolute growth yield is plotted in Fig. 2.10C against the viability at extraction (grey dots in panel B). The linear relation between absolute yield and viability shows that the efficiency of biomass recycling remains constant throughout starvation. The slope of

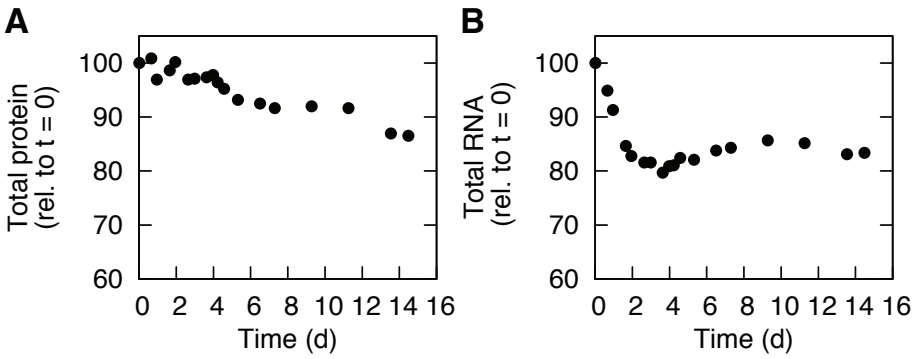

Figure 2.11: Nutrients loss during starvation. (A) Total protein and **(B)** RNA of a starved culture over 16 days, relative to the first extraction point shortly after glycerol exhaustion.

the line in Fig. 2.10C quantifies the yield, $\alpha = 0.18$, in units of "new cell" per "killed cell". In other words, it takes ≈ 5.5 killed cells to make one new cell.

2.8 Nutrients loss during starvation

That viable cells consume nutrients from dead cells for maintenance and for growth, depending on the amount of available dead cells, can be also directly observed by measuring the loss of biomolecules from the culture. Fig. 2.11 shows the loss of total protein and total RNA over 16 days of starvation. Such loss results to be not larger than 20% of the original content for both proteins and RNA, with the difference that total protein decreases gradually during the starvation period, while RNA initially decreases fast and then remains constant. This is probably due to turn-over of ribosomes after entry to starvation and degradation of mRNAs [151]. Since the majority of RNA is ribosomal rRNA folded into ribosomes (85%, [42, 152]), this finding implies that ribosomes are stable even after cell death, in contrast to other types of starvation [151]. However, it cannot be excluded that, even if not degraded, these ribosomes are broken and not functional. Interestingly, Houser et al. report that, when cells are starved of glucose, they show a quite uniform down-regulation of mRNA within the first 8 hours of starvation and constant transcription profiles after that [153]. Even if observed in a different type of starvation, these findings may support our measurements where RNA initially decreases and, then, remains constant. Finally, as we mentioned above, both proteins and RNA, even if decreasing, remain in the medium in high percentages respect to the initial value at the beginning of starvation. This may be due to the fact that *E. coli* probably manage to scavenge mainly small metabolites in the cultures and not big molecules. A more detailed study based on metabolomics and proteomics that identifies which nutrients are released by dead cells and which ones are uptaken by the viable cells is necessary.

2.9 RpoS regulon improves biomass recycling

We use the ability to quantify both yield and maintenance rate to dissect death rate contributions of a prominent example of a gene known to affect survival: the general stress response sigma factor encoded by *rpoS*, which regulates the expression of dozens of target genes [73, 84]. A Δ*rpoS* mutant displays a 1.8-fold increased death rate compared to the wild-type (see Fig. 2.12A). Using our protocol for measuring the maintenance rate, we find that β is only increased by about 15% percent in the Δ*rpoS* mutant (see Fig. 2.12B). Eq. (2.3) then predicts that the 1.8-fold increase of the death rate primarily stems from a decrease in the yield α. Indeed, we observe

that wild-type cells require ≈ 5.5 killed cells to make one new cell, whereas $\Delta rpoS$ mutant cells require about ten (Fig. 2.12C). This almost two-fold change in yield α could stem either from the release of fewer nutrients per dying cell or from less efficient usage of these nutrients. We disentangle these effects by quantifying the growth yield of wild-type cells on $\Delta rpoS$ cells that were killed by UV light and vice versa (see Fig. 2.12D and Fig. 2.13A,B). We find that a similar amount of nutrients is released by death of either strain, but that $\Delta rpoS$ cells use these less efficiently, resulting in the observed accelerated death during starvation. These results imply that during starvation, RpoS-mediated gene regulation gives a supply-side benefit, which almost doubles the biomass usage and decreases the death rate correspondingly. Metabolic genes are indeed known to be part of the RpoS regulon [79].

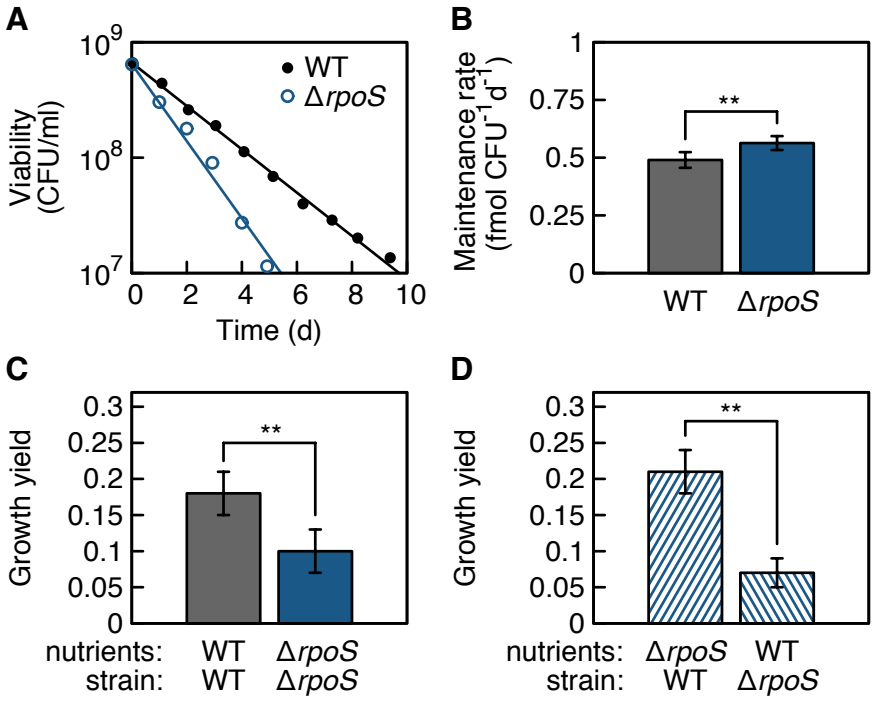

Figure 2.12: Impact of the general stress response sigma factor RpoS on survival. **(A)** Survival kinetics of *rpoS* knock-out mutants ($\Delta rpoS$, blue open circles) compared to wild-type cells (WT, black filled circles), cultured and starved in identical conditions (see Appendix A). The viability of $\Delta rpoS$ decreases at about twice the death rate compared to WT. The death rate is $\gamma_{\Delta rpoS} = 0.78 \pm 0.04$ d^{-1} (average of 12 independent experiments, see Table A.1 for details; slope of the blue line, value reported with one standard deviation). **(B)** Maintenance rate β, measured as described in Fig. 2.8 and Appendix A, is slightly higher for $\Delta rpoS$, $\beta_{\Delta rpoS} = 0.56 \pm 0.03$ fmol/(CFU $\cdot$ d) respect to WT, $\beta_{\mathrm{WT}} = 0.49 \pm 0.04$ fmol/(CFU $\cdot$ d). Error bars indicate one standard deviation of β values measured in independent experiments (each of them averaged between two replicates) at different times during starvation. The difference is significant (two-sample t-test, $p < 0.01$). **(C)** (Relative) growth yield for WT and $\Delta rpoS$ strains measured by growth of an inoculum on UV-killed cells of the same strain as described in Fig. 2.10 and Appendix A. Knock-out of *rpoS* leads a two-fold decreased in yield, compatible with the increase of death rate recorded in panel A. **(D)** (Relative) growth yield obtained by cross-mixing UV-sterilized culture and inoculum. While WT cells grow similarly well on $\Delta rpoS$ cells as on WT cells (shown in panel C), growth of $\Delta rpoS$ on WT is impaired. Data in panel C and D are taken in the first 12 hours of starvation and are averages of four independent measurements (each of them averaged between two replicates). Errorbars show one standard deviation. The differences in panels C and D are significant (two-sample t-test, $p < 0.01$). No differences in growth rate or yield are observed when WT and $\Delta rpoS$ cells are grown on glycerol as the carbon substrate.

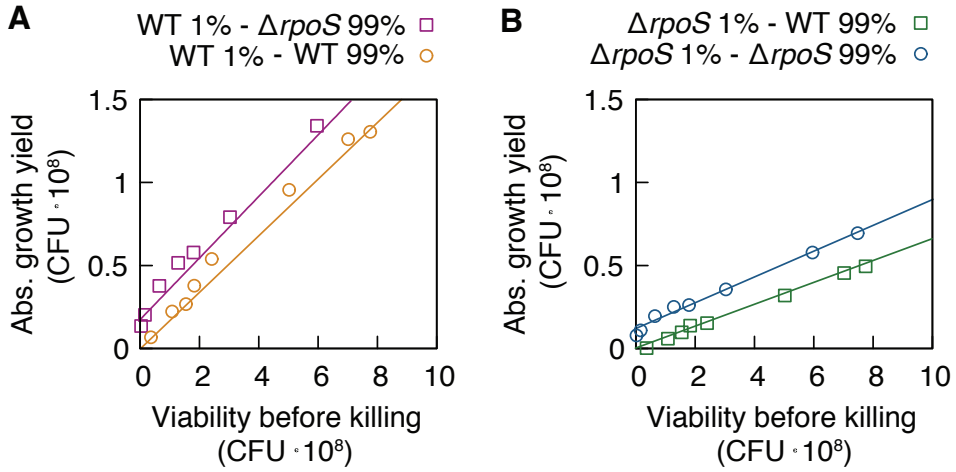

Figure 2.13: Metabolic challenges of Δ*rpoS* mutants. (A) Yield of WT cells. At different times (1h, 12h, 24h, 48h, 71h, 97h, 120h, 170h) during starvation of a WT and a Δ*rpoS* control culture, a fraction of WT cells is extracted from the control culture and mixed in two new samples with 99% of UV-sterilized WT cells (yellow circle) or 99% of UV-sterilized Δ*rpoS* cells (purple squares) respectively, see Appendix A. The absolute growth yield $(\max(N_G) - \min(N_G))$ of WT in both samples is plotted versus the viability in the starved culture before killing. Note that the yield decreases proportionally with the viability. The (relative) growth yields of WT cells $\alpha_G^{\mathrm{WT-WT}}$ and $\alpha_G^{\mathrm{WT-}\Delta rpoS}$, measurements for the yield α, are the ratios of the absolute growth yield on UV-killed cells to the viability in the starvation culture at the killing time. Their values are $\alpha_G^{\mathrm{WT1\%-WT99\%}} \approx 0.18$ and $\alpha_G^{\mathrm{WT1\%-}\Delta rpoS\mathrm{99\%}} \approx 0.21$. **(B)** Yield of Δ*rpoS* cells. Using the same method explained for panel A, a fraction of Δ*rpoS* cells is inoculated with 99% of WT cells (green squares) or 99% of UV-sterilized Δ*rpoS* cells (blue circles) respectively. In both samples, the absolute growth yield of Δ*rpoS* decreases proportionally with the viability at the extraction points during starvation with (relative) growth yields being $\alpha_G^{\Delta rpoS\mathrm{1\%-}\Delta rpoS\mathrm{99\%}} \approx 0.08$ and $\alpha_G^{\Delta rpoS\mathrm{1\%-WT99\%}} \approx 0.06$. First of all, these results show that the yield is significantly lower upon knock-out both in the case of nutrients released by WT UV-sterilized cells and by Δ*rpoS* UV-sterilized cells, indicating that Δ*rpoS* mutants cannot use released nutrients as well as WT cells do. This implies that the culture with Δ*rpoS* mutants contains nutrients accumulated over time that Δ*rpoS* mutants are not able to consume. Thus, when a culture of 1% of WT is mixed with 99% of a UV treated Δ*rpoS* culture, see panel A, the yield of WT is even higher than when the WT are mixed with 99% of a UV treated WT culture because the living WT can regrow on both nutrients released by UV sterilized cells and nutrients accumulated in the Δ*rpoS* culture $(\alpha_G{}^{\mathrm{WT1\%-}\Delta rpoS\mathrm{99\%}} > \alpha_G^{\mathrm{WT1\%-WT99\%}})$. The same effect is observed in panel B: the yield $\alpha_G^{\Delta rpoS\mathrm{1\%-}\Delta rpoS\mathrm{99\%}}$ is slightly higher than the yield $\alpha_G^{\Delta rpoS\mathrm{1\%-WT99\%}}$. We then interpret also the small offsets of the purple and blue fits in panels A and B as the result of nutrients released and not consumed by Δ*rpoS* mutants in the control cultures. In a hypothetical case of a Δ*rpoS* control culture with viability before killing equal to zero, the UV treatment would not provide nutrients because there would not be any cell to kill. However, adding 1% of living WT or Δ*rpoS* cells would still imply $\alpha > 0$ because living cells could regrow on nutrients left over time in the control culture by Δ*rpoS* previously dead cells.

2.10 Discussion

The data of this chapter show that the survival of carbon-starved *Escherichia coli* is a collective phenomenon. In particular, we (i) confirm that *E. coli* cells require nutrients to maintain their viability and quantify their maintenance rate, (ii) reveal that viable cells feed on cells that have perished, (iii) show that a stable steady-state decay of viability emerges due to a flux balance, and (iv) demonstrate that, in this steady-state, we can dissect how and how much, individual molecular components contribute to the death rate of the population. These results have several implications, which we discuss in the following.

2.10.1 Thermodynamic aspects of the steady-state exponential decay of viability

Even when not growing, a living bacterial cell is in an non-equilibrium state, with internal conditions (e.g., molecular concentrations of ions, metabolites, macromolecules, etc.) differing strongly from the outside conditions in the medium. Any spontaneous biochemical or physical process (e.g., leakage of ions and metabolites across the membrane or hydrolysis of RNA) will be directed towards chemical and thermodynamic equilibrium, deteriorating the state of the cell. The cell's maintenance processes must be directed against this spontaneous deterioration, requiring free energy, in the form of nutrients, due to the constraints of the second law of thermodynamics [154]. The existence of a nutrient demand for the maintenance of viability, as depicted in the model in Fig. 2.6A and measured in Fig. 2.8, is thus a natural consequence of the cell maintaining its non-equilibrium state and is required by thermodynamics. However, the magnitude of this demand, i.e. the rate β at which free energy is utilized for maintenance, is not a thermodynamic quantity, but is set by the kinetic processes that deteriorate the state of the cell. We found that, during the exponential decay of viability, cells obtain the required free energy by taking up nutrients released from dead cells (see Fig. 2.5A and Fig. 2.7B). Quantitatively, we inferred that a single, wild-type cell could survive about 20 days with the amount of carbon substrate required for one cell doubling. Moreover, our data reveal that, during the exponential decay of viability, the non-equilibrium state of the non-growing *E. coli* cells is stable. If at any point in time, due to a fluctuation, cells die at a higher rate, more resources leak into the medium, slowing down the decay of the remaining viable cells. This feedback of the energetic state of cells onto their death rate (see Fig. 2.6A) generates a flux balance between the nutrient outflux from the dead cells into the medium and the nutrient influx from the medium into the viable cells. As time progresses, and the number of viable cells decreases exponentially, the total outflux and the total influx decrease at the same rate, remaining in balance. However, the fluxes per cell are constant, such that individual viable cells are in a non-equilibrium steady-state. Constant non-vanishing fluxes are the hallmark of non-equilibrium steady-states [155].

2.10.2 Biological implications of the steady-state exponential decay of viability

Bacteria adapt their metabolism [156], their gene expression [79, 153] and other properties when transitioning from growth to a non-growing state. During this adaptation period, bacterial properties change and measurements depend on the point in time at which they are taken. However, within 24 hours into carbon starvation, an *E. coli* culture enters the steady-state exponential decay of viability (Fig. 2.2C). This non-equilibrium steady-state greatly simplifies the characterization of bacterial physiology. Death rate (Fig. 2.1B), cell size (Fig. 2.3), protein synthesis (Fig. 2.4), maintenance rate (Fig. 2.8 and Fig. A.2) and ability to feed on dead cells (Fig. 2.10) are constant in this steady-state, making measurements of cell properties robust and reproducible and eliminating the need to quantify physiology along time courses. This appealing aspect of the steady-state exponential decay of viability is analogous to steady-state exponential growth, during which the average properties of a bacterial cell do not change [33, 36, 37]. In both cases, exponential growth and exponential death, the physiology of the cell is stabilized by a flux balance. However, the nature of this flux balance is fundamentally different. In the case of balanced growth, it is an internal flux balance that stabilizes the relative fractions of different protein species within the exponentially growing proteome [41] (see Section 1.8.2). The time required to reach this balance after simple shifts in the growth medium typically ranges from less than an hour to a few hours [46]. In contrast, in the case of the exponential decay, it is an external balance between two global metabolic fluxes in the bacterial culture, the nutrient

outflux from the dead cells, dubbed "supply flux" in Fig. 2.6, and the nutrient influx into viable cells, which we refer to as the "demand flux". Our experiments indicate that a stable balance between supply and demand is established roughly 24 hours after carbon starvation (Fig. 2.2C). In principle, cells could also store nutrients to use for maintenance during starvation, rather than using nutrients released by dead cells. Our measured value for the maintenance rate β (Fig. 2.8) permits a rough estimate of the required storage size: a cell would need a reservoir of about five percent of the cell mass in order to survive just a single day. Another strategy to deal with starvation is to suppress the above-mentioned spontaneous processes that deteriorate the state of the bacterium. The extreme limit of this strategy is the formation of endospores, which are inactive and non-reproductive structures produced by certain bacteria, but not *E. coli*. Note, however, that because endospores are inactive, they cannot maintain any processes, and therefore their state will very slowly deteriorate. Endospores thus cannot establish a non-equilibrium steady-state.

2.10.3 Fitness and evolution under carbon starvation

Finally, we discuss the evolutionary implications of this work. How does the measured population death rate γ relate to fitness and selection? Fitness measures the ability of an organism to survive and reproduce in a specified environment. However, it is important to distinguish between fitness as a phenotype of an individual and fitness as a summary statistic of a given genotype [51]. Restricting our attention to a population of cells in a non-growing state, fitness of an individual is its probability to survive, while fitness of a genotype is a measure for the average change of the population size. In our case of a clonal population of bacteria in carbon starvation, some cells die early on, while others survive for a long time, despite having the same genotype. Thus, individual fitness is not a useful concept here. Instead, the cell-averaged fitness of the genotype is the relevant quantity for evolution. In our case, the (absolute) fitness of the genotype corresponds to the observed population death rate γ. This definition derives from the (Malthusian) fitness m, which is applicable whenever the number of viable cells changes exponentially, $N(t) = N(0)e^{mt}$ [51]. For a clonal bacterial population in a rich environment, m is equal to its growth rate μ, while $m = -\gamma$ under carbon starvation. From this perspective, our work reveals a natural way to decompose the fitness during carbon starvation, $m = -\gamma = -\beta/\alpha$, into a contribution from the maintenance rate β and a contribution from the yield α, which can be experimentally determined using our independent assays (see Fig. 2.8 and Fig. 2.10). To illustrate this, we used our assays to analyze how a wasteful protein activity increases the maintenance rate (Fig. 2.9), thereby decreasing fitness, and how the RpoS regulon improves the efficiency of nutrient recovery from dead cells (Fig. 2.11), increasing fitness. The underlying approach, which leverages the steady-state exponential decay of viability to quantitatively understand the determinants of bacterial survival under starvation, can now be broadly applied. As a measure of a genotype's ability to survive and reproduce, fitness determines how natural selection acts during evolution. In our case, we obtain information about selection in phases of carbon starvation. Consider, for instance, an evolutionary scenario where mutants of a gastrointestinal bacterium such as *E. coli* are generated during growth in the host (see Chapter 1) and microcolonies of the wild-type and the different mutants are dispersed into the environment outside the host where they starve. In this scenario, with different genotypes separated during starvation and directly competing during growth, we can use the fitness $m = -\gamma$ to determine the contribution to selection from the starvation phase. The dimensionless selection coefficient s quantifies how much the relative abundance of two species changes [157, 158],

$$s(t) = \gamma_{\mathrm{w}}^{-1} \frac{\mathrm{d}}{\mathrm{dt}} \ln \frac{N_{\mathrm{m}}(t)}{N_{\mathrm{w}}(t)}. \tag{2.7}$$

Here, $N_{\mathrm{m}}(t)$ and $N_{\mathrm{w}}(t)$ denote the viabilities of the mutant and wild-type species, respectively, whereas γ_{w} is the death rate of the wild-type species. If both mutant and wild-type have a constant death rate, then the selection coefficient is simply

$$s = 1 - \gamma_{\mathrm{m}}/\gamma_{\mathrm{w}} \tag{2.8}$$

consistent with the intuitive notion that the mutant is under positive selection during starvation, if its death rate is smaller than that of the wild-type and under negative selection otherwise. Using our result that the death rate is set by the maintenance rate and the yield, see Eq. (2.3), we can further decompose the selection coefficient according to

$$s = 1 - \frac{\beta_{\mathrm{m}}}{\alpha_{\mathrm{m}}}\frac{\alpha_{\mathrm{w}}}{\beta_{\mathrm{w}}}. \tag{2.9}$$

However, if the different genotypes are not separated during starvation, they must compete for nutrients released by dying cells. Eq. (2.9) then only provides a baseline expectation, against which the strength of such competition effects can be measured. Deciphering such competition effects is likely the key to understanding the intriguingly complex observed evolutionary dynamics of individual species [13, 159] and microbial communities [160].

Chapter 3

Slower growth of *E. coli* leads to longer survival in starvation

3.1 Introduction

Bacteria in nature live in a variety of environments, from stressful and nutrient-poor to ideal and nutrient-abundant. The average proliferation of *E. coli* through cycles of famine and feast, the fitness, depends not only on their ability to grow fast, but also on surviving long when conditions worsen. As we showed in the previous chapter, this is particularly important in carbon starvation of gram-negative bacteria: while gram-positive bacteria produce dormant spores that can survive millions of years [62, 63], gram-negative bacteria, such as *E. coli*, enter a death phase that leads to the exponential decay of viability. As our supply-demand model shows, these starved bacteria constantly require maintenance to prevent death. In this chapter, we study if *E. coli* can also adapt their physiology to prolong their survival chances in starvation.

A key signal for the upcoming starvation is a decrease of growth rate. When the culture approaches starvation, nutrient concentrations fall below the substrate affinity, nutrient uptake decreases and growth slows down [33]. As we said in Chapter 1, almost all major physiological parameters depend on growth rate, such as cell size and ribosome content [35], but also the detailed composition of the proteome [41, 45]. That is why we suspect that starvation survival depends on growth rate prior to nutrient depletion. However, it is not clear whether a better or a worse growth state is beneficial for the cell's future survival.

The first option is that slow growth on poor substrates leads to longer survival. When bacteria grow fast, they need to allocate large fractions of their proteome to biosynthesis. When growth slows down, this resource becomes free, the proteome can be remodeled and the expression of "starvation" proteins can be increased. Many of these "starvation" proteins were described [34, 79, 86, 88, 89, 161], including the general stress response regulated by RpoS [79]. This response was implicated in improved nutrient scavenging abilities [81, 89, 153], improved cellular protection against potential harm such as heat shock, osmotic shock, oxidative damage and acid stress [75, 79] and improved energy storage of glycogen or carbon residues [57, 162]. It is thus plausible, when growth slows down, that the ability of the bacteria to survive starvation increases.

A second option could be that fast growth on rich substrates allows longer survival because the cell can budget the abundant nutrients. For example, glycogen storage depends on the growth medium [163] and bacteria store more glycogen when entering non-carbon-limited

starvation [164]. Such additional nutrient could prolong survival. In addition, a better energy conversion efficiency for cells growing in rich medium [165] could allow bacteria to need fewer nutrients. Other evidence implicates increased levels of starvation inducible genes, such as the ones regulated by RpoS, to be detrimental when nutrients are scarce as they may decrease the cell's ability to scavenge resources [13, 166]. For example, the most common *rpoS* GASP mutation that confers competitive advantage in starvation conditions attenuates *rpoS* expression, rather than increasing it [78]. It is, thus, also plausible that fast growth allows the cells to adapt better to survival. Either way, growth and starvation phases seem closely intertwined, as suspected by many researchers in the past [86–89, 167–170].

Studying how the growth state influences survival is a non-trivial problem. The classical way of studying survival, letting bacteria deplete their nutrients, leads to a gradual decrease of growth rate and a gradual adaptation to stationary phase. As a result, because of these intermediate steps of adaptation, it is not clear how the state of the cell during growth influences survival after complete nutrient depletion. In this chapter, we choose a different approach and titrate growth rate by culturing *E. coli* in medium with different substrates [35], where each substrate supports a certain growth rate, or in a carbon limited chemostat. Before the cells reach starvation, we deprive each culture of its carbon substrate by washing the cells and we measure their survival. In the previous chapter, we saw that, during starvation, viability typically decreases with an exponential function with a certain death rate. We use this to correlate growth rate with death rate and show that slower growing cells will survive longer.

To investigate how *E. coli* achieves the reduction in death rate, we use the quantitative approach described in the previous chapter, which allows dissecting the individual contributions to death rate. We showed that the exponential decay of bacterial viability in carbon starvation is a collective phenomenon where viable bacteria feed on dead bacteria. During this exponential decay, death rate is given by the ratio of maintenance rate to the yield, representing biomass recycling. The first one quantifies the energy consumed per time to maintain basic cellular functions, while the second one measures the amount of nutrients recoverable from a dead cell. Here, we use this quantitative approach to show that the decrease in death rate for slowly growing bacteria is due to a decrease in the maintenance rate.

This work is a project collaboration with Dr. Severin Josef Schink and Prof. Dr. Ulrich Gerland. This chapter is adapted from Biselli E.*, Schink J. S.* and Gerland U., *Slower growth of E. coli leads to longer survival in starvation due to a decrease of the maintenance rate*, manuscript under submission (*co-first author).

3.2 Death rate in starvation depends exponentially on growth rate

To study how the growth state influences survival during starvation, we grow *E. coli* K-12 NCM3722 in media supplemented with different carbon substrates, see Fig. 3.1A. Bacteria grow exponentially and the growth rate (slope of the lines in Fig. 3.1A) depends on the carbon substrate. In rich media like LB (white symbols) bacteria grow fast, while in minimal medium supplemented with a poor carbon substrate like mannose (black symbols) they grow slowly.

Once the cultures have reached an optical density (OD_{600}) of about 0.5, we wash and resuspend them in carbon free medium (see Appendix B). This step removes left-over nutrients from

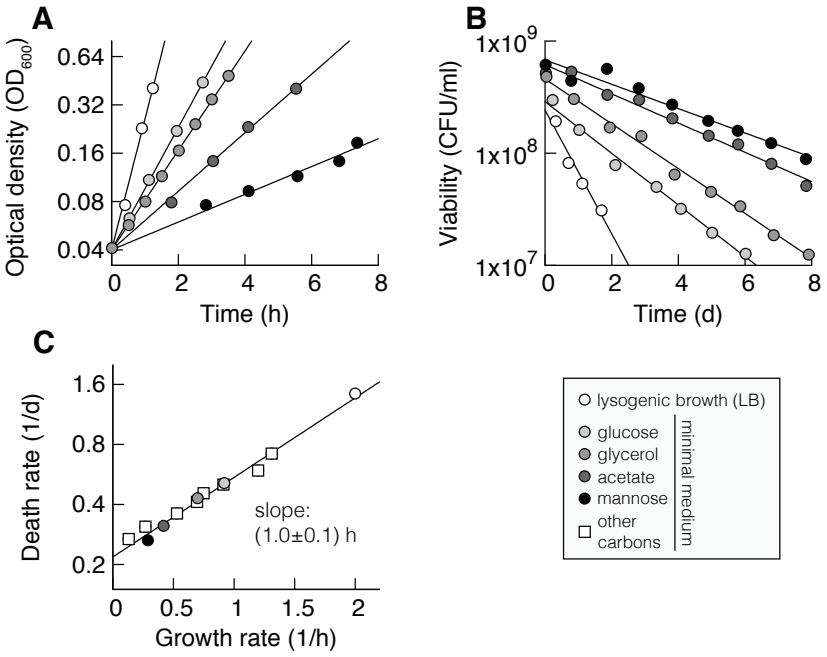

Figure 3.1: Death-growth rate dependence in different media. (A) Exponential growth of *E. coli* K-12 NCM3722, measured using optical density (OD_{600}), in lysogenic broth (LB, white circles) or minimal medium supplemented with different carbon sources, listed in the legend on the bottom right in a grey scale. All the cultures are grown in batch mode, see Appendix B. Growth rates (slope of the exponential fits) are summarized in Table B.1. **(B)** Bacterial viability in colony forming units (CFU) per ml of cultures from panel A after washing and re-suspension in carbon-free minimal medium. Death rates (slopes of the exponential fits) are summarized in Table B.1. Note that after the exponential decay shown here, mutants gradually take over and long-term survival can last months to years [13, 137, 148], as shown in Fig. 2.2. **(C)** Death rates of panel B plotted against growth rates of panel A shown as circles. Squares show data obtained using eight other carbon substrates, listed in Table B.1. Black line shows exponential fit to all data.

complex media like LB or fermentative by-products such as acetate and ensures that bacteria are starved of all external carbon substrates. We then follow survival by measuring bacterial viability by plate counting, see Fig. 3.1B. The number of colony forming units (CFU) per ml decreases exponentially for all cultures. The death rate (slope of the lines in Fig. 3.1B) depends on the medium, with cultures grown on LB dying more than 5-times faster than those on mannose (see Table B.1).

In Fig. 3.1C we plot death rates against growth rates. We show the five cultures from Fig. 3.1B, as well as eight more cultures, whose growth and death rates are listed in Table B.1. We find that death rate γ depends exponentially on growth rate μ (Fig. 3.1C; exponential fit: $\gamma = 0.20\mathrm{h}^{-1}\mathrm{e}^{\mu(1.0\pm0.1)\mathrm{h}}$). The exponential relation is intriguing for two reasons. First, death rate appears not to depend on the specific carbon used for growth, but instead on growth rate. This echoes Schaechter, Maaløe and Kjeldgaards seminal finding that the cellular composition does not depend on the specifics of the nutrient composition, but rather the resulting growth rate [35]. Second, other bacterial properties also scale exponentially with growth rate. Cell volume during growth, in particular, increases exponentially with growth rate ($\mathrm{V} = 0.43\mu\mathrm{m}^3\mathrm{e}^{\mu(1.35\pm0.04)\mathrm{h}}$), see Fig. B.1.

Next, we aim to understand how the bacteria manage to decrease their death rate. In the previous chapter, we found that death rate is determined by the ratio of maintenance rate to

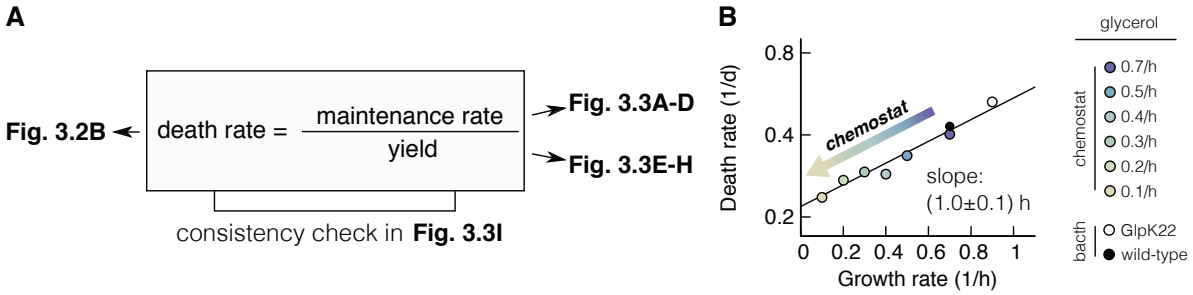

Figure 3.2: Death-growth rate dependence titrating growth rate on a single carbon source. (A) In carbon starvation, yield α (see Fig. 3.3A-D) and maintenance rate β (see Fig. 3.3E-H) determine the death rate γ (see panel B). Changes of maintenance rate and yield, measured for the death rates of panel B, can explain the observed change in death rate (see Fig. 3.3I). **(B)** Death rates of wild-type and GlpK22 mutants plotted versus growth rates. Wild type is grown in glycerol minimal medium in batch cultures (black circle) and in chemostat continuous cultures with growth rates coded in colors, see legend on the right. GlpK22 mutants (white circle) are grown in glycerol minimal medium in batch culture. The black line shows the fit of Fig. 3.1C.

yield, see Fig. 2.6 and Fig. 3.2A. To investigate whether the decrease of death rate in Fig. 3.1C is due to a change of the maintenance rate, the yield, or both, we perform a set of experiments where we measure death rate, yield and maintenance rate in varying growth conditions. Finally, we check if the measured changes of maintenance rate and yield can explain the observed change in death rate.

3.3 Titrating growth rate on a single carbon substrate

Maintenance rate is measured by quantifying how long bacteria can survive when they are given a small concentration of a nutrient. This nutrient should be the same nutrient for all experiments, in order for measurements to become comparable. For this reason, we perform a series of experiments at different growth rates, but on the same carbon substrate: glycerol. Slow growing cells grow in a chemostat in glycerol limited continuous culture (see Fig. B.2), where growth rate is set by the dilution rate, spanning from 0.1 h^{-1} to 0.7 h^{-1} (see Appendix B). For fast growth, we use a GlpK22 (NQ898) mutant without catabolic repression of the GlpK enzyme [171] that grows 30% faster than wild-type (WT) in batch culture in minimal medium supplemented with glycerol ($\mu_{\mathrm{GlpK22}} = 0.9\ h^{-1}$). As a control, wild-type cells are grown in batch culture in glycerol minimal medium ($\mu_{\mathrm{WT}} = 0.7\ h^{-1}$). After at least six generations in steady state growth, samples of cells in the chemostat are extracted, washed and starved in carbon-free minimal medium (see Appendix B). GlpK22 and wild-type are grown in batch cultures, washed and starved in carbon-free medium, too. During starvation, we observe that viability decreases exponentially and death rates span a range from 0.25 d^{-1} to 0.59 d^{-1} (see Fig. B.3 and Table B.1). Death rate is plotted versus growth rate in Fig. 3.2B, with the data following well the exponential fit from Fig. 3.1C, shown as a black line. These findings confirm that the death-growth correlation is independent of specific medium composition, but instead dependent only on growth rate.

3.4 Change of the yield with pre-starvation growth rate

Recycling of biomass from dead cells is one of the two determining factors of the death rate. The more nutrients a viable cell can scavenge from a dead cell, the more maintenance it can achieve

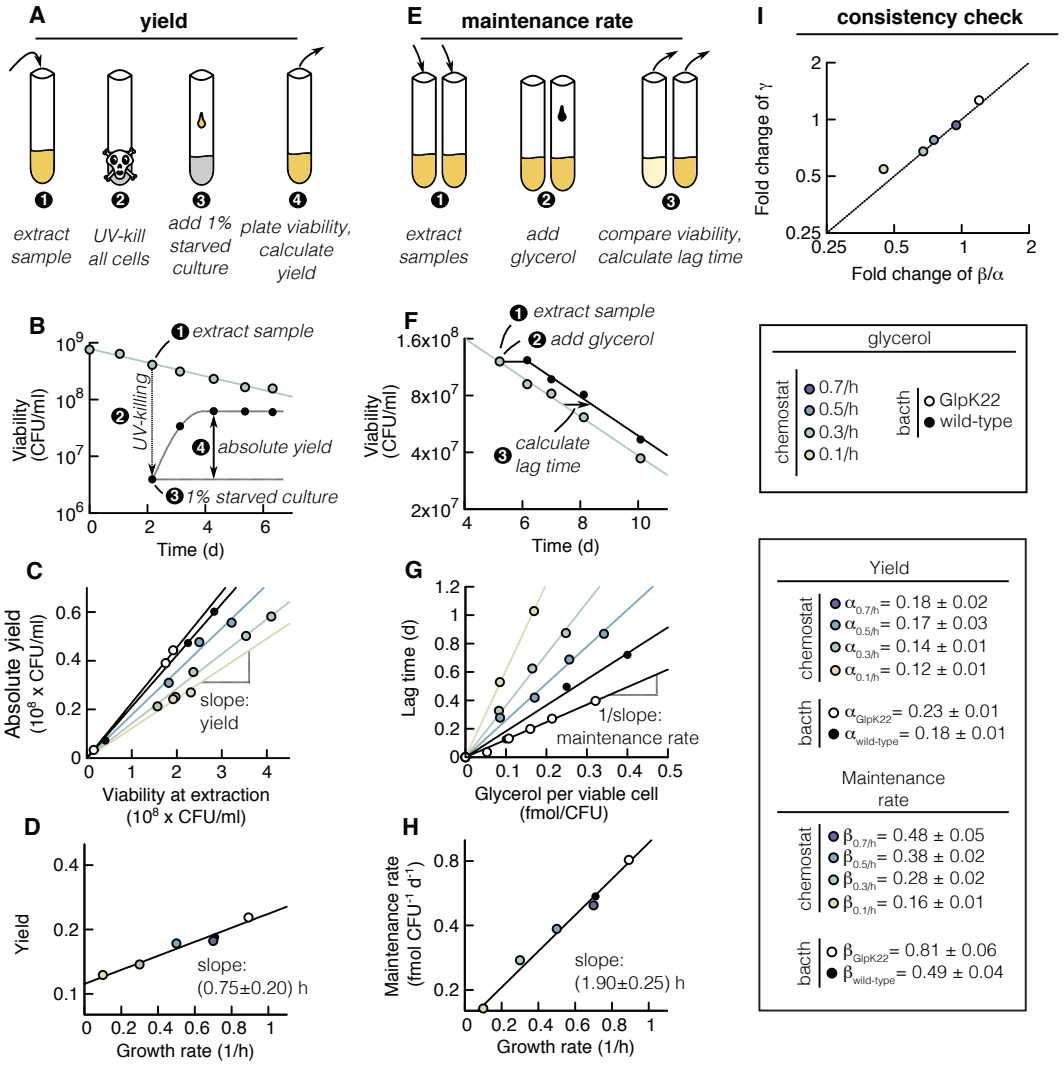

Figure 3.3: Quantification of maintenance rate and yield. (A) Graphical synopsis of the assay to measure the yield (see Appendix B for details). At different times during starvation, a sample is (1) extracted from a starved culture, (2) sterilized with UV-light (3) inoculated with 1% of the original starved culture and (4) regrowth is measured using plate counting. **(B)** Example experiment of the assay sketched in panel A. Cells previously grown at 0.3 h^{-1} in continuous culture are starved (green circles). After 2 days of starvation, a sample is (1) extracted and (2) UV-sterilized, see dashed line, followed by (3) inoculation of 1% of starved culture and (4) regrowth of the culture. The difference between the maximum viability after regrowth and the initial viability at point (3) is the absolute yield. **(C)** The absolute yield, measured at three different time points for each of the growth conditions shown in Fig. 3.2B, is plotted against the viability of the starvation culture at the extraction time. The yield is extracted as the slope of the linear fits. **(D)** Yield from panel C plotted versus growth rate. Black line shows a fit with a slope of 0.75 ± 0.20 h. **(E)** Graphical synopsis of the assay to measure the maintenance rate (see Appendix B for details). At one point during starvation, (1) a sample is extracted from a starvation culture and split into several tubes. (2) Different concentrations of glycerol are added to each tube, small enough to support survival, but not growth and (3) viability is measured. **(F)** Example experiment from a starved culture previously grown at a rate of 0.3 h^{-1} with a viability of $1.21 \cdot 10^8$ CFU/ml after 5 days of starvation. After (1) extraction and (2) addition of 40 µM of glycerol, the decay of viability is delayed (black circles) compared to a control without glycerol (green symbols). Per viable cell, the glycerol addition in this experiment is 0.33 fmol/CFU. After an initial period of survival, the culture with added glycerol (black) dies at the same rate as the control (green). The lag time fitted to this data is 1.0 days. **(G)** Lag time of the experiments of Fig. 3.2B for different glycerol concentrations. Lag increases linearly with glycerol concentration and maintenance rate is extracted as the inverse of the slope of the linear fits. **(H)** Maintenance rate values extracted from panel G plotted versus growth rate and fitted with an exponential function with a slope of 1.90 ± 0.25 h. **(I)** Consistency check of the equation in panel A. Fold changes of maintenance rate, FC(β), divided by the fold changes of the yield, FC(α), plotted versus the fold changes of death rate, FC(γ). All fold changes are relative to wild-type in batch, growing at 0.7 h^{-1}. The dashed line shows the unity line $\mathrm{FC}(\gamma) = \mathrm{FC}(\beta)/\mathrm{FC}(\alpha)$. Symbol color is identical in all panels and depicted in the legend on the right. Values of yield and maintenance rate for all experiments are shown in the panel on the right and in Table B.2.

and the longer it will survive. In the previous chapter, we showed that the yield can be quantified by measuring to what density bacteria grow when dead bacteria are provided as nutrients. For this case, the assay is sketched in Fig. 3.3A and described in Appendix B. In Chapter 2, we distinguished the growth yield measured from the yield, where the first one is proportional to the latter. For simplicity, here, we do not make this distinction and we only use the term yield. At different times during starvation, we (1) extract a sample of a starved culture, (2) UV-kill all cells in the sample, (3) add 1% of the original starved culture with viable cells and (4) measure regrowth by plating. Fig. 3.3B shows one exemplary measurement for bacteria previously grown at 0.3 h^{-1} in the chemostat (green symbols). As defined in Chapter 2, the difference between the maximum regrowth and the initial viability in the sample is the "absolute yield", see symbol (4) in Fig. 3.3B. In Fig. 3.3C, we show three measurements of the absolute yield plotted against the viability at extraction for each of the growth experiments from Fig. 3.2B. In this plot, the yield is the slope of the linear fit. It ranges from 12% for the slowest growth to 23% for the fastest growth (see Table B.2). This value represents the number of cells that can grow on one killed cell, i.e. a yield of 12% means that eight cells need to be killed to produce one new cell. The yield depends exponentially on growth rate, see Fig. 3.3D, with a slope of 0.75 ± 0.20 h.

3.5 Change of maintenance rate with pre-starvation growth rate

The maintenance rate is the second determining factor of the death rate (the first is the yield). The lower the maintenance rate, the less nutrients the cell has to consume to remain viable. As shown in the previous chapter, the maintenance rate can be quantified measuring how long bacteria can survive after the addition of a small amount of nutrient. For this case, the assay is sketched in Fig. 3.3E and described in Appendix B. At one point during starvation, we (1) extract several samples, (2) add different concentrations of glycerol and (3) compare viability between samples. An exemplary experiment for cells previously grown at a rate of 0.3 h^{-1} in the chemostat is shown in Fig. 3.3F. A concentration of 40 µM glycerol allows a culture (black symbols) to survive longer than the control culture (green symbols). The delay in the survival curves between the two experiments is the lag time, see symbol (3) in Fig. 3.3F. In Fig. 3.3G we show the lag time for different growth experiments and different glycerol concentrations. In this plot, the maintenance rate is the inverse of the slope of the linear fits. It ranges from 0.16 fmol/(d · CFU) for the slowest growth to 0.81 fmol/(d · CFU) for the fastest growth. The value of the maintenance rate represents the number of glycerol molecules a single cell needs to survive one day. Just as volume and yield, also the maintenance rate depends exponentially on growth rate, see Fig. 3.3H, but with a slope of about twice that of either, $\beta = 1.90 \pm 0.25$ h.

3.6 Changes of maintenance rate and yield explain changes of death rate

We finally compare if the changes of maintenance rate and yield are consistent with the changes observed in the death rates. According to the formula in Fig. 3.2A, death rate γ is set by maintenance rate β divided by yield α. In Fig. 3.3I we thus plot the fold change of the death rate, FC(γ), against the fold change of maintenance rate, FC(β), divided by the fold change of the yield, FC(α). Each change is relative to the death rate, maintenance rate and yield of the control culture: wild-type in batch (black symbols throughout Fig. 3.2 and Fig. 3.3). The dashed line shows the unity line, FC(γ) = FC(β)/FC(α). The data largely follow the dashed line, showing that our measurements of maintenance rate and yield capture the change of death rate.

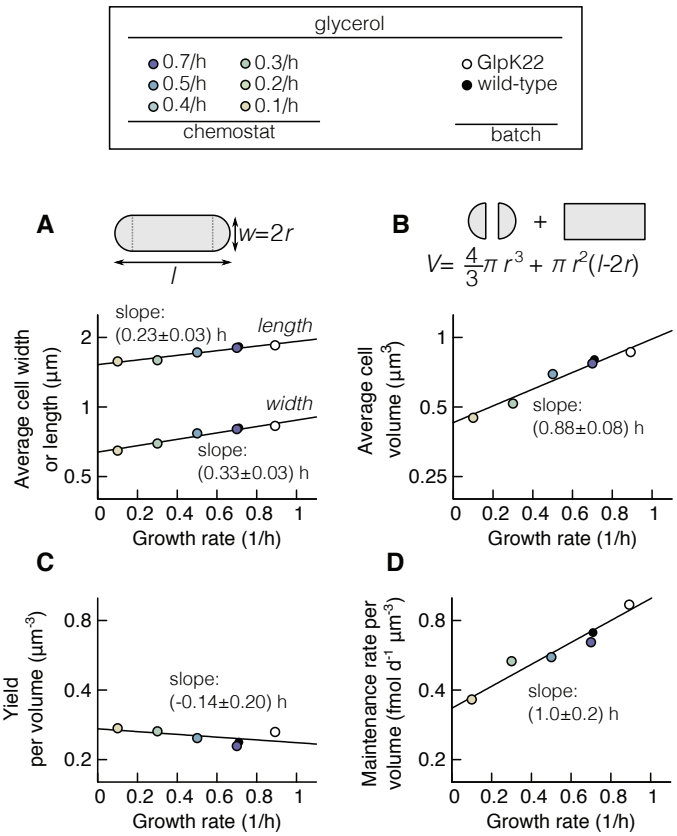

Figure 3.4: Normalization of maintenance rate and yield with cell volume. (A-B) Cell size during starvation. Length and width of the cells are measured with phase-contrast microscopy and the volume is computed considering cell shape as a cylinder with two semi-spheres, as described in the graphical synopsis at the top (see also Table B.3 and Appendix B). Each measurement is an average of 200 cells. **(A)** Measured length and width of wild-type cells starved in batch cultures and previously grown in the chemostat at different steady-state growth rates and of GlpK22 cells starved and previously grown in batch culture at $\mu = 0.9$ h^{-1} (see upper color legend). Black lines in the plot are exponential fits with slopes of 0.23 ± 0.03 h for length and 0.33 ± 0.03 h for width. For comparison, cell size during steady state growth was also measured and it is reported in Fig. B.1. Note that, as shown in Fig. 2.3, cell widths do not change from steady state growth to starvation, while lengths decrease. Both length and width increase exponentially with growth rate. **(B)** Starvation volume of the cells described in panel A, computed as explained in the graphical synopsis (see also Appendix B). In agreement with literature [35], it increases exponentially with growth rate (black line, exponential fit, slope of 0.88 ± 0.08 h). **(C-D)** Yield and maintenance rate per cell volume. **(C)** Yield and **(D)** maintenance rate measured as described in Fig. 3.3 are normalized per cell volume and plotted versus the previous growth rate of the cultures they refer to (see color legend at the top and Table B.3). The normalized yield is constant within the uncertainty, -0.14 ± 0.20 h. Maintenance rate increases significantly with a slope of 1.0 ± 0.2 h, matching the increase of the death rate, 1.0 ± 0.1 h, shown in Fig. 3.1C and Fig. 3.2B.

3.7 Change of cell volume with pre-starvation growth rate

One challenge with interpreting the data of yield and maintenance rate is that both parameters could depend on the cell size. The bigger a dead cell is, the more nutrient it could contain. The bigger a viable cell is, the more nutrients it might consume. As we showed in Fig. 2.3, cell size during starvation is generally lower than during growth, that is why we repeat the cell size determination previously performed during growth, Fig. B.1, for bacteria in starvation, see Fig. 3.4.

We determine length and width of individual starved bacteria from phase-contrast images,

see Appendix B. The average length and width increase exponentially with growth rate with slopes of 0.23 ± 0.03 h and 0.33 ± 0.03 h, respectively, see Fig. 3.4A and Table B.3. From the individual cell lengths and width, we calculate the volume of each cell by approximating the cell as a cylinder with two half spheres (top of Fig. 3.4B). The average cell volume increases also exponentially with growth rate with a slope of 0.88 ± 0.08 h, see Fig. 3.4B and Table B.3.

It is noteworthy that the logarithmic slopes of the volume dependence on growth rate (see Fig. 3.4B) and the recycling yield dependence on growth rate (see Fig. 3.3D) are indistinguishable within our experimental uncertainty. Consequently, normalizing recycling yield to cell volume results in a constant normalized yield, independent of growth rate within the statistical error (see Fig. 3.4C). Maintenance rate, on the other hand, still increases significantly when normalized to cell volume (see Fig. 3.4D), with a logarithmic slope of 1.0 ± 0.2 h. This growth rate dependence of the normalized maintenance rate matches (within error) our observed dependence of the death rate on growth rate (see Fig. 3.1C). Hence, our quantitative analysis suggests that slower growing *E. coli* cells subsequently survive longer in starvation because they adjusted their maintenance rate to a lower level.

3.8 Death-growth dependence does not hinge on *rpoS*

The general stress response regulator RpoS is often implicated with regulating the maintenance rate of *E. coli* [75, 79, 81]. RpoS is up-regulated during slow growth and almost 500 genes are correlated with its abundance [79]. In the previous chapter we showed that a knock-out of the *rpoS* gene increases the death rate via a decrease of the yield, while having only little influence on the maintenance rate. This finding is opposite to the death-growth dependence in this case, where the decrease of the death rate is mainly via a decrease of the maintenance rate.

To test if *rpoS*, despite this discrepancy, plays a role in the death-growth dependence, we grow *rpoS* knock-out mutants (Δ*rpoS*) in batch cultures using the same carbon substrates we used in Fig. 3.1C. If *rpoS* was responsible for the death-growth relation, its knock-out should abolish this relationship. During starvation, Δ*rpoS* mutants die exponentially as shown by some representative survival curves in Fig. 3.5A. In Fig. 3.5B, we plot the individual death rates against growth rates for Δ*rpoS* (blue symbols). As reference, we include the data for wild-type and GlpK22 mutants (black symbols) shown in Fig. 3.1 and Fig. 3.2. We find that the correlation between death rate and growth rate persists for Δ*rpoS*, confirming that the death-growth relation does not hinge on the general stress response RpoS. In accordance with this result, as shown in Chapter 2, the knock-out of *rpoS* increases maintenance rate during starvation by only 15%, much less than the 2.5-fold increase of maintenance rate observed in Fig. 3.4.

3.9 Discussion

In this chapter, we reveal the existence of a correlation between growth rate and death rate of *E. coli*, when they are first grown in media with carbon and then carbon starved. When corrected for changes in cell size, we find that the change of death rate is mainly due to a change of the maintenance rate. This cost increases exponentially with increasing growth rate, leading to an exponential increase of death rate with the pre-starvation growth rate.

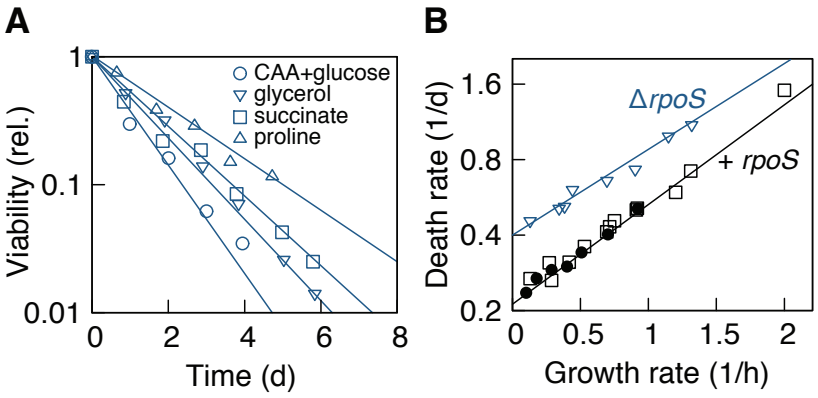

Figure 3.5: Δ*rpoS* death-growth rate dependence. (A) As for wild-type cells, independently on the carbon sources used during growth, Δ*rpoS* starvation following carbon depletion leads to an exponential decay of bacterial viability, measured in colony forming units (CFU) per ml, with death rate changing depending on previous growth rate. The panel shows the viability and exponential fits of four different cultures decreasing over time and previously grown in cas-aminoacids and glucose, glycerol, succinate and proline (see also Table B.4). Data are shown normalized to the highest viability value for each culture at the beginning of starvation. **(B)** Death rate of Δ*rpoS* plotted versus growth rate together with the corresponding values of wild-type cells and GlpK22 mutants carrying the *rpoS* gene (+ *rpoS*) already shown in Fig. 3.1C and Fig. 3.2B. Even if with a lower slope ($\gamma = 0.40\mathrm{h}^{-1}\mathrm{e}^{\mu(0.74\pm0.1)\mathrm{h}}$), Δ*rpoS* mutants still show an exponential dependence of death rates on growth rates suggesting that RpoS activation does not abolish the dependence.

3.9.1 Phenomenological scaling laws

Our results show that death rate γ, maintenance rate β and recycling yield α all increase exponentially with growth rate μ. Because cell volume V also scales exponentially with growth rate, we can derive phenomenological scaling laws between these physiological parameters of a cell. When dividing the slope of the exponential increase of yield and maintenance rate by the slope of volume increase, we find that the yield scales with volume to the power of $0.75/0.88 = 0.85$, i.e. roughly linear. This result is probably due to the fact that larger dead cells contain proportionally more biomass. Maintenance rate, on the other hand, scales with volume to the power of $1.90/0.88 = 2.16$, i.e. roughly squared. As a result, death rate scales linearly with cell volume, $\gamma = \beta/\alpha \sim V^2/V = V$, consistent with our observed logarithmic slopes for death rate and cell volume $1.0/0.88 = 1.13$. This interesting link among cell death rate, maintenance rate and cell size suggests that the latter can be one of the factors that contribute to the energetic cost of the cell in carbon starvation conditions. This hypothesis may be also supported by the fact that, at the molecular level, cell size, structure and integrity in stress conditions such as carbon limitation appear to be largely independent of RpoS [81, 172], which we showed not to be the main responsible of maintenance modulation in death-growth rate dependence. However, the finding that the maintenance rate scales with the volume squared was unexpected and if there is a causal link behind this scaling law is still unclear. Considering the relationship among cell death rate, maintenance rate and cell size, future measurements of death rate changes and relative cell size changes in different conditions can elucidate whether cell size is the only determinant of the observed maintenance increase, disentangling cell size effects from growth rate effects.

3.9.2 Maintenance rate modulation as a survival strategy in energy limited environments

A large proportion of bacteria on Earth live in energy-limited environments, such as the deep biosphere, where the energy flux available from buried organic carbon is less than 1% of the photosynthetically fixed carbon on the surface of our planet [58]. The survival strategies of these organisms are largely unknown because of the impossibility to reproduce their environmental conditions in laboratories and the difficulties in quantifying cell metabolic rates by direct measurements of chemical transformations or by reaction-transport modeling. By using these techniques, different studies have revealed that a huge amount of bacterial species either grow very slow, with doubling times between 1 and 3000 years [173–175], or, even more drastically, become dormant [176]. While some bacteria can form endospores that survive for millennia, vegetative bacteria have a minimum energy requirement to survive, the maintenance rate. It is clear that the ability to reduce and optimize the maintenance rate is crucial for maximizing survival fitness in these extreme energy limited environments. But how the cell can achieve this efficiency is still largely unclear. In this context, we provide evidence that bacteria have the ability to modulate their need for maintenance. Even if maintenance rate changes among different species were previously reported during exponential growth [90, 177, 178], to our knowledge, this is the first time that they are observed in starvation for a single species. We believe that our approach of linking maintenance rate and recycling yield changes to death rates will allow quantitative assessment of what strategies vegetative bacteria employ to survive extreme energy limited environments such as the deep biosphere.

3.9.3 Resource allocation during slow growth

As we said in the introduction of this chapter, when growth slows down, the proteome is remodeled and the expression of "starvation" proteins is increased. RpoS regulates the expression of many of these proteins and is key for survival of *E. coli* in stressful conditions [79]. The death-growth relationship found in this work, however, appears to be not regulated by RpoS, which is more involved in biomass recycling, than regulation of the maintenance rate, as shown in Chapter 2. This does not mean that RpoS and the general stress response are generally dispensable in starvation. RpoS improves biomass recycling, which manifests itself in the increase of the overall death rate for the *rpoS* knock-out in Fig. 3.5. Instead, this result implies that the molecular adaptation of the bacteria to survival is likely multifaceted, with *rpoS* playing a role that is independent of a second mechanism by which *E. coli* can decrease its maintenance rate.

3.9.4 Bacterial trade-offs between survival and growth may shape bacterial fitness

As the cell adjusts its physiology towards survival, it will inevitably become less adapted for growth. One reason for this trade-off is the proteome allocation problem of the bacteria (see Section 1.8.2 and [41]). Synthesizing proteins that protect bacteria and increase their survival chances is a clear fitness benefit in starvation. Because synthesis of these proteins needs nutrients, for building blocks and energy, this preparation must be done during growth. To synthesize these "protective proteins", bacteria need to allocate a certain part of their resources to it, which goes at the expense of growth-related proteins. The result is a slowdown of growth, i.e. a fitness cost. Metabolic trade-offs (between efficiency and throughput) or trade-offs in cell size (small versus big) could be additional constraints for *E. coli*.

This means that the cell's ability to survive and the cell's ability to grow fast are competing

objectives. Because fitness is the average proliferation across cycles of growth and death, fitness costs in one environment can be compensated with fitness benefits in others. As a result, investments in anticipation of changing environments can become a favorable strategy, as described for example for the overproduction of ribosomes that allows *E. coli* to quickly adapt to improved nutrient conditions [179–181], the preparation of *E. coli* to competitive environments [160] or antibiotic persistence [106].

The central finding of this work, that environments that support only slow growth lead to longer survival, means that *E. coli* increases its investment into survival when growth is decreasing, i.e. when the cells anticipate an approaching starvation. This implies that the increase of investment into better survival is major burden for the bacterial cell, which is only induced when necessary. Deciphering the mechanistic origin of the growth-death trade-off could shed light on the long-standing questions why *E. coli* has not maximized its growth rate during evolution.

Chapter 4

A thermal fuse in *E. coli* leads to survival at elevated temperatures

4.1 Introduction

In the last 20 years, increased antimicrobial therapy failures have fuelled research interest on bacterial persistence, the ability of a subpopulation of cells to tolerate antibiotics without having acquired resistance through genetic modification. Such ability allows microbial cultures to survive an antibiotic treatment and repopulate the host once treatment has stopped [104]. Tolerating antibiotics can also increase mutation rates and lead to genetically encoded antibiotic resistance [103, 125, 182]. Moreover, antibiotic persistence likely plays a role in human infections, where the lack of clearance of pathogenic bacteria by antibiotic treatment allows infections to recur [102, 104, 183]. Thus, a deeper understanding of the mechanisms of persisters formation is needed to develop strategies to ensure that antimicrobial therapies remain effective.

The main molecular mechanisms so far known to cause persistence lead to a non-growing, dormant state of the cells (see also Chapter 1), which prevents the corruption of the target [105, 132, 184–187]. For example, toxin-antitoxin systems [115, 187–189] stop protein synthesis [185], which renders the inhibition of growth-dependent processes like translation or peptidoglycan synthesis useless. Recovery kinetics from this dormancy state, which leads to the recurrence of the infection after antibiotic clearance, are usually complex and difficult to decipher because they depend on systems-parameters like cell density, e.g. quorum sensing [190] or the medium where cells are allowed to grow [191].

There exist multiple stresses that trigger the dormancy state, such as starvation [106, 192] or temperature increase [109, 193–195]. In particular, elevated temperature, i.e. fever, is a typical response for bacterial infections such as Tubercolosis, Salmonella, Thyphoid fever and *E. coli* urinary and respiratory tract infections [196]. These infections are often characterized by the presence of persister cells that impede drug efficacy and can lead to recurrence [102, 183, 197–200].

Progress has been made towards the molecular mechanism leading to dormancy at high temperatures. As we said in Chapter 1, the degradation of homoserine O-succinyltransferase (MetA) is one of the main factors limiting exponential growth above 37°C [95, 96, 201]. This enzyme is unstable, misfolds, aggregates and is eventually degraded [94]. Its thermal instability limits growth because MetA is an essential step of the biosynthetic pathway of methionine, a basic building block necessary for protein synthesis initiation and synthesis of the major methyl group

donor in cellular metabolism, S-adenosyl-L-methionine [202]. In this context, we hypothesize that by impeding methionine synthesis, MetA degradation leads to dormancy at high temperatures. This hypothesis is supported by the fact that the addition of exogenous methionine in bacterial culture at high temperature reduces the fraction of persister cells within the population [109].

How this growth limitation works quantitatively, however, remains unclear. In particular, MetA is also unstable and degraded at 37°C, with the decay rate being only 30% lower than at 45°C [98]. This minor change of the decay rate seems to be critical because at 37°C no significant amount of persistence is being formed. Furthermore, MetA degradation is a major fitness burden, as it reduces growth rate [98]. This growth defect can be prevented by stabilizing the enzyme with single nucleotide changes [92, 98, 180]. This raises the question why bacteria have evolved to degrade MetA. Because antibiotic treatment of febrile patients is a rather modern threat to bacteria, we recall the long-standing question if there exist an evolutionary advantage of the MetA-induced dormancy [96].

In this chapter, we investigate how MetA is involved in the molecular mechanism behind the dormancy state using a combination of quantitative experiments and modeling. Experimentally, we study the recovery from starvation at elevated temperatures. We show that, during recovery, there exist two distinct sub-populations in each culture: one being able to grow and the other one not. Using mathematical modeling, genetic and environmental perturbations, we show that the dormancy state is due to a combination of MetA degradation and a dual-use of methionine for protein synthesis and as a methyl-donor. We find that there is a certain threshold of MetA, below which bacteria cannot recover and become dormant. This threshold crucially depends on the MetA decay rate, explaining why the 30% decrease from 45°C to 37°C leads to a drastic decrease of persistence. Finally, we investigate possible fitness benefits of the dormancy state, uncovering that it not only protects bacteria against antibiotics, but also from heat shocks. This suggests that the thermally induced dormancy has initially evolved to protect bacteria when temperature rises.

This work is a project collaboration with Dr. Severin Josef Schink, Mariel García Huiman, Dr. Yu-Fang Chang, Prof. Dr. Markus Basan and Prof. Dr. Ulrich Gerland. A manuscript of the project is in preparation.

4.2 Short periods of starvation lead to long lag times

We study bacterial physiology at elevated temperatures, up to 45°C, which is the maximuml temperature that allows *E. coli* growth in our protocol. In particular, we are interested in how *E. coli* is recovering from short periods of starvation. In our protocol, *E. coli* K-12 NCM3722 is cultured in minimal medium until the carbon substrate glycerol is depleted. After a certain period of starvation (see Fig. C.1 for starvation at high temperatures), the culture is then diluted into fresh medium with new glycerol, as illustrated in the cartoon of Fig. 4.1A and described in detail in Appendix C. By measuring the optical density of the culture throughout the experiment, see Fig. 4.1B-D, we observe that this protocol induces long lag times prior to recovery (e.g. after 5 h of starvation, a culture recovers after about 12 h).

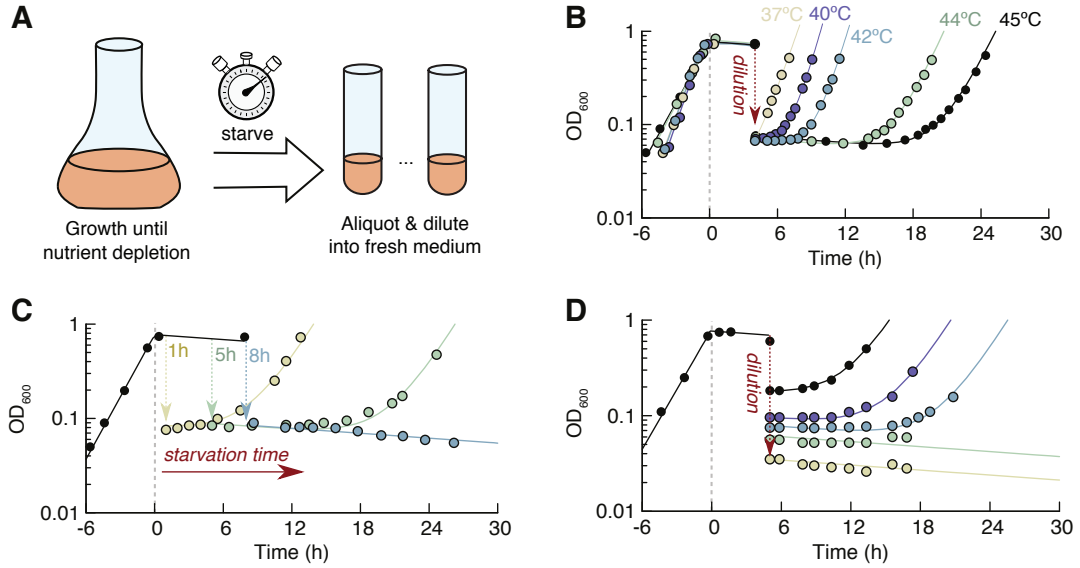

Figure 4.1: Dependence of lag times on culture conditions. **(A)** Experimental protocol to study cell dormancy at high temperatures (see also Appendix C): a culture of cells is grown and starved at the desired temperature; at a certain time during starvation, a sample is extracted from the culture, diluted 8 fold in fresh minimal medium and supplemented with glycerol to allow cell regrowth. Then, regrowth is measured by OD_{600} measurements over time and lag times are quantified as explained in Appendix C. **(B)** Using the protocol explained in panel A, cells are first grown at different temperatures (37°C (yellow), 40°C (violet), 42°C (blue), 44°C (green) and 45°C (black)) until nutrient depletion (dashed grey line) and let starved for 4 h. Then, regrowth upon starvation is monitored by OD_{600} measurements: the lag time increases with temperature ($\sim$ 1 h at 37°C, $\sim$ 2 h at 40°C, $\sim$ 4 h at 42°C, $\sim$ 8 h at 44°C and $\sim$ 10 h at 45°C). **(C)** The protocol explained in panel A is applied at different times during starvation at 45°C: cells are diluted and re-supplemented with glycerol after 1 (yellow), 5 (green) or 8 h (blue) of starvation and their regrowth is monitored by OD_{600} measurements. The lag time increases with longer starvation time. In particular, no recovery appears to be possible if cells are re-supplemented with glycerol after 8 h of starvation (blue). **(D)** Following the protocol explained in panel A, after 5 h of starvation, starved cells at 45°C are diluted with different dilution factors (3, 6, 8, 10, 15 fold corresponding to black, violet, blue, green, yellow) and regrowth is monitored by OD_{600} measurements over time: the more the culture is diluted, the longer is the lag time and no recovery is possible above 8-fold dilution. In panels B, C and D, data of growth before starvation are fitted with exponential functions. Data of regrowth are fitted with the function: $N = N_1 e^{-\gamma t} + N_2 e^{\mu t}$ where N is the optical density.

4.3 Lag times depend on culture conditions

These lags depend on several key parameters of our protocol. One important parameter is temperature. We find that lag times increase gradually, from 37°C to 45°C, see Fig. 4.1B. A second important parameter is the starvation time. We find that with longer starvation times, lag times increase, see Fig. 4.1C. For starvation times longer than 8 h at 45°C, cultures do not recover within the 3 days of the experiment. A third important parameter is the culture density. The more the culture is diluted into fresh medium, i.e. the lower OD_{600}, the longer they take to recover, see Fig. 4.1D. Since all cells come from the same culture and are only split at the point of the dilution, this experiment shows that not only the internal state of the cells determines the lag time, but also the environment of the cells.

4.4 Lag times are due to methionine limitation

As we said in Chapter 1, for *E. coli*, it is known that degradation of homoserine O-succinyltransferase (MetA) is one of the limiting factors of exponential growth above 37°C [95, 96, 201]. This enzyme

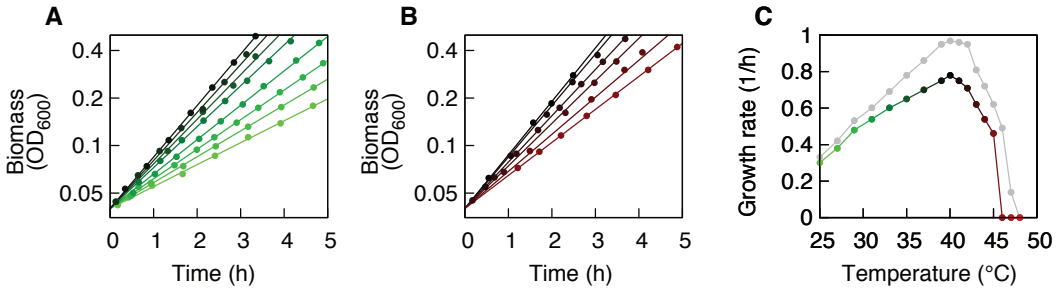

Figure 4.2: Growth rate dependence on temperature with and without methionine. **(A)** Exponential growth of *E. coli* K-12 NCM3722 in glycerol minimal medium at 25, 27, 29, 31, 33, 35, 37, 39°C (from bright to dark green), measured using optical density (OD_{600}). **(B)** Exponential growth of *E. coli* K-12 NCM3722 in glycerol minimal medium at 40, 41, 42, 43, 44, 45°C (from bright to dark red), measured using optical density (OD_{600}). Lines in panels A and B are exponential fits. **(C)** Green-red data: growth rates of the cells at different temperatures extracted from the slopes of the exponential fits in panels A and B. Each value is an average of three independent experiments (see Table C.1). Grey data: growth rates of the cells grown at the same temperatures of the cultures in panels A and B with the additional supplementation of exogenous methionine. Values are also averages of three independent repeats (see Table C.1). With increasing temperature and, consequently, MetA degradation, methionine becomes limiting and its supplementation increases cell growth rate, reaching the maximum value of 0.97 h^{-1} at 40°C compared to the corresponding 0.78 h^{-1} in the culture without methionine at the same temperature.

is unstable, misfolds, aggregates and is eventually degraded [94]. As a result of the unstable MetA, *E. coli* grows about 30% slower in the absence of methionine at temperatures above 37°C, see Fig. 4.2.

To test if the long lag phases are methionine-dependent, we supplement the medium with methionine during the recovery phase. In the presence of methionine, the culture immediately recovers, see Fig. 4.3, showing that the lag is caused by methionine limitation, which is likely the result of MetA degradation.

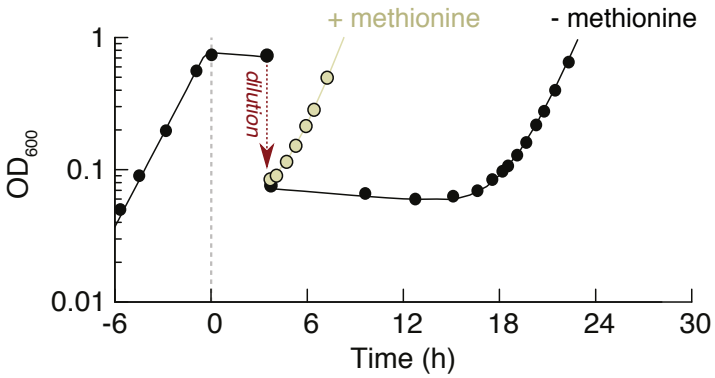

Figure 4.3: Lag times dependence on methionine. Example of an experiment performed as explained in Fig. 4.1A after 4 h of starvation at 45°C: when no methionine is added (black), cells experience a lag time of ∼ 10 h, while, in the presence of methionine, cell regrowth occurs immediately (yellow). Data of growth before starvation are fitted with an exponential function. Data of regrowth are fitted with the function: $N = N_1 e^{-\gamma t} + N_2 e^{\mu t}$ where N is the optical density.

4.5 Single-cell time-lapse of growth recovery

For the methionine-limited culture, there are two scenarios for how a long lag time could arise. Either there is a homogeneous population of cells that recover after a long time or there are two subpopulations, a large non-growing population and a small growing population. In the second case, the lag time would be given by the time it takes for the small, growing population to take over. To distinguish between these two scenarios, we measure the recovery of the cells during the lag time at the single cell level: we extract samples of a starved culture at 45°C and plate them on agar pads supplemented with minimal medium and glycerol. We stain the bacteria with propidium iodide (red) for membrane permeability to detect cell death and monitor growth by time-lapse microscopy (see Appendix C). Fig. 4.4A shows two snapshots, 2 h and 8 h after nutrient addition, from a time-lapse movie of 300 single cells. The culture, previously starved for 5 h, shows three distinct populations. One population, 15%, stains positive for cell permeability and is likely dead. A second population, 5%, recovers after about 2 hours, and after 8 h has formed micro-colonies (white arrow). A third population, 80%, stains negative for cell permeability, but does not grow within the 24 h of this time lapse. If the agar pad is also supplemented with methionine, see Fig. 4.4B, this non-growing population is absent and only permeability-stained bacteria (red) do not recover. This result shows that the viable population splits into a growing and a non-growing part and that the non-growing cells are methionine limited.

4.6 Growth-dormancy model

In order to understand how, within an isogenic population, a non-growing subpopulation can get trapped in a state of methionine limitation, while at the same time a growing subpopulation can recover, we build a quantitative model. The model is summarized in Fig. 4.5A and describes the dynamics of two major components of the system: internal methionine concentration c_{met} (solid lines) and active MetA abundance (dashed lines). The goal of the model is to yield quantitative predictions on how the lag time depends on experimental parameters. In Appendix C we show a detailed derivation of the model and in Tables C.2, C.3, C.4, C.5 we estimate model parameters based on published measurements.

First, we dedicate our attention to the internal methionine concentration c_{met}. As methionine is limiting at high temperatures [96], we model growth rate μ as being dependent on the methionine concentration,

$$\mu = \kappa_{\mathrm{p}} c_{\mathrm{met}} \tag{4.1}$$

where κ_{p} is a rate constant.

The dynamics of the methionine concentration is determined by synthesis, import and consumption of this metabolite (see Fig. C.2). As MetA is the limiting step in synthesis [96], we model the production flux as being proportional to the MetA abundance ϕ_{MetA}, defined as the fraction of the proteome that is MetA, $j_{\mathrm{MetA}} = h\phi_{\mathrm{MetA}}$. If methionine is present in the medium, it can be taken up, giving an import flux j_{in}. Finally, we consider that methionine is consumed in several pathways in bacteria. The two major ones are protein synthesis and S-adenosylmethionine (SAM) synthesis, the major methyl donor of the cell [202]. We can estimate the methionine flux to protein synthesis from the methionine concentration inside the cell that is bound in proteins, $c_{\mathrm{met}}^{\mathrm{pro}} = 27.5$ mM, see Table C.3 for the estimation. The resulting methionine

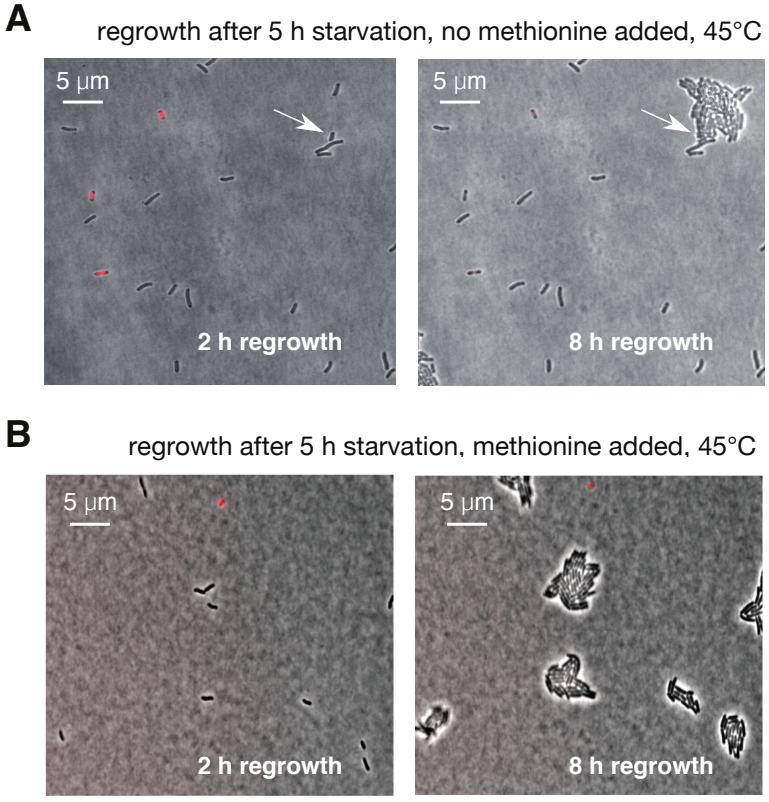

Figure 4.4: Population-wide dormancy determines methionine-dependent lag times. Time-lapse snapshots of cell regrowth at 45°C on agar pads supplemented with minimal medium and glycerol. After 5 h of starvation in batch culture, samples of the culture are extracted, stained with propidium iodide to detect dead cells (see Appendix C) and spread on agar pads without **(A)** or with **(B)** methionine. The regrowth of the cells is monitored over time and, in the absence of methionine, shows a population-wide dormancy ($\sim 80\%$), as only 5% of the cells regrow (the white arrow indicates the single cell regrowing) and 15% is dead (red). If the agar pad is also supplemented with exogenous methionine, the dormant population is absent and only permeability-stained bacteria do not recover.

consumption flux is $j_\mathrm{p} = c_\mathrm{met}^\mathrm{pro}\mu$, for a cell growing at growth rate μ.

During growth, the majority of the methionine flux drains into S-adenosyl-methionine (SAM). While much of this SAM is recycled back to methionine in the SAM cycle, it is also used for biosynthesis of polyamines, such as spermidine, which are important for survival in stress conditions [203]. Of these metabolites, spermidine is present at a particularly high intracellular concentration of about $c_\mathrm{spe} = 1.4$ mM [93]. Because one methionine is consumed per spermidine, we can estimate the fraction of the methionine flux that is used for spermidine synthesis as $c_\mathrm{spe}/c_\mathrm{met}^\mathrm{pro} = (1.4\mathrm{mM})/(27.5\mathrm{mM}) = 5\%$. Since polyamine synthesis is an overall small part of the cell's biomass, we assume that the drainage flux saturates at some level and choose to model it as a saturating function of the internal methionine concentration. These reactions permanently drain methionine at a rate $j_\mathrm{d} = k_\mathrm{d} c_\mathrm{met}/(c_\mathrm{met} + K_\mathrm{M})$, with $k_\mathrm{d} = c_\mathrm{spe}\mu$. All these fluxes, combined with a dilution due to growth, μc_met, yield the following dynamics of the internal methionine concentration:

$$\frac{\mathrm{d}c_\mathrm{met}}{\mathrm{d}t} = j_\mathrm{MetA}(\phi_\mathrm{MetA}) + j_\mathrm{in} - j_\mathrm{p}(c_\mathrm{met}) - j_\mathrm{d}(c_\mathrm{met}) - \mu c_\mathrm{met}. \tag{4.2}$$

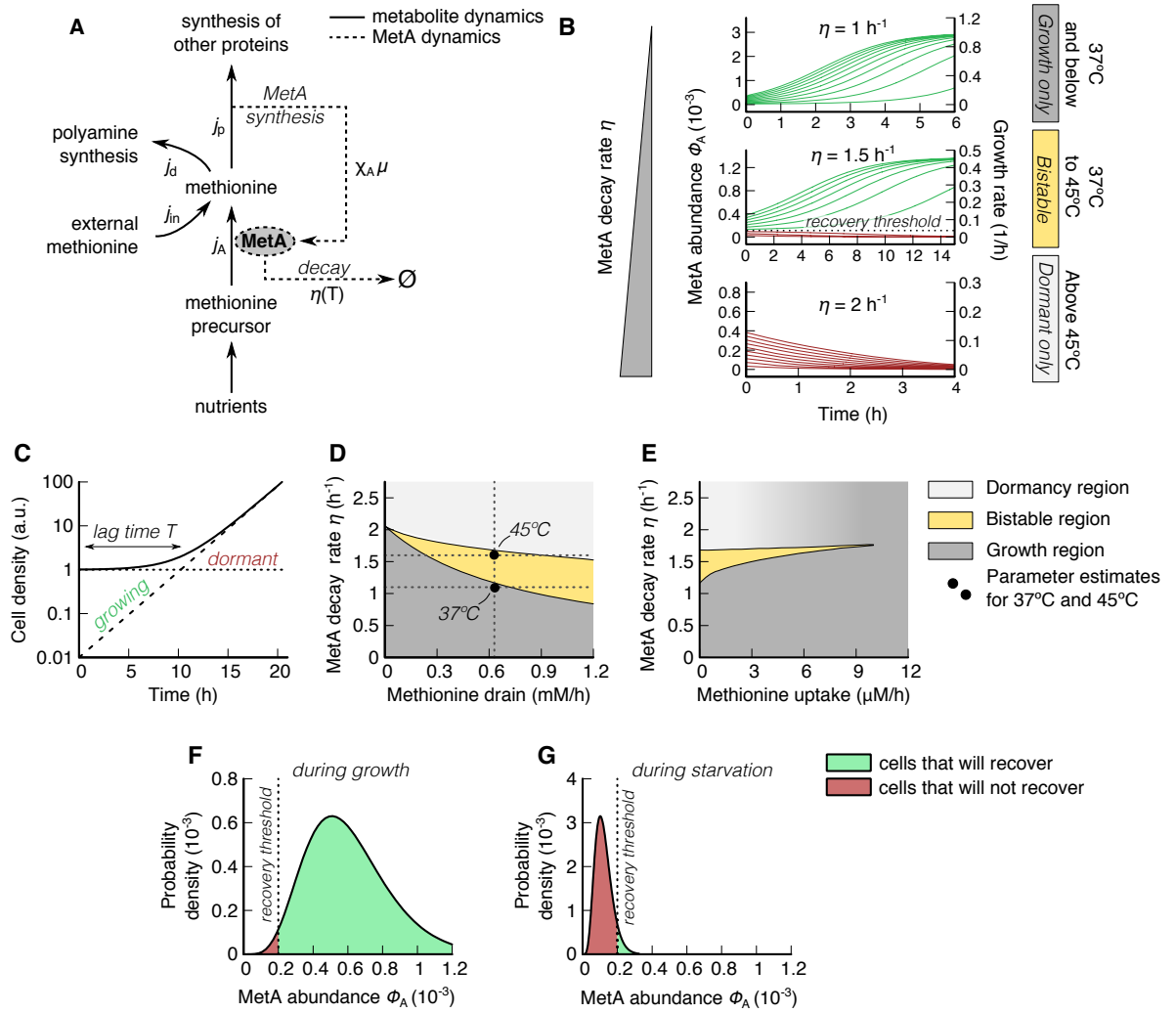

Figure 4.5: Growth-dormancy model. (A) Metabolite dynamics (continuous arrows): nutrients are uptaken by the cell from the environments to build methionine precursors, which are used by MetA to start the production flux of methionine j_{MetA}. At the same time, methionine can be also directly uptaken from the environment, if present (import flux j_{in}). Methionine is then partially consumed in polyamines synthesis (drain flux j_{d}) and protein synthesis (consumption flux j_{p}). MetA dynamics (dashed arrows): methionine is used to produce MetA, at a rate $\chi_{\mathrm{MetA}}\mu$. The latter is again used to produce methionine, while also degrading with temperature at a rate $\eta(\mathrm{T})$. **(B)** Numerical results of the dynamics of the model (see also Appendix C). MetA abundance values are computed at different cell growth rates for three increasing MetA decay rates η (grey bar on the left). In all the panels, green trajectories tend to the stable point of growth, while red trajectories tend to the stable point of dormancy. The top panel represents the stable regime of growth (dark grey, 37°C or below), the central panel represents the bistable regime (yellow, from 37°C to 45°C) and the bottom panel represents the dormancy regime (light grey, above 45°C). **(C)** Representative sketch of the recovery dynamics in the bistable regime. Cell population is initially split into a small fraction of growing cells (red) and a large fraction of dormant cells (green). The time it takes for the growing fraction to equal the dormant fraction and take over is the lag time (see Section C.2.5 in Appendix C for the lag time calculation). **(D)** Stability diagram showing the system behaviours in the growth regime (dark grey region), dormancy regime (light grey region) and bistable regime (yellow region) in function of the parameters MetA decay rate and methionine flux used to produce polyamines (methionine drain). Black dots: estimates of system values at 37°C and 45°C, derived from measurements in the literature, summarized in C.2. **(E)** Stability diagram in function of the parameters MetA decay rate and uptake rate of external methionine. The shaded region (light grey to dark grey) indicates the shift of the system from the dormancy to the growth regime. **(F-G)** Gamma distribution of MetA abundance during growth **(F)** and starvation **(G)** for the values written in Section 4.10. Green and red area indicate the probability density of MetA abundance values that allow (green) and not allow (red) growth.

The second component of the model is the dynamics of the MetA abundance, ϕ_{MetA}, defined as a protein mass fraction. MetA is synthesized during growth at rate $\chi_{\mathrm{MetA}}\mu$, where χ_{MetA} is the fraction of the newly synthesized proteome that is MetA. Since we are interested in the regime of low methionine abundance, we assume that χ_{MetA} is set constantly to full expression. In addition to dilution by growth, $\mu\phi_{\mathrm{MetA}}$, the MetA abundance decays at a constant rate, $\eta(\mathrm{T})\phi_{\mathrm{MetA}}$ [95, 98]. The decay rate $\eta(\mathrm{T})$ is temperature T dependent [98] and includes any process that renders MetA unfunctional, from degradation [95] to thermal aggregation [94]. Combined, the dynamics of the MetA abundance reads

$$\frac{\mathrm{d}\phi_{\mathrm{MetA}}}{\mathrm{d}t} = \chi_{\mathrm{MetA}}\mu(c_{\mathrm{met}}) - (\eta(\mathrm{T}) + \mu(c_{\mathrm{met}}))\phi_{\mathrm{MetA}}. \tag{4.3}$$

The dynamics of methionine concentration and MetA abundance have very different time scales. While concentrations of metabolites like methionine typically change within seconds to minutes [156], the protein abundance changes within tens of minutes to hours [46]. For the growth dynamics of the cell, however, the combined dynamics of both contributions is important. This is because dynamics of methionine and MetA are intertwined: MetA is required to synthesize methionine and methionine in turn is required to synthesize MetA - the motif of a positive feedback loop.

4.7 Recovery dynamics

The results of the dynamics can be obtained numerically (see Appendix C) and are shown in Fig. 4.5B: at low temperature, where MetA decay rate is low, all cells regardless of their initial state recover to growth (top panel, green trajectories). We call this the "growth regime". At high temperatures, where MetA decay rate is high, none of the cells recover, i.e. they become dormant (bottom panel, red trajectories). We call this the "dormancy regime". At intermediate temperature, the population splits depending on the initial MetA abundance. Cells above a certain recovery threshold accumulate MetA and start growing (green trajectories), while cells below the threshold do not (red trajectories). Because both growth and non-growth are stable states, we call this state the "bistable regime".

4.8 Recovery dynamics in the bistable regime

In the bistable regime, the population can contain bacteria that are growing and others that are dormant. As a result, the recovery dynamics of such mixed population will show a characteristic lag before growth becomes exponential again, see Fig. 4.5C. This lag time is the key experimental observable of Fig. 4.1 and it depends on how many bacteria are in the dormant and growing state. In order to understand how the lag time depends on experimental parameters, we will next study the parameter dependency of the theoretical solution from Eqs. (4.1) to (4.3), followed by studying how the heterogeneity of the population arises from heterogeneous gene expression.

4.9 Condition dependency of the bistable regime

By studying the fixed points of the system, i.e. the steady states of constant methionine concentrations and MetA abundance, $\mathrm{d}c_{\mathrm{met}}/\mathrm{d}t = 0$ and $\mathrm{d}\phi_{\mathrm{MetA}}/\mathrm{d}t = 0$, we can understand under which conditions the cell is in which of the three regimes of Fig. 4.5B and what sets the position of the "recovery threshold" in the bistable regime (yellow).

The results of the fixed points analysis, detailed in the Appendix C, show that the behaviour of the system crucially depends on MetA decay rate, dual usage of methionine for protein synthesis and SAM cycle and methionine uptake. Here, we discuss these dependencies. In Fig. 4.5D, we plot the solutions of the systems at the steady states (growth, dormancy and bistable regimes, see Section C.2.10 in Appendix C) in the space of the parameters MetA decay rate and methionine flux used to produce polyamines such as spermidine. The bistable regime (yellow region) exists for intermediate decay rates and depends on the methionine drain. Above this region, no growth is possible (light grey region) because MetA decays faster than it is produced. For small decay rates, enough MetA is synthesized, that even residual amounts of MetA can restart the cycle of MetA synthesis (dark grey region).

The two black dots in Fig. 4.5D are our estimates of the steady states system values for wild-type at 37°C and 45°C, derived from measurements in the literature, summarized in Tables C.2, C.3 and C.4. The decay rate of MetA for 37°C lies only in the growth regime, while the decay rate at 45°C lies in the bistable regime. This means that MetA decay at 37°C can lead to complete recovery of the population, despite only being 30% smaller than at 45°C because synthesis outpaces decay of MetA. We further see that if there is no methionine drain into spermidine, there is no bistable regime. This is because the synthesis of spermidine from methionine competes with protein synthesis for the same pool of methionine and can thus modulate the protein synthesis rate. This dual usage of methionine is an integral part of the system and essential for the bistable regime.

In Fig. 4.5E, we plot again the solutions of the systems at the steady states (growth, dormancy and bistable regimes, see Section C.2.10 in Appendix C) in the space of the parameters MetA decay rate and uptake rate of external methionine. For higher methionine uptake, the bistable regime disappears. In addition, the presence of a methionine influx leads to growth even at high MetA decay rates (shaded region - grey to white). This is because synthesis of methionine becomes obsolete when external methionine is supplied.

4.10 Population partitioning is set by heterogeneous gene expression

Whether a cell recovers or stays dormant depends on its MetA abundance. Individual cells within the population can have different MetA abundances because of stochastic effects. Gene expression, for example, is highly heterogeneous during growth and leads to large variations in protein abundance between cells. This heterogeneity can have a strong impact on recovery dynamics and lag times in nutrient shifts [204]. Therefore, we suspect it to be a relevant factor in determining how many cells can recover at elevated temperatures. Protein abundance due to heterogeneous gene expression can be well described by a gamma distribution [205, 206]

$$p(\phi_{\mathrm{MetA}}) = \frac{{\phi_{\mathrm{MetA}}}^{a-1} e^{\phi_{\mathrm{MetA}} b^{-1}}}{\Gamma(a) b^a} \tag{4.4}$$

where a is the number mRNA synthesized per cell cycle and b the number of proteins synthesized per mRNA. Due to the nature of the gamma distribution, the square root of the inverse of a also equals the noise, $\sqrt{a^{-1}} = \sigma/\xi$, and b equals the Fano factor, $b = \sigma^2/\xi$, where σ is the standard deviation and $\xi = ab$ is the average MetA abundance. As an example, in Fig. 4.5F we show the gamma distribution for an average MetA abundance of $\xi_{\mathrm{MetA}} = 6.13 \cdot 10^{-4}$, estimated from a copy number of about 1700 [207], and noise $\sqrt{a^{-1}_{median}} = 0.4$, typical for proteins of this

abundance, see Table C.2 [206].

During starvation, MetA will decay. Due to the large initial copy number of MetA (∼1700, see Table C.2), the stochasticity in MetA abundance arising from the stochastic decay process is small, about $\sqrt{1700}^{-1} < 1\%$ compared to the inherited heterogeneous gene expression, $\sqrt{a_{median}^{-1}} = 40\%$, discussed in the paragraph above. For this reason, we model the decay of MetA abundance as a deterministic exponential decay, given by the decay rate η. During starvation, MetA abundance distribution shown in Fig. 4.5F will shift to the left, see Fig. 4.5G, and only a small number of cells will have a MetA abundance above the recovery threshold. The position of the threshold and the distribution of the MetA abundance together determine how large the growing fraction of the population is and thus determines the lag time of the population.

4.11 Derivation of quantitative lag time predictions

Based on the discussion above we can derive how the lag time depends on the parameters of the system. The goal is to test these dependencies experimentally. We find that the average MetA prior to starvation (mean MetA pre-expression ξ_{MetA}), the starvation time τ and the decay rate η determine the MetA abundance distribution, while the MetA growth threshold is determined by nutrient quality and methionine uptake from the environment. We derive these mathematical dependencies in Appendix C and find that the lag time can be approximated as

$$T_{\mathrm{lag}} \approx \mathrm{const} + \phi_{\mathrm{MetA}}^{\mathrm{th}} b^{-1} e^{\eta\tau} \tag{4.5}$$

which depends approximately

- exponentially on starvation time τ,
- exponentially on MetA decay rate η,
- linearly on the inverse of the mean MetA pre-expression $\xi = ab$,
- linearly on the growth threshold $\phi_{\mathrm{MetA}}^{\mathrm{th}}$.

The growth threshold, in turn, depends linearly on nutrient quality and methionine uptake, as explained in Appendix C.

4.12 Experimental tests of the lag time predictions

We next test experimentally if these predictions hold. In Fig. 4.6A we plot lag time against starvation time for the three experiments shown in Fig. 4.1C and 2 more on a semi-exponential scale. Cultures starved for more than 8 hours do not recover within 3 days. Longer starvation times allow longer and thus more thorough decay of MetA. As predicted by Eq. (4.5), we find that the lag time T_{lag} increases exponentially with starvation time τ.

To test if lag time is indeed determined by MetA abundance and not a different thermally-degraded protein, we titrate MetA expression prior to starvation. In Fig. 4.6B, we show the lag time against the inducer concentration (cTc) for a strain containing the titratable element $\mathrm{P}_{LTet-O1}$-*metA* in the absence of the native *metA* gene, see Appendix C. We find that when *metA* pre-expression is increased, lag time decreases, qualitatively confirming that the average

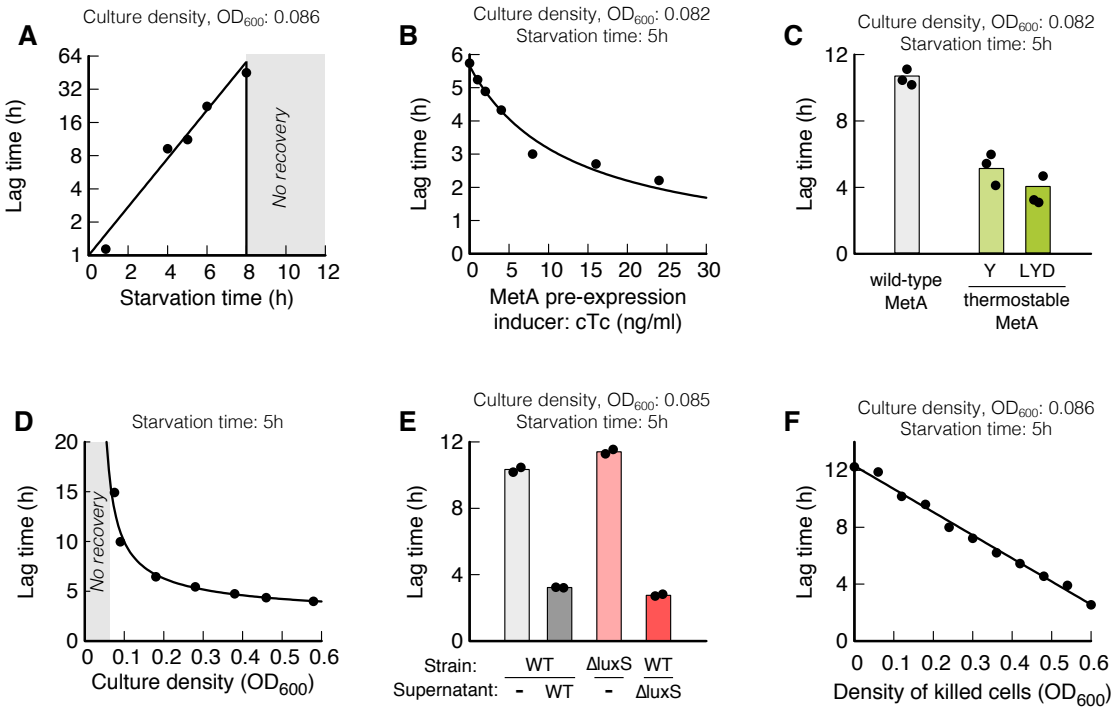

Figure 4.6: Tests of the growth-dormancy model. In all of the following tests of the model, the lag time of the cells is measured by performing the experiment explained in Fig. 4.1, at 45°C. **(A)** The lag time measured for the three experiments of Fig. 4.1C and two more is plotted against starvation time and it increases exponentially with it (black line), as predicted by the growth-dormancy model. When cultures are starved for more than 8 hours, they do not recover within three days. **(B)** The lag time of a strain containing the titratable element $P_{LTet-O1}$-*metA* is measured after 5 h of starvation and plotted against the inducer concentration (cTc), representing the average MetA pre-expression, ξ_{MetA}. As predicted by the model, lag time decreases with increasing cTc, as $T_{\mathrm{lag}} \approx 1/(\mathrm{A} + \mathrm{B} \cdot c(\mathrm{cTc}))$ (black line), as the P_{tet} system is linear in cTc concentration with some basal expression pattern [46]. **(C)** The lag time of MetA thermostable mutants LYD and Y (green) is measured after 5 h starvation and compared to the corresponding lag time of the wild-type strain (light grey). Black dots represent different experimental results (three for each strain) and show that the increase of MetA thermostability reduces of about 2/3 the lag time. **(D)** After 5 h starvation, a starved culture of wild-type cells is split and diluted into fresh minimal medium (see Appendix C) with different dilution factors in different cultures supplemented with glycerol. The higher the dilution factor, the lower the OD_{600} (black line, $T_{\mathrm{lag}} \approx 1/(A + B \cdot \ln(\mathrm{OD}_{600}))$). The lag time measured is plotted against the optical density of the culture upon dilution. The plot shows that it decreases with increasing optical density. **(E)** After 5 h starvation, a starved culture is diluted into the supernatant and supplemented with glycerol. The lag time measured (dark grey) is 1/3 of the lag time measured in fresh minimal medium (light grey), free of nutrients released by dead cells. The same experiment is performed with a $\Delta luxS$ strain, where the autoinducer 2 (AI-2) is knocked-out and signal molecules are not released in the supernatant. Both the $\Delta luxS$ culture diluted into fresh medium (light pink) and the one diluted into its supernatant (dark pink) show lag times similar to the ones of the wild-type strain. **(F)** After 5 hours of starvation, a wild-type culture is split and diluted in cultures with different percentage of UV-light killed cells. The lag time measured is plotted against the percentage of UV-light killed cells in the culture: the higher the number of dead cells in the medium, the lower the lag time (linear fit, black line.

MetA abundance determines the lag time. The model predicts the inverse of lag time, T_{lag}^{-1}, to increase linearly with the average MetA pre-expression, ξ_{A}, see Eq. (4.5). Because expression from the P_{tet} system is linear in cTc concentration c(cTc) with some basal expression pattern [46], i.e. $\xi_{\mathrm{MetA}} = \mathrm{A} + \mathrm{B} \cdot c(\mathrm{cTc})$, we fit $T_{\mathrm{lag}} \sim 1/(\mathrm{A} + \mathrm{B} \cdot c(\mathrm{cTc}))$ to the data of Fig. 4.6B.

As an alternative to titration of MetA abundance, we can also decrease the decay rate of

MetA using stabilized mutants (see Appendix C), where MetA half-life at 45°C is 107 min compared to 36 min in the wild-type strain [98]. Stabilization of MetA leads to a decrease of lag time, see Fig. 4.6C, confirming the importance of MetA decay.

Finally, we turn to the concentration dependence of lag time observed in Fig. 4.1D. In Fig. 4.6D we show the lag time against the optical density of the culture for the experiments of Fig. 4.1D and additional measurements. At high densities, cultures recover fast, while, for densities below $OD_{600} = 0.08$, bacteria do not recover within the two days of the experiment. At all densities, cultures recover in the presence of methionine, as in Fig. 4.3. Diluting the culture into the supernatant can similarly decrease lag time, showing that the medium contains molecules that alter the recovery, see Fig. 4.6E. This effect is independent of the autoinducer 2 (AI-2) system, which some bacteria use for quorum sensing, see Fig. 4.6E.

We hypothesize the density dependence of the lag time is due to nutrient recycling from dead bacterial biomass. Such cannibalistic use of dead cells is common for bacteria in nutrient-limited conditions, as we showed in Chapter 2. During the 5 h of starvation about one third of the bacteria have perished due to heat stress. To test if biomass recycling is important, we add bacteria killed with UV-light to the recovery medium. We find that the higher the number of dead bacteria, the lower the lag time, see Fig. 4.6F. Cannibalism of dead bacterial biomass can lead to recovery of methionine and other nutrients. While we cannot distinguish how much of the lag time reduction is due to uptake of other nutrients and how much due to uptake of methionine, we see that according to the model, see Eq. (4.5), both methionine uptake and improvement of nutrient quality should lead to a linear decrease of the lag time, as they decrease the growth threshold $\phi^{\mathrm{th}}_{\mathrm{MetA}}$. This linear prediction fits the data of Fig. 4.6F well.

4.13 Fitness benefit of dormancy

Considering all of the above results together, it appears that a rather intricate system regulated by MetA decay is responsible for shutting-off growth and forcing cells into a dormant state when stressful conditions such as starvation and high temperatures occur. Interestingly, as we said in Chapter 1, MetA temperature sensitivity is not exclusive to *E. coli*, but it was found also in other mesophilic bacteria of the family *Enterobacteriaceae* [99] and in *Bacillus polymyxa* [100]. Moreover, a single nucleotide change is sufficient to stabilize MetA [92, 180], making it an evolutionarily easily accessible target. This suggests that there is an evolutionary benefit in degrading MetA, as hypothesized almost 50 years ago [96].

4.14 Dormancy leads to bacterial antibiotic persistence at high temperatures

Long lag times mean that a large fraction of the population is dormant. Typically, bacteria in such dormant states tolerate antibiotic treatment because the antibiotic targets are not corrupted [105, 132, 184–186, 203]. This implies that the bacterial populations at elevated temperatures should have a high degree of antibiotic persistence. To quantify bacterial antibiotic persistence during these long lag times before regrowth at high temperatures, we repeat the experiment performed to study the lag times, described in Fig. 4.1A, with the additional supplementation of ampicillin. We grow *E. coli* at different temperatures (37, 40, 42 and 45°C) in minimal medium supplemented with glycerol. After 5 h of starvation, we dilute the culture 8 fold, we supplement it with ampicillin and glycerol and we measure survival in colony forming

units per volume (CFU/ml) (see Appendix C). Fig. 4.7A shows, for each temperature, the biphasic survival kinetics, sign of the presence of persister cells [106]: a fast, initial decay of viability followed by a "plateau", which indicates the survival fraction of cells that tolerate antibiotics. At higher temperatures, the initial decay becomes slower and the "plateau" increases from 37°C to 45°C. If ampicillin is added not during starvation, but during exponential growth, the fraction of persisters still increases with temperature, but the fraction of survivors is 10% of the survival fraction when cells are previously starved (see Fig. C.3), indicating that starvation is a main persistence trigger.

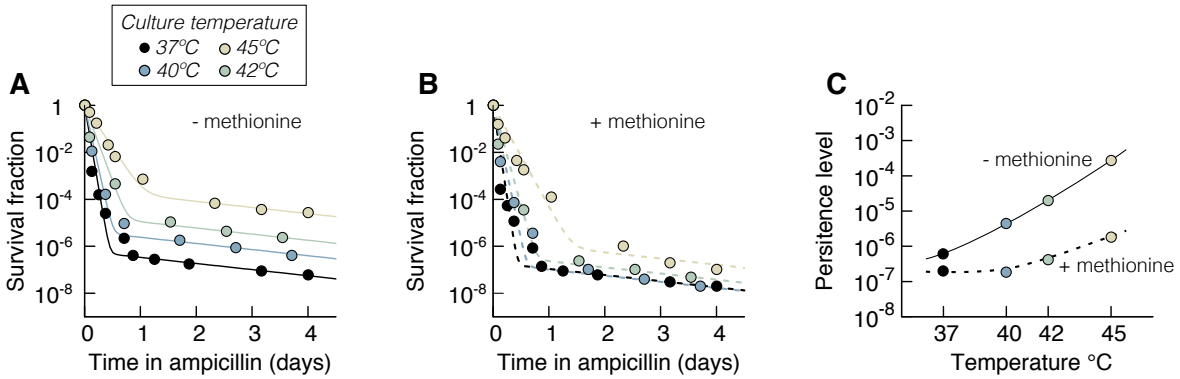

Figure 4.7: Antibiotic persistence. (A) Cells are grown in minimal media with glycerol at 37, 40, 42 and 45°C (different colours, as explained in the legend). After 5 h of starvation, ampicillin is added into the culture (see Appendix C). The survival curves of the cultures are plotted against time. They all show the bi-phasic kinetics typical for persister cells [104]. This final survival fraction increases with temperature. **(B)** The experiment performed in panel A is repeated with additional exogenous methionine in combination with ampicillin treatment (see Appendix C). Colours correspond to the same temperatures of panel A. In this case, the survival fraction does not show an increase higher than 10% with increasing temperature. Lines in panels A (continuous) and B (dashed) indicate the bi-phasic fits $N = N_1 e^{-\gamma_1 t} + N_2 e^{-\gamma_2 t}$ where N is the cell viability and $N_1 + N_2 = 1$. γ_1 indicates the rate of viability decrease in the first phase, while γ_2 is the rate of viability decrease in the second phase and is the same for all curves. **(C)** The final viability values ($\approx N_2$) extracted from panel A (−methionine) and B (+methionine) are plotted versus temperature. Colours correspond to the ones in the previous panels. In the absence of methionine (continuous line), compared to 37°C, persistence increases up to a factor of 1000 at 45°C, while up to 99% of it can be abolished when methionine is added (dashed line).

Previous works showed that, when cells are treated with antibiotics, the addition of exogenous methionine to the culture reduces the frequency of persisters [109]. To investigate the phenomenon in our case, we repeat the experiment shown in Fig. 4.7A, but we also add exogenous methionine in the culture, before antibiotic addition (see Appendix C). As a result, the "plateau" level of persisters at high temperature decreases (see Fig. 4.7B). By fitting the bi-phasic dynamics of the experiments with and without exogenous methionine in Fig. 4.7A,B, we extract the "plateau" levels at different temperatures, see Fig. 4.7C. Compared to 37°C, persistence increases a factor of 10 at 40°C and a factor of 1000 at 45°C, while up to 99% of it can be abolished when methionine is added. These experiments show that the existence of a dormant subpopulation at elevated temperatures leads to an increased persistence of the population to antibiotic treatment.

4.15 Dormancy allows bacterial survival in heat shocks

Antibiotic persistence is certainly beneficial for bacteria in infections if antibiotics are used as treatment. In addition, we ask if there exist a protective feature of the decay of unstable MetA

in a more natural context . Because the MetA decay is temperature dependent, we hypothesize that MetA decay and the induction of dormant state is a preparation strategy for high temperatures.

To test this, we check if growing bacteria are more susceptible to heat shocks than dormant bacteria. In Fig. 4.8A we show survival of a growing and non-growing culture, both kept at 37°C and shifted to 50°C. The non-growing culture was starved of the carbon substrate for 3 hours prior to the temperature shift. We find that the growth state has a strong effect on survival. Only one in a thousand growing bacteria survive the first 15 minutes of the heat shock, while non-growing bacteria survival is virtually unharmed. Then, both cultures show a gradual decrease in viability.

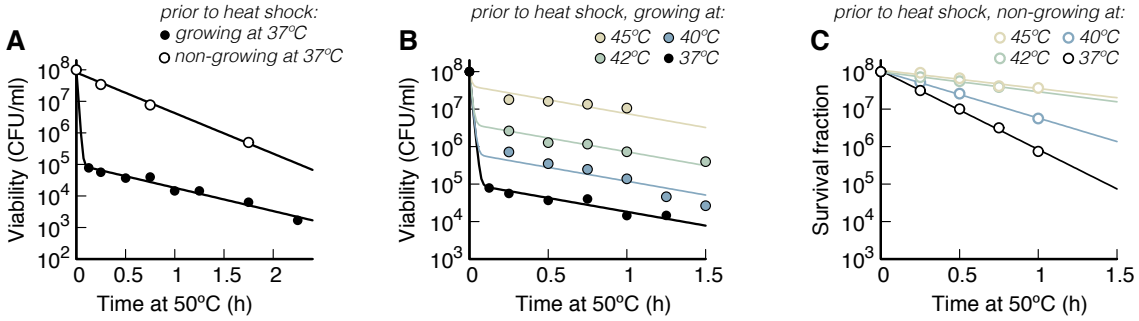

Figure 4.8: Survival in heat shocks. (A) Survival kinetics upon temperature shift from 37°C to 50°C of exponentially growing and starved wild-type cells. Cells are grown in minimal media with glycerol at 37°C. When $OD_{600} \sim 0.3 - 0.4$, one culture (black circles) is supplemented again with glycerol to avoid glycerol exhaustion and shifted to 50°C. Another culture (white circles) is grown until glycerol exhaustion. After 3 h of starvation, the culture is shifted to 50°C. Then, cell viability is measured over time by plate counting in both cases. Cell viability in the first case drops of a factor 1000 within the first 15 minutes, while it slowly decreases exponentially in the second case. **(B)** Survival kinetics of exponentially growing wild-type cells upon temperature shift from 37, 40, 42, 45°C (black, blue, green, yellow respectively) to 50°C. Cells are grown in minimal media with glycerol at different temperatures. When $OD_{600} \sim 0.3 - 0.4$, the cultures are supplemented again with glycerol to avoid glycerol exhaustion and shifted to 50°C. Then, cell viability is measured over time by plate counting. The higher the temperature, the smaller is the initial drop of viability and more cells survive. **(C)** Survival kinetics of wild-type starved cells upon temperature shift from 37, 40, 42, 45°C (black, blue, green, yellow respectively) to 50°C. Cells are grown in minimal media with glycerol at different temperatures until glycerol exhaustion. After 3 h of starvation, the cultures are shifted to 50°C. Then, cell viability is measured over time by plate counting. As they are starved, in all the cultures cells survive more than in panel B and, again, the higher the temperature, the slower is the viability decay. In all panels, lines are the fits of the data. For cells previously growing exponentially (filled circles), the fit function is $N = N_1 e^{-(100/\mathrm{h})t} + N_2 e^{-\gamma t}$ with N indicating the cell viability. For starved cells (empty circles), the fit function is $N = N(0)e^{-\gamma t}$.

At higher temperature, MetA decay increases and more cells become dormant. We then expect that the higher the initial temperature of the culture, the higher the number of dormant cells that survive after heat shocks. Indeed, when we repeat the experiment of Fig. 4.8A for temperatures between 40°C and 45°C, we find that the surviving fraction of cells increases with increasing growth temperature, see Fig. 4.8B,C.

This suggests that in anticipation of a deadly heat shock, the bacterial population splits into a growing and non-growing fraction. The growing fraction would make use of the abundant nutrients and proliferate, while the non-growing fraction would survive a further increase of the temperature. This could be a classic example of a "bet-hedging" strategy that can optimize bacterial fitness [208, 209].

4.16 Discussion

In this chapter, we shed light on the mechanism by which *E. coli* cells become dormant at elevated temperatures and how it affects the physiology of the population. Depending on the decay of the unstable MetA and the dual-use of methionine for protein synthesis and as a methyl-donor, cells may or may not get trapped in a state of low methionine concentration that does not allow growth, thereby splitting the community in two sub-populations of growing and dormant cells. With our combination of theoretical model and experiments, we found that:

- a dormant subpopulation forms at high temperatures;
- dormant bacteria are trapped in a state of methionine limitation due to the architecture of the methionine and MetA cycle and the high MetA decay rate;
- this dormancy seems to protect bacteria from antibiotic treatment and heat shocks.

4.16.1 Thermally unstable MetA as a thermal fuse

In electrical engineering, devices are protected from excessive heat with thermal fuses. Such a thermal fuse will cut-off electric current by physically disintegrating itself, e.g. melting, under heat stress. The fuse has the role of an emergency protection, kicking in when other regulatory mechanisms have failed, in order to protect more expensive machinery such as a motor. In a similar manner, we interpret MetA as a biological thermal fuse. It becomes increasingly unstable at higher temperatures and physically disintegrates, i.e. misfolds and becomes inactive. The resulting cut-off in amino acid synthesis stops growth and protects the organism from death in a heat shock.

4.16.2 Antibiotic and thermal persistence as "bet-hedging" strategies of survival

This thermal fuse leads to a dormant subpopulation that may be part of a bacterial "bet-hedging" strategy in preparation to unpredictable, catastrophic events such as antibiotics and heat shocks. For such a "bet-hedging" strategy, an isogenic population splits into different phenotypes to maximize the time-average population fitness [210]. In our case, during favourable conditions, the growing subpopulation can proliferate, while the dormant subpopulation is an unprofitable burden. If the catastrophic event sets in, however, the growing subpopulations dies off and only the non-growing subpopulation survives. Any one-sided strategy would yield a catastrophic outcome in either one of the environments. The heterogeneity in populations, however, ensures safe proliferation through cycles of growth and stress and improves the overall fitness of the population, analogue to many established scenarios of "bet-hedging" in bacteria [127, 211–213].

4.16.3 The potential of methionine in medical treatments to fight persistence

Elevated temperatures are often encountered by pathogenic bacteria as the body temperature of hosts increase. This cardinal response of the host organism, fever, has been conserved throughout warm and cold-blooded vertebrates for over 600 million years of evolution [214]. Independent of whether the formation of a dormant subpopulation was evolutionarily beneficial for the bacteria, in the present antibiotic era, this dormant subpopulation poses a substantial threat because

it leads to antibiotic persistence and can impair the efficacy of antibiotic treatment.

In this context, our study shows that the large number of dormant cells at fever temperatures is abolished by the addition of methionine, which recovers the cells from their dormant state and expose them to the lethal effects of antibiotics. This could allow methionine to improve strategies employed against persistence. For example, methionine could be useful in intermittent antibiotic treatments. From the first observations of bacterial persistence in the 1940s, it is indeed known that the majority of persisters recover after antibiotic clearance [105]. This evidence has fuelled the idea of applying intermittent antibiotic treatments to patients with the aim to kill in different rounds bacteria waking up from dormancy and re-growing [105, 215]. The same approach is used to directly fight antibiotic resistance by alternating different classes of antibiotics exhibiting comparable spectra activities to avoid the development of resistance to one specific agent [31]. In this context, administration of methionine may help in homogenizing persister recovery upon antibiotic treatment and facilitate complete microbial clearance. Alternatively, methionine could also be administered directly in combination with antibiotics. A successful example of such strategy is the treatment of chronic lung infections by *Pseudomonas aeruginosa* in mouse models. Methionine was found to inhibit biofilm formation and increase the sensitivity to antibiotics [216]. By promoting growth of dormant bacteria, methionine is a prime candidate to reduce persistence *in vivo*, especially in chronic infections characterized by recurrent fever, where the number of persister cells is likely to increase with temperature. More so, because no adverse effects towards methionine administration have been reported in adults or children with a single dose of 100 mg/kg body weight [217].

Chapter 5

Conclusions

The findings presented in this thesis establish a new phenomenological approach to understand how cellular components affect *E. coli* physiology in the growth-arrest phase, where stresses, such as starvation and temperature increase, force the cells to activate strategies of survival.

We first revealed why *E. coli* die exponentially when starved of carbon by showing that viable bacteria recycle nutrients from dead bacteria and use them for maintenance. A stable steady-state exponential decay of viability emerges as a collective phenomenon due to a balance between a supply and a demand flux of nutrients. The observed collective death rate, representing the fitness of the population, is then determined by the maintenance rate of viable cells and the amount of nutrients recovered from dead cells, the yield, which can be experimentally determined using our independent assays. This relationship provides a mean to break down bacterial fitness into its molecular contributions during starvation. To illustrate this, we used our assays to show that the cost of a wasteful enzyme during starvation increases maintenance and thereby the death rate, while the benefit of the stress response sigma factor RpoS improves biomass recycling, decreasing the death rate.

In line with the quantitative approach developed in the last decade to dissect costs and benefits of molecular contributions to cell physiology during the exponential growth phase [40], the model presented here requires a minimum of molecular level information and it is based upon a "top-down" approach that relies on the empirical law of the exponential decay of viability. This is essential when studying the growth-arrest phase, where the alternative "bottom-up" approach is often impossible, due to the lack of knowledge of many processes regulating death and survival. Moreover, the non-equilibrium steady-state aspect of the exponential decay of viability greatly simplifies the characterization of bacterial physiology, as cell properties remain constant and their measurements are robust and reproducible, in analogy with the measurements during steady-state exponential growth. Finally, in the context of evolution, the revealed interplay between death rate, maintenance rate and yield may provide information about natural selection in carbon starvation. The dissection of fitness into its contributions for two different species may indeed help in estimating how much the relative abundance of the species changes during starvation and in competitive environments.

Secondly, we uncovered a correlation between the growth rate of *E. coli* in media with carbon and their death rate when they are carbon starved, by developing a new controlled and quantitative way to bring bacteria from different physiological states into starvation. Cells were grown at different growth rates in different substrates or in a carbon limited chemostat. They were then deprived of the carbon substrate and their survival was measured during starvation.

This approach allowed us to measure quantitative changes in death rate as function of the cell's growth rate, as opposed to the classical "entry into stationary phase" of the bacterial life cycle, where bacteria continuously adapt as the nutrient quality of the medium worsens [33, 79]. We then used the relationship between death rate, maintenance rate and yield to dissect changes of the death rate into their underlying contributions. In this way, we showed that, when corrected for changes in cell size, the change of death rate is mainly due to a change of the maintenance rate. This cost increases exponentially with increasing growth rate, meaning that slower growing cells survive longer during starvation because they need less energy.

The interesting link among cell death rate, maintenance rate and cell size suggests that the latter can be one of the factors that contribute to the energetic cost of the cell in carbon starvation conditions. Moreover, our finding that environments supporting only slow growth lead to longer survival means that *E. coli* increases its investment into survival when growth is decreasing and starvation is approaching. This investment represents a fitness cost during growth, but it becomes a benefit during starvation. Thus, fitness costs in one environment can be compensated with fitness benefits in others. This result supports the idea that bacteria do not optimize growth rate at all costs: alternative factors that determine bacterial fitness, as competition, adaptation and death prevention, force them to continuous trade-offs between slow and fast growth. This is particularly interesting if inserted in the ecological context of bacterial life in energy-poor environments such as the deep biosphere. It is indeed estimated that about $3 \cdot 10^{29}$ microorganisms reside in the subsurface of the Earth, probably living with a very low energy flux [58]. Our finding that starved bacteria can modulate their maintenance rate may contribute to understanding life's basal energy requirements and the survival strategies of many species living in extreme conditions. This is crucial for understanding the biological potential of these largely uncharacterized environments.

Finally, we showed how the combination of starvation and high temperature stresses induce the activation of a thermal fuse in *E. coli* cells that leads to the formation of a dormant and antibiotic persistent subpopulation, even when nutrients are again available. This fuse is implemented by a thermally unstable enzyme, MetA, in the methionine synthesis pathway. Depending on the decay of the unstable MetA and the dual-use of methionine for protein synthesis and as a methyl-donor, cells can grow or be dormant. In particular, as our model showed, the existence of the dormant state is due to a bistability in the system, that critically depends on the MetA decay rate. If this decay rate drops below a certain threshold, the dormant state disappears and all bacteria can recover. However, at fever-like and higher temperatures, the fraction of dormant bacteria is always present and not only survives antibiotic treatment, but also heat shocks.

From an evolutionary perspective, these findings suggest that this thermal fuse has originally evolved as a protection mechanism to defend cell vulnerability from temperature increase. Thus, MetA switch-off at high temperatures may be a bacterial strategy of survival when facing temperature stress and could be inserted among the different molecular mechanisms that lead to dormancy in order to optimize the fitness of the entire population [127, 211]. Using a "bet-hedging" strategy, the population splits into different phenotypes to maximize the probability of survival in anticipation of environmental changes [210]. Such phenotypic heterogeneity reduces the variance in cell numbers over time, providing competitive advantage in environments that change unpredictably. This is particularly interesting for clinical applications, as we showed that these dormant cells, induced by fever-like temperatures, can tolerate antibiotics. Fever is the first natural response of warm and cold-blooded vertebrates to many bacterial infections that stimulate the innate and adaptive immune system of the host [214]. Thus, a main evolutionary

advantage of MetA switch-off in bacteria may be the protection against fever. In this context, the finding that the addition of exogenous methionine speeds up cell recovery from the dormant state is crucial, as it exposes the cell to the lethal effect of antibiotics. Its administration, which does not appear to be toxic within 100 mg/kg of human body weight [217], could indeed facilitate the complete microbial clearance in bacterial infections, when combined with antibiotics treatments. In times of increasing prevalence of multi-resistant pathogens, elucidation of the molecular mechanisms underlying antibiotic tolerance and the development of new clinical therapies to fight it are imperative.

Appendices

Appendix A

Death rate of starved *E. coli* is set by maintenance cost and recycling yield

A.1 Methods

A.1.1 Strains

All strains used in this study are derived from wild-type *E. coli* K-12 strain NCM3722 [218]. Strain NQ354 ($\Delta lacI$) is a *lacI* knock-out mutant [44]. *rpoS* knockout was transferred from JW5437-1 to NCM3722 via P1 transduction to yield strain NQ1191.

A.1.2 Culture medium

The culture medium used in this study was based on N^-C^- minimal medium [219], containing K_2SO_4 (1 g), $K_2HPO_4 \cdot 3H_2O$ (17.7 g), KH_2PO_4 (4.7 g), $MgSO_4 \cdot 7H_2O$ (0.1 g) and NaCl (2.5 g) per liter. The medium was supplemented with 20 mM NH_4Cl, as nitrogen source, and 5 mM glycerol, as the sole carbon source. 1 mM IPTG was added to media when necessary to fully induce the native *lac operon*. All chemicals were purchased from Carl Roth, Karlsruhe, Germany.

A.1.3 Growth protocol

Before each experiment, cells were taken from $-80°C$ glycerol stock and streaked out on an LB agar plate. Growth was then carried out in three steps: seed culture, pre-culture and experimental culture, each cultured at 37°C in a water bath shaker at 250 rpm. The seed culture was prepared with fresh LB medium and inoculated with a single colony. The pre-culture was performed in medium identical to the experimental culture, inoculated with a small amount of seed culture previously washed by centrifugation. The size of the inoculum was chosen such that the pre-culture grown overnight was still growing exponentially in the morning of the experiment. Cells performed at least ten doublings in the pre-culture. Inoculation into pre-warmed experimental culture in the morning was chosen such that cells performed at least three additional doublings in the experimental culture before growth was measured. The limiting nutrient in the growth medium, 5 mM glycerol, was depleted at an optical density (OD_{600}) of around 0.5 and a cell density of about $5 \cdot 10^8$ CFU/ml. Due to the high affinity of the glycerol uptake system (K_M of about 5 µM [147]), the period in which growth was affected by the changing glycerol concentration was short. Due to the absence of acetate excretion of this strain in this medium [143], no significant amount of metabolizable waste products remained in the medium. Instead of inducing starvation by glycerol depletion, cells could also be washed

by centrifugation (3000 RCF for 3 min) with no significant differences in the death rate. For small culture volumes, 5 ml of experimental culture were grown in 20 mm x 150 mm glass test tubes (Fisher Scientific, Hampton, NH, USA) with disposable, polypropylene Kim-Kap closures (Kimble Chase, Vineland, NJ, USA). Larger volumes, 25, 50 and 100 ml were grown in 125, 250 and 500 ml baffled Erlenmeyer flasks (Carl Roth), respectively, and Kim-Kap closures. All cultures were grown in a shaking water bath (WSB-30, Witeg, Wertheim, Germany) with water bath preservative (Akasolv, Akadia, Mannheim, Germany). To measure growth, at each time point, a 200 µl sample was extracted and optical density was measured using a 1 mm path length Sub-Micro Cuvette (Starna, Ilford, United Kingdom) at 600 nm in a Spectrophotometer (Genesys 20, ThermoScientific. Waltham, MA, USA).

A.1.4 Starvation

Viability was measured by plating on LB agar and counting the colony forming units (CFU) after an incubation period of 12 hours at 37°C. Samples were diluted in fresh N^-C^- minimal medium without carbon substrate and spread on LB agar using Rattler Plating Beads (Zymo Research, Irvine, CA, USA). LB agar was supplemented with 25 µg/ml 2,3,5-triphenyltetrazolium chloride to stain colonies and increase contrast for automated colony counting (Scan 1200, Interscience, Saint-Nom-la-Bretche, France) of 100-200 colonies per Petri dish (92 x 16 mm, Sarstedt, Nmbrecht, Germany). Staining or automation of counting had no significant effect on viability measurements or accuracy, compared to un-stained, manually counted samples ($< 1\%$ systematic error).

A.1.5 Survival on supernatant

In order to measure cell survival on the supernatant of a starved culture, starved cells from an exponentially dying culture were diluted 4.5-fold to a density of $N \sim 6 \cdot 10^7$ CFU/ml both into supernatant of the same control culture and into fresh medium free of carbon used as a control. At this dilution, cells showed a clear lag, while for dilution to lower cell concentrations, regrowth of cells was observed. In order to measure cell viability on the supernatant without dead cells, a sample of the supernatant of a control culture was extracted and frozen at the end of exponential growth when all the cells in the culture were still viable and there were no dead cell in the supernatant. After 2 days of starvation of the control culture, the frozen supernatant was defrosted and starved cells from the control culture were diluted 4.5-fold to a density of $N \sim 6 \cdot 10^7$ CFU/ml into this supernatant. In all the cases, the supernatant was extracted by vacuum filtering the desired amount of control culture using 0.2 mm PES filter units. Viability of the new test tubes containing supernatant and fresh medium respectively was measured every day by plate counting. The lag time was calculated by measuring the average viability ratio of the number of viable cells in the culture with supernatant addition, N_{SN}, and the number of viable cells in the control culture with fresh medium, N_{FM}, as $T = \ln(< N_{\mathrm{SN}}/N_{\mathrm{FM}} >)/\gamma$.

A.1.6 Time-lapse video of survival

The existence of cryptic growth was checked using time-lapse microscopy. Cells grown in batch culture until glycerol depletion were extracted, stained with propidium iodide to detect loss of membrane integrity and filled into an Ibidi µ-Slide. The µ-Slide I Ibidi with one channel (wxlxh= 5x50x0.4 mm, 100 µl volume) and two reservoirs of 600 µl volume was used. The two reservoirs were completely filled with starved culture and sealed with parafilm to reduce evaporation. Cells were monitored for 6 days with continuous acquisition of phase-contrast and fluorescence images every 30 min, using a Nikon Ti-E microscope with the Nikon Imaging Software NIS Elements

4.40 (Nikon, Tokyo, Japan). A phase contrast Plan Apo 100x oil objective was used, with numerical aperture of 1.45 and a refractive index of 1.515 (Nikon, Tokyo, Japan) and an Andor Zyla VSC-02357 camera (Zyla-5.5, Andor, Belfast, Northern Ireland) with a binning of 1x1, a readout rate of 200 MHz and an exposure time of 200 ms. Conversion gain was set on 1/3 Dual gain and the spurious noise filter was activated. The calibration from length units to pixel was defined as 0.07 µm/px. Measurements were performed with activated perfect focus system and a PriorScan III drive stage.

A.1.7 Live/dead stain

Established commercial BacLight LIVE/DEAD (Thermo Fisher Scientific Inc., Waltham, Massachusetts, USA) staining was used when cells were microscopically imaged, according to manufacturing specifications.

A.1.8 UV sterilization

In order to UV-sterilize cell cultures, a sample was extracted from the control culture and pipetted into a Sarstedt 92x16 mm plastic Petri dish to increase surface area and facilitate exposure. The Petri dish was then placed in a peqlab PCR Workstation Pro workbench equipped with two General Electric G25t8 25W UV-lamps for sterilization. The Petri dish was placed directly under the lamps without lid and irradiated at 254 nm for 30 min. Complete sterilization was confirmed by plating 100 µl directly on an agar plate and checking the absence of regrowth. This treatment was chosen under the assumption that it presumably preserves the nutritional content of the cell, as opposed to chemical or temperature treatments, and is complete, as opposed to mechanical methods.

A.1.9 Lag time caused by addition of UV-killed cells

To quantify the influence of an addition of UV-killed cells on the death of the carbon starved cells, a fraction of an exponentially dying culture was extracted and UV-sterilized using the above described method. The UV-sterilized culture was then mixed with the starved culture at different mixing ratios. Since both viable and UV-sterilized cultures originated from the same culture, the ratio of viable cells N to UV-killed cells N_{UV} was equal to the volume mixing ratio. After the addition of UV-killed cells, viability was measured at least every 24 hours by plate counting both in the control culture (N) and in the samples with added UV-killed cells (N_+). The lag time was then calculated as $T = \ln(< N_+/N >)/\gamma$, where the brackets denote the time average of the ratio during the exponential decay that follows the initial lag time and both viabilities were normalized to 100% at the time-point of extraction.

A.1.10 RNA measurements

To measure RNA concentration in the sample, ultraviolet (UV) absorbance at a wavelength of 260 nm was used. Concentration was calculated using the 260 nm reading and a conversion factor based on the extinction coefficient for each nucleic acid (A260 of 1.0 = 40 µg/ml for RNA). The method is based on the one used by [220] with modifications as described in [44].

A.1.11 Total protein measurements

Total protein was quantified using commercial micro BCA assay. To measure concentration, the sample was added to the tube or plate containing the prepared BCA Working Reagent. After a

30-minutes incubation at 37°C and cooling to room temperature, the resultant purple color was measured at 562 nm.

A.1.12 Quantification of the maintenance rate

In order to quantify the maintenance rate β during starvation, at different times during starvation, samples of at least 3 ml were extracted from an exponentially decaying culture and a small amount of glycerol was added in each of them. The amount of glycerol was chosen in such a way that cells could not grow substantially using the supplied carbon substrate. In particular, at each time-point, in different samples, 10, 20, 30 and 40 µM of glycerol were added to cultures of approximately 10^8 CFU/ml. In comparison, the growth yield on 40 µM is around $4{\cdot}10^6$ CFU/ml, i.e. only 4% of the viability at addition. After glycerol addition, cell viability was measured at least every 24 hours by plate counting both in the control culture $N(t)$ and in the samples with glycerol added $N_{\rm gly}(t)$. The lag time was then calculated as $T = \ln(< N_{\rm gly}/N >)/\gamma$, where the brackets denote an average over all time points after the initial lag, when all cultures are in exponential decay. Using the theoretical expression of T, see Eq. (2.6), for each day, β was extracted from the inverse of the slope of the linear fit of the experimental lag times plotted versus the amount of glycerol added per cell (see Fig. 2.8).

A.1.13 LacY titration

LacY activity was titrated by adding the isopropyl β-D-1-thiogalactopyranoside (IPTG), which inhibits repression of the *lac* operon, at different time-points during growth at saturating concentrations (1 mM). The earlier IPTG was added to the culture during growth the more LacY was expressed until the end of growth. Lac expression is about 100-fold lower during starvation than during growth, see Fig. 2.4F, and does not significantly alter the high expression levels inherited from growth. LacZ activity (co-expressed with LacY) was measured in each culture using the Miller-Assay [221], using the protocol described in [44].

A.1.14 Quantification of the yield

In order to quantify changes of the yield α, the growth yield during starvation was measured both for WT and Δ*rpoS* strains: at different times during starvation (from 0 to 7 days), 3 to 15 ml of the control culture was extracted, UV-sterilized and mixed in a 99% to 1% ratio with untreated, starved culture. Viability of the growth curve $N_{\rm G}$ was then measured every 12-24 h by plate counting. The growth yield $\alpha_{\rm G}$, proportional to the yield α, was calculated as the ratio of the absolute growth yield, $\max(N_{\rm G}) - \min(N_{\rm G})$, where $\min(N_{\rm G})$ is the inoculation viability and $\max(N_{\rm G})$ the maximal viability reached at the end of growth, to the viability in the control culture at the extraction point during starvation $N(t_{\rm ex})$.

A.1.15 Statistical analysis

Values of the main quantities μ, γ, α and β are averages of at least three experimental repeats, reported with one standard deviation.
Statistical significance of α and β values between wild-type and Δ*rpoS* strains was calculated with a two-sample t-test ($p<0.01$).

A.2 Supplementary Figures

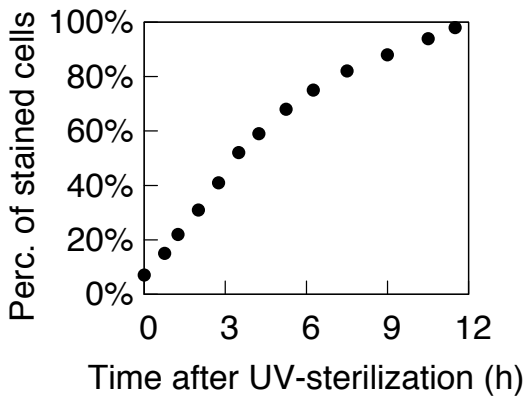

Figure A.1: Loss of membrane integrity after UV sterilization. After UV sterilization, performed as described in Section A.1.8, the culture loses its entire viability. At different times after UV sterilization, samples are extracted and cells stained using a commercial Live/Dead stain (see Section A.1.7), which reports a loss of membrane integrity. Within 4 h, half of the UV-killed cells loose its membrane integrity. This loss of membrane integrity after UV irradiation is fast compared to the half-life of the population during starvation, which is about 1.6 days.

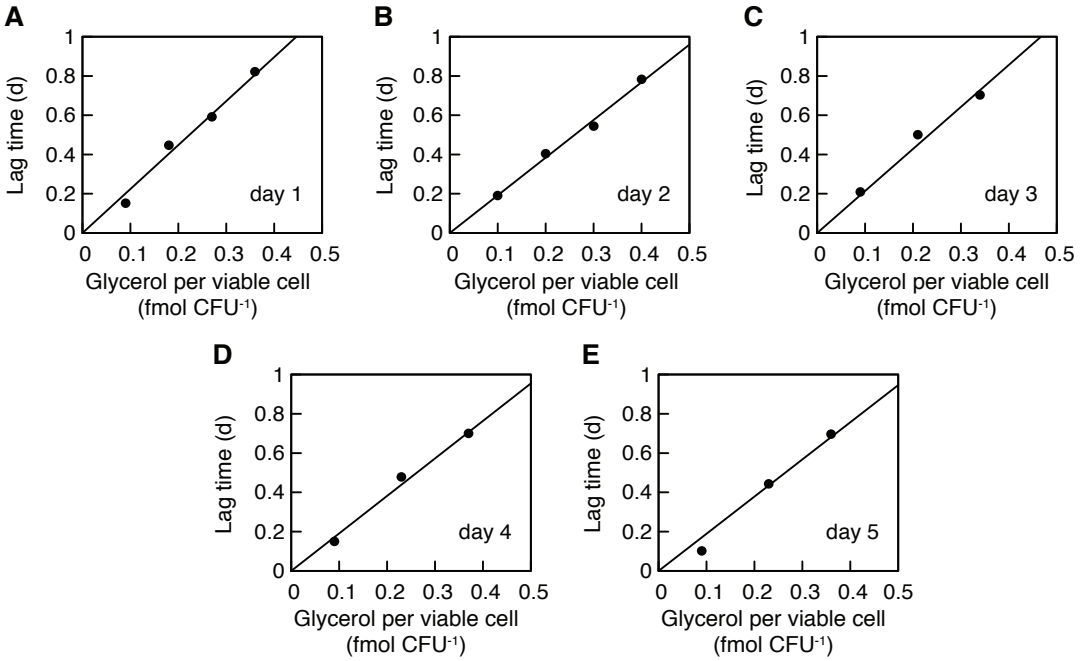

Figure A.2: Lag times due to glycerol addition after starvation. Fig. 2.8B shows a 1 day starved culture with a viability of 10^8 CFU/ml that is supplemented with 40 µM of glycerol prolonging the survival of the cells. Per viable cell, the glycerol addition in this experiment is 0.4 fmol/CFU. The same experiment is repeated after 2,3,4,5 days of starvation, using different glycerol concentrations (see Section A.1.12). **(A-E)** Lag times recorded at different days increase linearly with the amount of supplemented glycerol. From the inverse of the slopes of the black lines in these panels, we calculate the maintenance rate $\beta = (0.49 \pm 0.04)$ fmol/(CFU $\cdot$ d), as shown in Fig. 2.8.

A.3 Supplementary Table

Repeat n.	Wild-type (1/d)	Δ*rpoS* (1/d)
1	0.43	0.77
2	0.41	0.74
3	0.41	0.74
4	0.46	0.84
5	0.43	0.74
6	0.46	0.84
7	0.41	0.74
8	0.48	0.77
9	0.50	0.82
10	0.41	0.74
11	0.38	0.84
12	0.41	0.72
Average	0.43 ± 0.04	0.78 ± 0.04

Table A.1: Death rates of wild-type cells and Δ*rpoS* mutants. Representative selection of death rates fitted to 12 independent experiments of the exponential decay of viability of wild-type and Δ*rpoS* mutants (Fig. 2.1B and Fig. 2.12A). The average value is reported with one standard deviation.

Appendix B

Slower growth of *E. coli* leads to longer survival in starvation

B.1 Methods

B.1.1 Strains

All strains used in this study are derived from wild-type *E. coli* K-12 strain NCM3722 (WT) [218]. *rpoS* knockout was transferred from JW5437-1 to NCM3722 via P1 transduction to yield strain NQ1191. Glycerol kinase mutant GlpK22 [171] was transferred via P1 transduction to yield strain NQ898.

B.1.2 Culture medium

The culture medium used both in the chemostat and in batch cultures is based on N^-C^- minimal medium [219], containing K_2SO_4 (1 g), $K_2HPO_4 \cdot 3H_2O$ (17.7 g), KH_2PO_4 (4.7 g), $MgSO_4 \cdot 7H_2O$ (0.1 g) and NaCl (2.5 g) per liter. The medium was supplemented with 20 mM NH_4Cl, as nitrogen source, and 5 mM glycerol, as the sole carbon source. All chemicals were purchased from Carl Roth, Karlsruhe, Germany.

B.1.3 Growth protocol

Before each experiment, cells were taken from $-80°C$ glycerol stock and streaked out on an LB agar plate.

Growth in batch cultures

For growth in batch cultures, the same protocol described in Appendix A was applied. However, due to acetate excretion in the medium in the presence of carbon sources different from glycerol and at growth rates higher than 0.7 h^{-1} (e.g. growth of NQ898) [143], before entry into starvation, cells were centrifuged (3000 RCF for 3 min), washed and re-supplemented with medium free of carbon to avoid survival on waste products such as acetate. When no left-nutrients are available, this washing step does not alter cell physiology.

Growth in chemostat

Growth was carried out in three steps: seed- and pre-culture in batch mode and continuous culture in a chemostat. The first two steps were performed at 37°C in a water bath shaker

at 250 rpm (WSB-30, Witeg, Wertheim, Germany) with water bath preservative (Akasolv, Akadia, Mannheim, Germany). The seed culture was prepared with fresh LB medium and inoculated with a single colony from the LB agar plate. The pre-culture was performed in medium identical to the continuous culture, inoculated with a small amount of seed culture previously washed by centrifugation. The size of the inoculum was chosen such that the pre-culture grown overnight was still growing exponentially in the morning of the experiment. The seed culture was performed in 20 mm x 150 mm glass test tubes (Fisher Scientific, Hampton, NH, USA) with disposable, polypropylene Kim-Kap closures (Kimble Chase, Vineland, NJ, USA). The pre-culture had a volume of 200 ml and was performed in 500 ml baffled Erlenmeyer flasks (Carl Roth) and Kim-Kap closures. Once cells in the pre-culture have performed at least ten doubling and the optical density of the culture had reached the value $OD_{600} \approx 2$, 100 ml of the pre-culture were inoculated in 1 l of minimal medium supplemented with glycerol in the chemostat. Cells grew in such medium for ≈ 2 h in batch mode, reaching $OD_{600} \approx 0.5$ at the time of glycerol depletion. Then, continuous culture mode was applied and cells were grown in a constant volume of 1 l at 37°C with air-pressured spilling out the effluent at this volume, while the flow rate was controlled by the pump speed of the incoming feed. The bioreactor used was a Infors HT, Labfors 5 with 2.0 l glass vessel, controlled by its intrinsic Control-Software. Air flow at 2 vvm and stirrer speed of 500 rpm were applied to keep the dissolved oxygen concentration with the relative pO_2 greater than 90% for all experiments, to avoid limiting in oxygen. pH was kept at 7 ± 0.2 by a pH probe and automatic addition of a solution of 2% H_3PO_4. Optical cell density was kept constant between 0.35 and 0.55. Different dilution rates were established by changing the pump speed and the cultivations were performed from low to high growth rates (0.1, 0.2, 0.3, 0.4, 0.5, 0.7 h^{-1}). For each growth rate, steady state growth was reached within few minutes after setting the growth rate. However, to obtain a complete turn-over of the cells in the culture, for each growth rate chosen, six generations were performed before extracting the sample for starvation. It has been reported that glucose-limited chemostat cultivations strongly select for loss or attenuation of RpoS function in *E. coli* so that mutations occur in *rpoS* after 30 generations [161]. To avoid this possibility in our glycerol case, the experiment did not run for more than 30 generations.

B.1.4 Starvation protocol

For each growth rate in batch culture and chemostat, cells were centrifuged (3000 RCF for 3 min), washed and re-suspended in minimal medium free of carbon in 20 mm x 150 mm glass test tubes (Fisher Scientific, Hampton, NH, USA) with disposable, polypropylene Kim-Kap closures (Kimble Chase, Vineland, NJ, USA). The tubes were placed in the water bath shaker at 250 rpm as the seed- and pre-cultures and viability was measured by plating on LB agar and counting the colony forming units (CFU) after an incubation period of 12 hours at 37 degrees. For each growth rate, three tubes of starved cultures were monitored in order to have 3 experimental repeats of cell behavior during starvation. For each growth rate in the chemostat, after six generations, samples of the culture were extracted from the chemostat, using a SI Sample Syringe (20 ml, with 3-Way valve and check valve, C-Flex inlet) to avoid contaminations and to flush the line prior to sampling. In this way the line being sampled did not have residual fluid left in it from an earlier sample. At the extraction time, a sample of the chemostat culture was immediately plated on LB agar plates through dilution steps to check for contaminations and mutations in the chemostat. Then, cells were washed and starved as described above. For growth rates of 0.3 and 0.7 h^{-1}, two independent chemostat and starvation runs were performed. Samples were diluted in fresh N^-C^- minimal medium without carbon substrate and spread on LB agar using Rattler Plating Beads (Zymo Research, Irvine, CA, USA). LB agar was supplemented with 25 µg/ml of

2,3,5-triphenyltetrazolium chloride to stain colonies and increase contrast for automated colony counting (Scan 1200, Interscience, Saint-Nom-la-Bretche, France) of 100-200 colonies per Petri dish (92 x 16 mm, Sarstedt, Nümbrecht, Germany). Staining or automation of counting had no significant effect on viability measurements or accuracy, compared to un-stained, manually counted samples ($< 1\%$ systematic error).

B.1.5 Quantification of yield and maintenance rate

Maintenance rate and yield were measured as described in Appendix A. Measurements were performed for starved cultures of WT previously grown in the chemostat at growth rates of 0.1, 0.3, 0.5 and 0.7 h^{-1}, respectively, and for the starved culture of GlpK22 (NQ898) previously grown in batch mode at growth rate of 0.9 h^{-1}.

Yield

In order to quantify changes of the yield α, the absolute yield during starvation was measured both for WT and $\Delta rpoS$ strains: at different times during starvation (from 0 to 7 days) 3 to 15 ml of the control culture was extracted, UV-sterilized and mixed in a 99% to 1% ratio with untreated, starved culture. Viability of the growth curve N_{G} was then measured every 24 h by plate counting. The yield α, was calculated as the ratio of the absolute growth yield, $\max(N_{\mathrm{G}}) - \min(N_{\mathrm{G}})$, where $\min(N_{\mathrm{G}})$ is the inoculation viability and $\max(N_{\mathrm{G}})$ the maximal viability reached at the end of growth, to the viability in the control starved culture at the extraction point before killing (Fig. 3.3A-D).

Maintenance rate

In order to quantify the maintenance β during starvation, after 5 days of starvation, samples of at least 3 ml were extracted from an exponentially decaying culture and a small amount of glycerol was added in each of them. The amount of glycerol was chosen in such a way that cells could not grow substantially using the supplied carbon substrate. In particular, at each time-point, in different samples, 10, 20, 30 and and 40 µM of glycerol were added to cultures of approximately 10^8 CFU/ml. After glycerol addition, cell viability was measured at least every 24 hours by plate counting both in the control culture $N(t)$ and in the samples with glycerol added $N_{\mathrm{gly}}(t)$. The lag time was then calculated as $T = \ln(< N_{\mathrm{gly}}/N >)/\gamma$, where the brackets denote an average over all time points after the initial lag, when all cultures are in exponential decay. Using the theoretical expression of T, derived in Chapter 2, for each day, β was extracted from the inverse of the slope of the linear fit of the experimental lag times plotted versus the amount of glycerol added per cell (Fig. 3.3E-H).

B.1.6 Live/dead stain

As in Appendix A, the established commercial BacLight LIVE/DEAD (Thermo Fisher Scientific Inc., Waltham, Massachusetts, USA) staining was used when cells were microscopically imaged, according to manufacturing specifications.

B.1.7 Measurements of cell size

To measure cell size, samples from batch or continuous cultures were extracted, stained, placed on a cover slide and imaged with phase-contrast microscopy, using a Nikon Ti-E microscope with a Plan Apo 100x oil objective (numerical aperture of 1.45 and a refractive index of 1.515). The used camera was an Andor Zyla VSC-02357, with a binning of 1x1, a readout rate of 200 MHz and an exposure time of 200 ms. Conversion gain was set on 1/3 Dual gain and the spurious noise filter was activated. The calibration from length units to pixel was defined as 0.07 µm/px. Measurements were performed with an activated perfect focus system, taking 10x10 image frames and moving the sample with a PriorScan III drive stage after each acquisition step. Cell areas were then manually determined using the Nikon Imaging Software NIS Elements 4.40 (Nikon, Tokyo, Japan). For each growth rate, at least 200 cells were analyzed to determine averaged length and width. Cell volume was computed as $V = \pi(w/2)^2(l-w) + (4/3)\pi(l/2)^3$ where w=width and l=length of each cell, whose shape was considered as a cylinder (with base ray equal to w/2 and height equal to $(l-w)$) with two semi-spheres at the ends (with ray equal to $w/2$).

B.1.8 Statistical analysis

μ values in the chemostat are reported with an error of 5%, due the chemostat accuracy.
μ values in batch cultures and γ values are the averages of at least three experimental repeats, reported with one standard deviation.
Values of cell lengths, widths and volume are the averages of 200 microscopy measurements, reported with one standard deviation.
α and β values are the slopes of the fits (see Section B.1.5) reported with 95% confidence bounds.
α and β values normalized per cell volume are reported with error propagation, where we consider an instrument error of 5% for the volume measurements.
Error of the exponential fits of cells size, yield, maintenance and death rate plotted against growth rates are reported with 95% confidence bounds.

B.2 Supplementary Figures

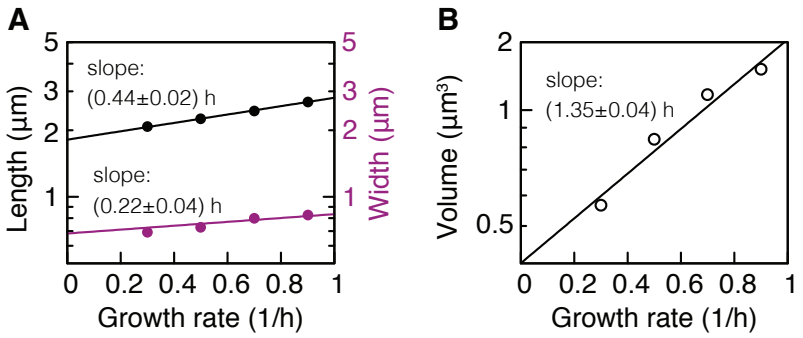

Figure B.1: Size of wild-type cells and GlpK22 mutants during steady state growth. (A) Measured length (black) and width (purple) of wild-type cells growing in the chemostat at different steady-state growth rates ($\mu = 0.3, 0.5, 0.7$ h^{-1} and GlpK22 cells growing in batch culture at $\mu = 0.9$ h^{-1}). Black and purple lines are exponential fits. Measurements are in agreement with data reported in [222], within a standard deviation of 0.22. **(B)** Volume of the cells computed as explained in Fig. 3.4 (see also Section B.1.7). In agreement with literature [35], volume increases exponentially with growth rate (black line, exponential fit).

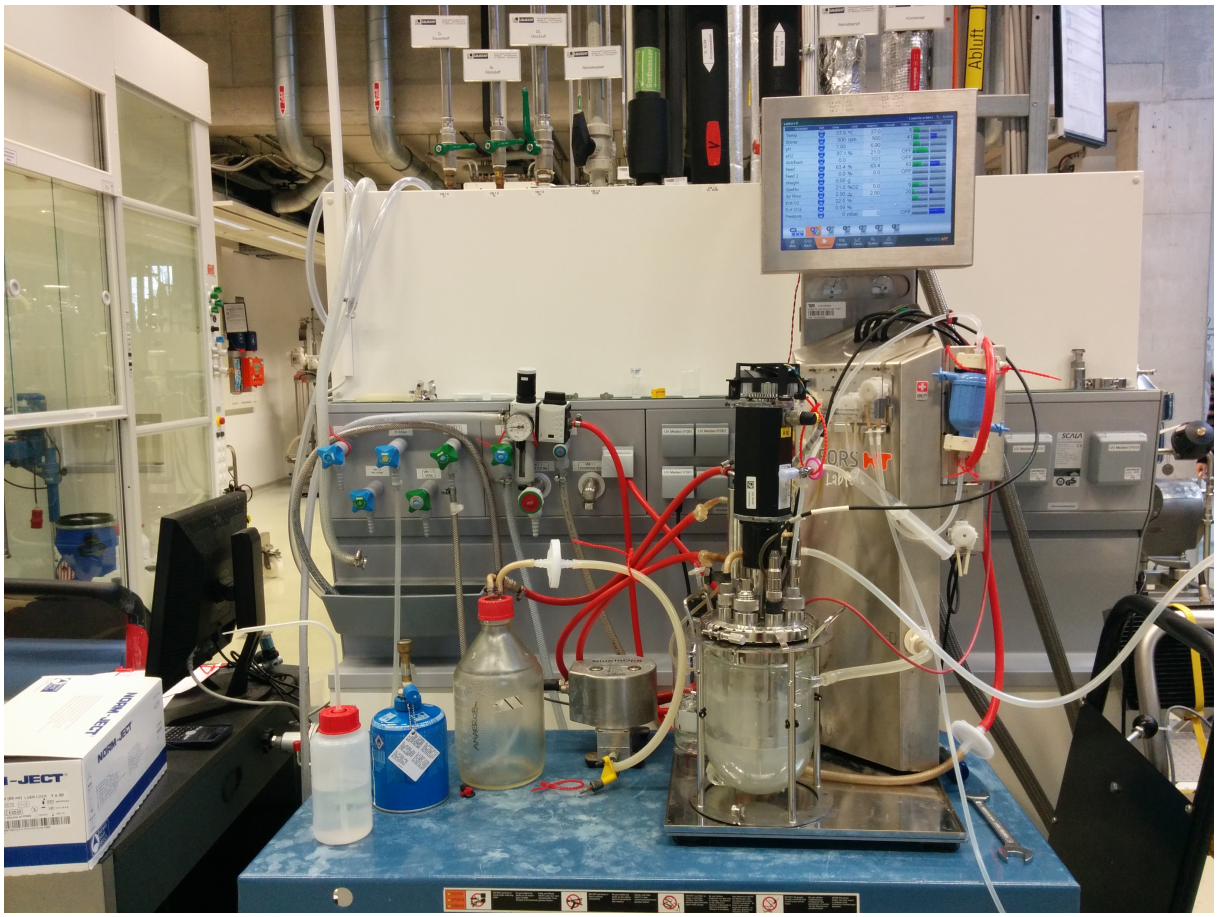

Figure B.2: Bioreactor used for continuous culture. Experimental setup for continuous culture: the bioreactor Infors HT, Labfors 5 with 2.0 l glass vessel, controlled by its intrinsic Control-Software, works with air flow at 2 vvm, stirrer speed of 500 rpm, relative pO_2 greater than 90%, pH at 7 ± 0.2 and optical cell density OD_{600} between 0.35 and 0.55. Cells grow in a constant volume of 1 l, where the flow rate is controlled by the pump speed of the incoming feed, at 37°C. Different dilution rates are established by changing the pump speed. We thank Dr. Dominik Maslak and Prof. Dirk Weuster-Botz for providing the experimental set-up and technical support.

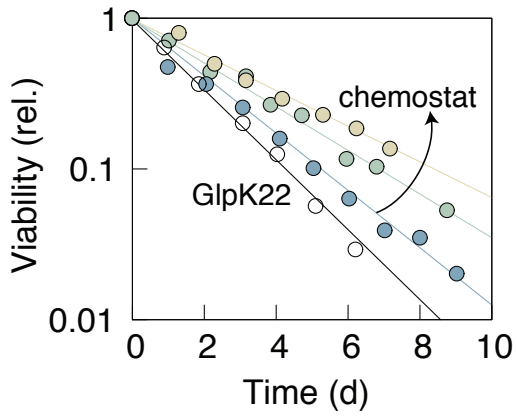

Figure B.3: Survival kinetics of wild-type cells and GlpK22 mutants after growth rate titration. Survival kinetics of wild-type cells grown in chemostat at growth rates $\mu = 0.3, 0.5, 0.7$ h^{-1} (colored data) and GlpK22 mutants grown in batch at $\mu = 0.9$ h^{-1} (white circles). Symbols and colors correspond to the ones in the legend of Fig. 3.2. Experimental data are shown normalized to the highest viability value at the beginning of starvation. All the cultures die exponentially, spanning a range from 0.25 d^{-1} (WT previously grown at 0.3 h^{-1}, yellow circles) to 0.59 d^{-1} (GlpK22, previously grown at 0.9 h^{-1}, white circles).

B.3 Supplementary Tables

Strain	Growth mode	Carbon source	Growth rate (1/h)	Death rate (1/d)
WT	batch	LB	2.00 ± 0.01	1.44 ± 0.05
WT	batch	CAA+Glucose	1.31 ± 0.01	0.72 ± 0.08
WT	batch	CAA + Glycerol	1.20 ± 0.01	0.59 ± 0.02
WT	batch	Glucose	0.92 ± 0.01	0.51 ± 0.03
WT	batch	Lactose	0.91 ± 0.01	0.50 ± 0.01
WT	batch	Xylose	0.75 ± 0.01	0.45 ± 0.01
WT	batch	Glycerol	0.70 ± 0.01	0.43 ± 0.04
WT	batch	Succinate	0.69 ± 0.01	0.41 ± 0.03
WT	batch	CAA	0.53 ± 0.01	0.36 ± 0.02
WT	batch	Acetate	0.42 ± 0.01	0.31 ± 0.02
WT	batch	Mannose	0.29 ± 0.01	0.26 ± 0.01
WT	batch	Proline	0.27 ± 0.01	0.31 ± 0.03
WT	batch	Glutamate	0.13 ± 0.01	0.27 ± 0.02
WT	chemostat	Glycerol	0.70 ± 0.03	0.40 ± 0.04
WT	chemostat	Glycerol	0.50 ± 0.02	0.34 ± 0.03
WT	chemostat	Glycerol	0.40 ± 0.02	0.30 ± 0.04
WT	chemostat	Glycerol	0.30 ± 0.01	0.29 ± 0.04
WT	chemostat	Glycerol	0.20 ± 0.01	0.26 ± 0.04
WT	chemostat	Glycerol	0.10 ± 0.01	0.25 ± 0.02
GlpK22	batch	Glycerol	0.90 ± 0.01	0.59 ± 0.04

Table B.1: Growth and death rates of wild-type cells and GlpK22 mutants. Wild type cells (WT) and GlpK22 mutants (NQ898) are grown in batch or continuous cultures in minimal medium supplemented with different carbon sources. Growth rate values in the chemostat are reported with an error of 5%, due to the feeding pump. Growth rate values in batch cultures and death rate values are averages of three independent experimental repeats, reported with one standard deviation. Note that the wild-type culture grown at 0.7 h^{-1} in the chemostat shows a death rate of $\gamma_{\mu=0.7/h} = 0.40 \pm 0.04$ d^{-1}, which is in good agreement with the batch culture value $\gamma_{batch} = 0.43 \pm 0.04$ d^{-1}, where cells also grow at 0.7 h^{-1}.

Strain	Growth mode	Growth rate (1/h)	Death rate (1/d)	Yield	Maintenance rate (fmol/(CFU · d))
WT	chemostat	0.1 ± 0.01	0.25 ± 0.02	0.12 ± 0.01	0.16 ± 0.01
WT	chemostat	0.3 ± 0.01	0.29 ± 0.04	0.14 ± 0.01	0.28 ± 0.02
WT	chemostat	0.5 ± 0.02	0.34 ± 0.03	0.17 ± 0.03	0.38 ± 0.02
WT	chemostat	0.7 ± 0.03	0.40 ± 0.04	0.18 ± 0.02	0.48 ± 0.05
WT	batch	0.7 ± 0.01	0.43 ± 0.04	0.18 ± 0.01	0.49 ± 0.04
GlpK22	batch	0.9 ± 0.01	0.59 ± 0.04	0.23 ± 0.01	0.81 ± 0.06

Table B.2: Yield and maintenance rate values. Yield and maintenance rate values of wild-type cells (WT) and GlpK22 mutants (NQ898) grown in batch or continuous cultures in minimal medium supplemented with glycerol. Relative growth rates and death rates are also reported (see also Table B.1). Yield and maintenance values are reported with 95% confidence bounds.

Strain	Growth mode	Growth rate (1/h)	Death rate (1/d)	Length (µm)	Width (µm)	Volume (µm^3)	Yield (1/µm^3)	Maintenance rate (fmol/(CFU · d· µm^3))
WT	chemostat	0.1 ± 0.01	0.25 ± 0.02	1.57 ± 0.39	0.65 ± 0.11	0.45 ± 0.17	0.27 ± 0.04	0.36 ± 0.05
WT	chemostat	0.3 ± 0.01	0.29 ± 0.04	1.59 ± 0.38	0.69 ± 0.10	0.52 ± 0.18	0.26 ± 0.03	0.53 ± 0.06
WT	chemostat	0.5 ± 0.02	0.34 ± 0.03	1.72 ± 0.21	0.77 ± 0.09	0.69 ± 0.21	0.25 ± 0.05	0.55 ± 0.05
WT	chemostat	0.7 ± 0.03	0.40 ± 0.04	1.80 ± 0.48	0.80 ± 0.10	0.77 ± 0.20	0.23 ± 0.03	0.64 ± 0.08
WT	batch	0.7 ± 0.01	0.43 ± 0.04	1.83 ± 0.35	0.81 ± 0.11	0.80 ± 0.23	0.23 ± 0.02	0.68 ± 0.06
GlpK22	batch	0.9 ± 0.01	0.59 ± 0.04	1.85 ± 0.38	0.83 ± 0.14	0.86 ± 0.24	0.26 ± 0.02	0.94 ± 0.09

Table B.3: Yield and maintenance rate values per cell volume. Yield and maintenance rate per cell volume values reported with relative length, width and volume of wild-type cells (WT) and GlpK22 mutants (NQ898) grown in batch or continuous cultures in minimal medium supplemented with glycerol. Relative growth rates and death rates are also reported (see also Table B.1). Cell length and width values are averages of 200 cells, reported with one standard deviation. Cell volume is calculated from length and width as described in Methods, also reported with one standard deviation. We then estimate that cell volumes are determined only to about 5%, due to limitations of phase contrast microscopy. These uncertainties of cell volume measurements are propagated into recycling yield and maintenance rate per volume.

Strain	Growth mode	Carbon source	Growth rate (1/h)	Death rate (1/d)
Δ*rpoS*	batch	CAA+Glucose	1.32 ± 0.01	0.88 ± 0.05
Δ*rpoS*	batch	CAA+Glycerol	1.15 ± 0.01	0.74 ± 0.03
Δ*rpoS*	batch	Xylose	0.73 ± 0.01	0.73 ± 0.01
Δ*rpoS*	batch	Glycerol	0.70 ± 0.01	0.72 ± 0.02
Δ*rpoS*	batch	Succinate	0.69 ± 0.01	0.61 ± 0.04
Δ*rpoS*	batch	Acetate	0.44 ± 0.01	0.60 ± 0.04
Δ*rpoS*	batch	Mannose	0.38 ± 0.01	0.53 ± 0.05
Δ*rpoS*	batch	Proline	0.34 ± 0.01	0.50 ± 0.03
Δ*rpoS*	batch	Glutamate	0.13 ± 0.01	0.46 ± 0.01

Table B.4: Growth and death rates of Δ*rpoS* mutants grown in different media. Growth and death rates of Δ*rpoS* mutants grown in batch cultures in minimal medium supplemented with different carbon sources. Growth rate and death rate values are averages of three independent experimental repeats, reported with one standard deviation.

Appendix C

A thermal fuse in *E. coli* leads to survival at elevated temperatures

C.1 Supplementary Material for the growth-dormancy model

In this section, we derive theoretical solutions for the model discussed in Chapter 4. In particular, we focus on the stability analysis, the MetA recovery threshold and the derivation of the lag times. In addition, we make a detailed estimation of the theoretical parameters of the model from measurements in the literature.

C.1.1 Stability analysis

We discuss the stability of the non-linear equation system proposed in Eq. (4.1), Eq. (4.2), Eq. (4.3) of Chapter 4. The standard approach to stability analysis requires derivation of the two nullclines of the system, where 1) the methionine concentration and 2) the active MetA abundance are constant [223]. At the intersection of the two nullclines, we find the "fixed points". When the system evolves, the cells will relax towards the stable fixed points (and away from the unstable fixed points). In our case, the possible stable fixed-point positions are growth or dormancy and their existence is discussed thereafter. We first derive the nullclines and then the criteria for the existence of the fixed points.

In Eq. (4.2) of Chapter 4 we derived the dynamics of the internal methionine concentration as

$$\frac{\mathrm{d}c_{\mathrm{met}}}{\mathrm{d}t} = j_{\mathrm{MetA}}(\phi_{\mathrm{MetA}}) + j_{\mathrm{in}} - j_{\mathrm{p}}(c_{\mathrm{met}}) - j_{\mathrm{d}}(c_{\mathrm{met}}) - \mu c_{\mathrm{met}} \tag{C.1}$$

with the individual contributions being

$$j_{\mathrm{MetA}} = h\phi_{\mathrm{MetA}}, \tag{C.2}$$

$$j_{\mathrm{p}} = c_{\mathrm{met}}^{\mathrm{pro}} k_{\mathrm{p}} c_{\mathrm{met}} = c_{\mathrm{met}}^{\mathrm{pro}} \mu, \tag{C.3}$$

$$j_{\mathrm{d}} = k_{\mathrm{d}} g(c_{\mathrm{met}}), \tag{C.4}$$

$$j_{\mathrm{in}} = \mathrm{const} > 0, \tag{C.5}$$

$$\mu = k_{\mathrm{p}} c_{\mathrm{met}}, \tag{C.6}$$

$$g(c_{\mathrm{met}}) = c_{\mathrm{met}}/(K_{\mathrm{M}} + c_{\mathrm{met}}). \tag{C.7}$$

The nullcline of the methionine concentration is defined as the curve in the space of ϕ_{MetA} and c_{met}, in which $\mathrm{d}c_{\mathrm{met}}/\mathrm{d}t = 0$. Setting Eq. (C.1) to zero, we get

$$\frac{\mathrm{d}c_{\mathrm{met}}}{\mathrm{d}t} = f_1(\phi_{\mathrm{MetA}}, c_{\mathrm{met}}) = h\phi_{\mathrm{MetA}} + j_{\mathrm{in}} - c_{\mathrm{met}}^{\mathrm{pro}} k_{\mathrm{p}} c_{\mathrm{met}} - k_{\mathrm{d}} g(c_{\mathrm{met}}) - k_{\mathrm{p}} c_{\mathrm{met}}^2 = 0. \tag{C.8}$$

By solving this equation for ϕ_{MetA} and defining new parameters: $a_1 = c_{\mathrm{met}}^{\mathrm{pro}} k_{\mathrm{p}} h^{-1}$, $a_2 = k_{\mathrm{d}} h^{-1}$ and $a_3 = k_{\mathrm{p}} h^{-1}$, as well as $\tilde{j}_{\mathrm{in}} = j_{\mathrm{in}} h^{-1}$, we derive the nullcline of the methionine concentration,

$$\phi_{\mathrm{MetA}} = a_1 c_{\mathrm{met}} + a_2 g(c_{\mathrm{met}}) + a_3 c_{\mathrm{met}}^2 - \tilde{j}_{\mathrm{in}}. \tag{C.9}$$

Next, we discuss the MetA abundance, where the dynamics was derived in Chapter 4 in Eq. (4.3). Setting Eq. (4.3) to zero, we get

$$\frac{\mathrm{d}\phi_{\mathrm{MetA}}}{\mathrm{d}t} = f_2(\phi_{\mathrm{MetA}}, c_{\mathrm{met}}) = \chi_{\mathrm{MetA}} \mu(c_{\mathrm{met}}) - (\eta(\mathrm{T}) + \mu(c_{\mathrm{met}}))\phi_{\mathrm{MetA}} = 0. \tag{C.10}$$

By solving for ϕ_{MetA}, we obtain the nullcline for the active MetA abundance to be

$$\phi_{\mathrm{MetA}} = \chi_{\mathrm{MetA}} c_{\mathrm{met}}/(\tilde{\eta} + c_{\mathrm{met}}), \tag{C.11}$$

where we define a new variable $\tilde{\eta} = \eta k_{\mathrm{p}}^{-1}$ and use $\mu = k_{\mathrm{p}} c_{\mathrm{met}}$ from Eq. (4.1) of Chapter 4.

The fixed points of the system are found at the intersection of both nullclines, i.e.

$$\chi_{\mathrm{MetA}} \frac{c_{\mathrm{met}}^*}{(\tilde{\eta} + c_{\mathrm{met}}^*)} = \phi_{\mathrm{MetA}} = a_1 c_{\mathrm{met}}^* + a_2 g(c_{\mathrm{met}}^*) + a_3 c_{\mathrm{met}}^{*2} - \tilde{j}_{\mathrm{in}} \tag{C.12}$$

where c_{met}^* is the fixed-point of the methionine concentration. The fixed-point of the MetA abundance ϕ_{MetA}^* can then be obtained by plugging in c_{met}^* into either nullcline.

Depending on the parameter regime, there are either one, two or three fixed-points in the regime $c_{\mathrm{met}} \geq 0$ and $\phi_{\mathrm{MetA}} \geq 0$. We can get vital information about the system by calculating stability criteria analytically. We consider the simplest case of no external methionine influx $\tilde{j}_{\mathrm{in}} = 0$, where the trivial solution of the fixed-point equation, Eq. (C.12), is $c_{\mathrm{met}}^{\mathrm{d}} = 0$ and $\phi_{\mathrm{MetA}}^{\mathrm{d}} = 0$. This fixed-point corresponds to dormancy, thus the superscript "d", because in this case the steady state growth rate is zero, $\mu^{\mathrm{d}} = k_{\mathrm{p}} c_{\mathrm{met}}^{\mathrm{d}} = 0$. This fixed-point can either be stable, i.e. the cell will stop growing when close to this fixed-point, or unstable, i.e. the cell will start growing, even at very low c_{met} and ϕ_{MetA} levels. The stability can be checked using the Jacobian matrix of the system, defined as

$$J = \begin{pmatrix} \frac{\partial f_1}{\partial c_{\mathrm{met}}} & \frac{\partial f_1}{\partial \phi_{\mathrm{MetA}}} \\ \frac{\partial f_2}{\partial c_{\mathrm{met}}} & \frac{\partial f_2}{\partial \phi_{\mathrm{MetA}}} \end{pmatrix}.$$

At the trivial fixed point $c_{\mathrm{met}}^{\mathrm{d}} = 0$ and $\phi_{\mathrm{MetA}}^{\mathrm{d}} = 0$, we find

$$J = \begin{pmatrix} -h(a_1 + a_2/K_{\mathrm{M}}) & h \\ \chi_{\mathrm{MetA}} k_{\mathrm{p}} & -\eta \end{pmatrix}.$$

The stability of the fixed point can then be checked by computing the trace

$$\tau = \frac{\partial f_1}{\partial c_{\mathrm{met}}} + \frac{\partial f_2}{\partial \phi_{\mathrm{MetA}}} \tag{C.13}$$

and the determinant

$$\Delta = \frac{\partial f_1}{\partial c_{\mathrm{met}}}\frac{\partial f_2}{\partial \phi_{\mathrm{MetA}}} - \frac{\partial f_1}{\partial \phi_{\mathrm{MetA}}}\frac{\partial f_2}{\partial c_{\mathrm{met}}} \tag{C.14}$$

of the Jacobian matrix [223]. Because the trace $\tau = -(h(a_1 + a_2/K_{\mathrm{M}}) + \eta)$ is negative, the stability is determined solely by the sign of the determinant $\Delta = h(a_1 + a_2/K_{\mathrm{M}})\eta - h\chi_{\mathrm{MetA}}k_{\mathrm{p}}$. If $\Delta > 0$, then the dormancy fixed-point is stable.

This condition is met if

$$\eta > \frac{\chi_{\mathrm{A}}k_{\mathrm{p}}}{a_1 + a_2/K_{\mathrm{M}}} \tag{C.15}$$

which can be formulated in terms of the original parameters as

$$\eta > \frac{\chi_{\mathrm{MetA}}h}{c_{\mathrm{met}}^{\mathrm{pro}} + k_{\mathrm{d}}/(k_{\mathrm{p}}K_{\mathrm{M}})}. \tag{C.16}$$

To get an analytical estimate for the stability criterium of the growth fixed-point, we make several simplifying assumptions. We first note that the MetA abundance nullcline levels to a constant, $\phi_{\mathrm{MetA}} \to \chi_{\mathrm{MetA}} = \mathrm{const}$, for high methionine concentrations, while the methionine nullcline increases monotonically to infinity in the same limit, $\phi_{\mathrm{MetA}} \to \infty$. Thus, if at low methionine concentrations, the methionine nullcline is ever lower than the MetA abundance nullcline, these two nullclines will cross and create a fixed-point at finite growth, $c_{\mathrm{met}}^{\mathrm{g}} > 0$ and $\phi_{\mathrm{MetA}}^{\mathrm{g}} > 0$, where the superscript "g" stands for growth.

There are two possibilities for the methionine nullcline f_1 to be lower than the MetA abundance nullcline f_2. The first option is that for very low methionine concentration, $0 < c_{\mathrm{met}} \ll K_{\mathrm{M}}$, the methionine nullcline increases less than the MetA abundance nullcline, $\mathrm{d}f_1/\mathrm{d}c_{\mathrm{met}} < \mathrm{d}f_2/\mathrm{d}c_{\mathrm{met}}$. Testing this was the essence of the stability analysis done for the dormancy fixed-point: if the dormancy fixed point is stable, $\mathrm{d}f_1/\mathrm{d}c_{\mathrm{met}} > \mathrm{d}f_2/\mathrm{d}c_{\mathrm{met}}$; if the dormancy fixed point is unstable, $\mathrm{d}f_1/\mathrm{d}c_{\mathrm{met}} < \mathrm{d}f_2/\mathrm{d}c_{\mathrm{met}}$. The second option is that, at a higher methionine concentration, the methionine nullcline becomes lower than the MetA nullcline again. We estimate the regime where this happens, by comparing the two nullclines at relatively low methionine concentrations $K_{\mathrm{M}} \ll c_{\mathrm{met}} \ll c_{\mathrm{met}}^{\mathrm{g}}$, in the regime where the drain has already saturated, i.e. $g(c_{\mathrm{met}}) = 1$, but the methionine concentration is still low compared to the steady state, $c_{\mathrm{met}}^{\mathrm{g}}$.

In this regime, the methionine nullcline can be approximated as $f_1 \approx a_1 c_{\mathrm{met}} + a_2$, by omitting quadratic terms in Eq. (C.9). The MetA abundance nullcline in the same regime can be approximated as $f_2 \approx \chi_{\mathrm{MetA}}\tilde{\eta}^{-1}c_{\mathrm{met}}$, when we omit higher order terms in Eq. (C.11). Combined, these two approximations yield that, if $a_1 c_{\mathrm{met}} + a_2 < \chi_{\mathrm{MetA}}\tilde{\eta}^{-1}c_{\mathrm{met}}$, then the methionine nullcline lies below the MetA nullcline.

As a upper limit, we can then conclude that, if

$$\tilde{\eta} < \frac{\chi_{\mathrm{MetA}}}{a_1} \tag{C.17}$$

or, in the original parameters,

$$\eta < \frac{\chi_{\mathrm{MetA}} h}{c_{\mathrm{met}}^{\mathrm{pro}}} \tag{C.18}$$

then, at low methionine concentrations, the methionine nullcline can lie below the MetA nullcline and the growth fixed-point exists.

From the above analysis we conclude that three distinct regimes exist. First, if

$$\eta > \frac{\chi_{\mathrm{MetA}} h}{c_{\mathrm{met}}^{\mathrm{pro}} + k_{\mathrm{d}}/(k_{\mathrm{p}} K_{\mathrm{M}})}, \tag{C.19}$$

the cells do not grow. Second, if

$$\frac{\chi_{\mathrm{MetA}} h}{c_{\mathrm{met}}^{\mathrm{pro}} + k_{\mathrm{d}}/(k_{\mathrm{p}} K_{\mathrm{M}})} < \eta < \frac{\chi_{\mathrm{MetA}} h}{c_{\mathrm{met}}^{\mathrm{pro}}}, \tag{C.20}$$

both a stable growth and dormancy fixed-points exist. Third, if

$$\eta < \frac{\chi_{\mathrm{MetA}} h}{c_{\mathrm{met}}^{\mathrm{pro}}}, \tag{C.21}$$

only a growth state exists.

C.1.2 Calculation of the recovery threshold

In the case the environment permits two stable fixed-points, growth and dormancy, the question is in which will an individual cell end. To address this question, we calculate the necessary MetA abundance for recovery, called "recovery threshold" in Chapter 4. Above this threshold, the cell will have enough MetA to start producing more methionine and, conversely, more MetA. Below the threshold, too much methionine is drained, the degradation of MetA is faster than the production of new MetA and the cells will end in a stable state of dormancy.

Separation of time-scales

In starvation, the internal metabolite concentrations will drop quickly, i.e. $c_{\mathrm{met}} \approx 0$, and the MetA abundance will decay slowly,

$$\left.\frac{\mathrm{d}\phi_{\mathrm{MetA}}}{\mathrm{d}t}\right|_{c_{\mathrm{met}}=0} = -\eta \phi_{\mathrm{MetA}}. \tag{C.22}$$

During this decay, at some point, the cell will cross a threshold $\phi_{\mathrm{MetA}}^{\mathrm{th}}$, below which it cannot recover.

To estimate the dynamics following the nutrient recovery, we first simplify the dynamics of the system. We find that at low methionine concentrations, $c_{\mathrm{met}} \approx 0$, the dynamics of the internal methionine concentration, Eq. (4.2) in Chapter 4, can be approximated as

$$\left.\frac{\mathrm{d}c_{\mathrm{met}}}{\mathrm{d}t}\right|_{c_{\mathrm{met}}=0} = j_{\mathrm{in}} + h\phi_{\mathrm{MetA}}. \tag{C.23}$$

Eq. (C.23) means that in the absence of methionine, there is no protein production, no drain to polyamine synthesis and, because there is no growth, there is no dilution. The dynamics is entirely determined by production, $h\phi_{\mathrm{MetA}}$, and import, j_{in}. To get an estimate of the time-scale of this recovery, we calculate the rate change of methionine production

$$\left.\frac{\mathrm{d}\log c_{\mathrm{met}}}{\mathrm{d}t}\right|_{c_{\mathrm{met}}=0} = \frac{j_{\mathrm{in}} + h\phi_{\mathrm{MetA}}}{c_{\mathrm{met}}} \gg \frac{j_{\mathrm{in}} + h\phi_{\mathrm{MetA}}}{c^{\mathrm{g}}_{\mathrm{met}}} \approx 80\mathrm{h}^{-1}, \tag{C.24}$$

where we used the upper bound that the methionine concentration c_{met} is lower than the growth steady state $c^{\mathrm{g}}_{\mathrm{met}} = 1.5 \cdot 10^{-4}$ M. In comparison, the dynamics of the MetA abundance at $c_{\mathrm{met}} \approx 0$ is still mostly determined by degradation, as synthesis is small. We thus can estimate the rate change of the MetA abundance as

$$\left.\frac{\mathrm{d}\log \phi_{\mathrm{MetA}}}{\mathrm{d}t}\right|_{c_{\mathrm{met}}=0} = -\eta \approx -1.6\mathrm{h}^{-1}. \tag{C.25}$$

When we compare Eq. (C.24) with Eq. (C.25), we see that methionine relaxes much faster than MetA. This common feature of cellular metabolism allows us to separate the dynamics of the system into a fast and slow phase. We now use this to calculate the unstable fixed-point.

Calculation of the unstable fixed-point

The fact that the time scale of methionine recovery is faster than MetA means that, first, methionine concentration will increase, until consumption of methionine matches production. This is mathematically given by the nullcline $\mathrm{d}c_{\mathrm{met}}/\mathrm{d}t = 0$, Eq. (C.8), at a constant ϕ_{MetA} that equals the initial condition. Thereafter, both c_{met} and ϕ_{MetA} will slowly increase or decrease together, until they finally converge to either the growth or dormancy steady state.

Whether they increase or decrease depends on whether the fast phase ends at a position above or below the unstable fixed-point on the methionine nullcline. A cell that starts from the threshold $c_{\mathrm{met}} = 0$ and $\phi^{\mathrm{th}}_{\mathrm{MetA}}$ will land on the unstable fixed-point, $c_{\mathrm{met}} = c^{\mathrm{unst}}_{\mathrm{met}}$ and $\phi_{\mathrm{MetA}} = \phi^{\mathrm{unst}}_{\mathrm{MetA}}$.

Because during this phase ϕ_{MetA} is largely constant, we conclude that the threshold abundance of MetA, $\phi^{\mathrm{th}}_{\mathrm{MetA}}$, is roughly equal to the MetA abundance at the unstable fixed point,

$$\phi^{\mathrm{th}}_{\mathrm{MetA}} \approx \phi^{\mathrm{unst}}_{\mathrm{MetA}}. \tag{C.26}$$

We can calculate the position of the unstable fixed point related to the above discussion of the two stable fixed points that led to the conditions of the three stability regimes, Eq. (C.19), Eq. (C.20), Eq. (C.21).

In the regime around the unstable fixed point, drain has saturated, $g(c_{\mathrm{met}}) = 1$. At the same time, c_{met} is still much smaller than that at the growth fixed-point, $c^{\mathrm{g}}_{\mathrm{met}}$. Mathematically, this regime is given by $K_{\mathrm{M}} \ll c_{\mathrm{met}} \ll c^{\mathrm{g}}_{\mathrm{met}}$. In this case, the methionine nullcline is given by $\phi_{\mathrm{MetA}} \approx a_1 c_{\mathrm{met}} + a_2 - \tilde{j}_{\mathrm{in}}$ and the MetA abundance nullcline is given by $\phi_{\mathrm{MetA}} \approx \chi_{\mathrm{MetA}} \tilde{\eta}^{-1} c_{\mathrm{met}}$. Solving the MetA abundance nullcline for c_{met} and inserting it into the methionine nullcline gives us an estimate for the unstable fixed point,

$$\phi^{\mathrm{unst}}_{\mathrm{MetA}} = \frac{a_2 - \tilde{j}_{\mathrm{in}}}{1 - a_1 \tilde{\eta} \chi^{-1}_{\mathrm{MetA}}} \tag{C.27}$$

or, written in the original parameters,

$$\phi^{\mathrm{unst}}_{\mathrm{MetA}} = \frac{1}{h} \frac{k_{\mathrm{d}} - j_{\mathrm{in}}}{1 - h c^{\mathrm{pro}}_{\mathrm{met}} \eta \chi^{-1}_{\mathrm{MetA}}}. \tag{C.28}$$

Eq. (C.28) then defines the growth threshold, because of Eq. (C.26).

C.1.3 Calculation of the lag time

In this section, we aim to estimate the lag times of the population. Lag times are caused by the recovery of a small, growing subpopulation. For this reason, we first study the heterogeneity of gene expression that leads to the subpopulations, second, what determines the size of the subpopulations and third, how the size of the subpopulations affects the lag time.

Heterogeneity in MetA abundance

We investigate how the existence of a threshold can lead to a separation of the population into two growth and dormancy states. Generally, it is known that gene expression is a highly heterogeneous process, due to the stochastic synthesis and degradation of mRNAs and proteins [205, 206]. Phenomenologically, the abundance of proteins such as MetA is well described by a gamma distribution [205, 206],

$$p(\phi_{\mathrm{MetA}}) = \frac{\phi_{\mathrm{MetA}}^{a-1} e^{-\phi_{\mathrm{MetA}} b^{-1}}}{\Gamma(a) b^a}, \tag{C.29}$$

where a is the number of mRNA synthesized per cell cycle and b the number of proteins synthesized per mRNA. Due to the nature of the gamma distribution, the square root of the inverse of a also equals the noise, $\sqrt{a^{-1}} = \sigma/\xi$, and b equals the Fano factor, $b = \sigma^2/\xi$, where σ is the standard deviation and $\xi = ab$ is the average. In Table C.2, Table C.3, Table C.4, we estimate the average MetA abundance, $\phi^*_{\mathrm{MetA}} = 6.13 \cdot 10^{-4} = \xi$. In order to estimate the noise, we take the median noise, $\sqrt{a^{-1}_{median}} = \sigma/\xi$, of proteins with an average copy number of more than 10 [206] and find $\sqrt{a^{-1}_{median}} = 0.4$. We use this value to plot the gamma distribution of MetA in Chapter 4.

Calculation of lag times

During starvation, the abundance of MetA decays exponentially due to thermal inactivation [98],

$$\phi_{\mathrm{MetA}}(t) = \phi_{\mathrm{MetA}}(0) e^{-\eta t}, \tag{C.30}$$

and the MetA abundance in many cells will fall below the threshold $\phi^{\mathrm{th}}_{\mathrm{MetA}}$ required for growth, calculated in Eq. (C.28). By saying that all cells above the threshold will recover and cells below the threshold will not recover, we implicitly neglect gene expression noise during recovery.

We can calculate the number of recovering cells by integrating the probability distribution, Eq. (C.29), obtained after a starvation time τ, from the growth threshold $\phi^{\mathrm{th}}_{\mathrm{MetA}}$ to infinity,

$$\Pi(\phi^{\mathrm{th}}_{\mathrm{MetA}}, \tau) = \int_{\phi^{\mathrm{th}}_{\mathrm{MetA}}}^{\infty} p(\phi_{\mathrm{MetA}}(\tau)) \mathrm{d}\phi_{\mathrm{MetA}}. \tag{C.31}$$

We can estimate the resulting lag time by assuming that recovery of individual cells is fast. Then, lag time will be entirely determined by a growing population Π (growing immediately at growth rate μ) and a dormant population $1 - \Pi$ (that will never grow). These dynamics of the two subpopulations and the resulting lag time is sketched in Chapter 4 in Fig. 4.5C.

The resulting biomass growth of the population, is given by

$$M(t) = M(0)((1 - \Pi(\phi^{\text{th}}_{\text{MetA}}, \tau)) + \Pi(\phi^{\text{th}}_{\text{MetA}}, \tau)e^{\mu t}). \tag{C.32}$$

In order to calculate the lag time, we study the asymptotic growth, when the growing subpopulation has out-grown the non-growing population. In this regime, $\Pi(\phi^{\text{th}}_{\text{MetA}}, \tau)e^{\mu t} \gg 1$, and the biomass growth reaches

$$M(t) = M(0)\Pi(\phi^{\text{th}}_{\text{MetA}}, \tau)e^{\mu t} = M(0)e^{\mu(t-T_{\text{lag}})} \tag{C.33}$$

with the lag time

$$T_{\text{lag}} = \frac{1}{\mu}\ln\left(\frac{1}{\Pi(\phi^{\text{th}}_{\text{MetA}}, \tau)}\right). \tag{C.34}$$

Scaling of lag time with physiological parameters

To understand the impact of experimental perturbations, such as these performed in Chapter 4, we look for analytical scaling laws between the measurable output lag time and biological parameters such as MetA pre-expression, starvation time and MetA decay rate. For this, we note that long lag times are caused by very small growing subpopulations. The growing subpopulation $\Pi(\phi^{\text{th}}_{\text{MetA}}, \tau)$ becomes small when the threshold $\phi^{\text{th}}_{\text{MetA}}$ is much larger than the mean of the distribution $p(\phi_{\text{MetA}}(\tau))$. Thus, the growing subpopulation is represented by the tail of the gamma distribution, which is exponential with MetA abundance $\phi_{\text{MetA}}(t)$ that decreases during starvation, and is given by

$$p(\phi_{\text{MetA}}) \propto e^{-\phi_{\text{MetA}}(t)b^{-1}}. \tag{C.35}$$

We can then obtain the growing subpopulation after a certain starvation time τ using Eq. (C.31),

$$\Pi(\phi^{\text{th}}_{\text{MetA}}, \tau) \propto e^{-\phi^{\text{th}}_{\text{MetA}}b^{-1}e^{\eta\tau}}. \tag{C.36}$$

The growing subpopulation thus scales with a

- double-exponential form with starvation time τ,
- double-exponential form with MetA decay rate η,
- exponentially with the growth threshold $\phi^{\text{th}}_{\text{MetA}}$,
- exponentially with the inverse of MetA mean pre-expression $\xi = ab$.

By plugging in the growing subpopulation, Eq. (C.36), our derivation of lag time, Eq. (C.34), we find the scaling law of lag time:

$$T_{\text{lag}} \propto \text{const} + \phi^{\text{th}}_{\text{MetA}}b^{-1}e^{\eta\tau}. \tag{C.37}$$

In summary, lag time scales approximately

- exponentially with starvation time τ,
- exponentially with MetA decay rate η,
- linearly with the growth threshold $\phi^{\text{th}}_{\text{MetA}}$,
- linearly with the inverse of the mean MetA pre-expression $\xi = ab$.

C.1.4 Estimates on physiological parameters

Using published physiological characterization of *E. coli*, we can estimate the parameters used in the theory. The results are summarized in Table C.2, Table C.3, Table C.4 and Table C.5.

Growth physiology

At 45 degrees, *E. coli* in minimal medium supplemented with glycerol has a growth rate of about $\mu^g = 0.45$ h^{-1}, see Table C.1 and Table C.2. The typical cell volume in minimal medium is about $V = 1.3$ µm^3 $= 1.3 \cdot 10^{-15}$ l, with a protein mass of about M=165 pg [93]. The exact numbers of volume and mass do not matter for the bistability conditions, but serve the purpose to estimate parameters such as the MetA copy number per cell.

Methionine and related compounds

The internal concentration of free methionine (molar mass $m_{\mathrm{met}} = 149$ g/mol) in cells growing in minimal medium is about $c^{\mathrm{g}}_{\mathrm{met}} = 150$ µM [224]. Based on this internal methionine concentration, we can calculate the proportionality constant between methionine concentration and growth rate, $k_{\mathrm{p}} = \mu^{\mathrm{g}} c^{\mathrm{g}^{-1}}_{\mathrm{met}} = 3.0 \cdot 10^3$ M/h.

The spermidine concentration, the major polyamine that drains methionine, is found at about $c_{\mathrm{spe}} = 1.4$ mM [93]. The synthesis of each spermidine requires one S-adenosyl-methionine, which is directly draining the methionine pool. The resulting byproduct, S-methyl-thioadenosine, cannot be recycled back to methionine without passage through MetA.

While the spermidine pool is 10-fold larger than the free methionine pool, we note that the majority of the methionine is bound inside proteins, where they make up about 3.23% of the protein mass, see Table C.3. This corresponds to a methionine concentration of about $c^{\mathrm{pro}}_{\mathrm{met}} = 3.23\% M m^{-1}_{\mathrm{met}} V^{-1} = 27.5$ mM.

Thus, we conclude that during growth, about 27.5 mM / 1.4 mM = 20 fold more methionine goes into protein synthesis than into spermidine synthesis. In terms of systems parameters, this ratio can be written as

$$\frac{k_{\mathrm{d}}}{\mu^{\mathrm{g}} c^{\mathrm{pro}}_{\mathrm{met}}} = \frac{1}{20} \tag{C.38}$$

where we assume that $g(c_{\mathrm{met}})$ is saturated at $g(c_{\mathrm{met}}) = 1$ at full growth.

Enzymatic parameters of MetA

From the measured copy number of MetA, $N_{\mathrm{MetA}} = 1711$ [207], we can estimate the abundance $\phi_{\mathrm{MetA}} = N_{\mathrm{MetA}} m_{\mathrm{MetA}} M^{-1} N_{\mathrm{A}}^{-1} = 6.13 \cdot 10^{-4}$, if we use the Avogadro number, $N_{\mathrm{A}} = 6.022 \cdot 10^{23}$ mol^{-1}, the typical cell mass $M = 165$ pg and the molar mass of MetA, $m_{\mathrm{MetA}} = 3.56 \cdot 10^4$ g/mol. From the MetA abundance, we estimate the methionine production rate by MetA, h, as $h = (c_{met} + c^{pro}_{met}) \mu^{\mathrm{g}} \phi^{\mathrm{g}-1}_{\mathrm{MetA}} = 20.3$ M/h.

The decay rate of MetA is about $\eta(37°\mathrm{C}) = 1.1$ h^{-1} at 37°C and increases to $\eta(45°\mathrm{C}) = 1.6$ h^{-1} at 45°C [98]. In order to maintain a steady state MetA abundance of $\phi^{\mathrm{g}}_{\mathrm{MetA}} = 6.13 \cdot 10^{-4}$ at grow rate $\mu^{\mathrm{g}} = 0.45$ h^{-1}, the synthesis fraction of MetA, defined as the fraction of the protein

mass synthesis that is directed to MetA, has to be $\chi_{\mathrm{MetA}} = \phi_{\mathrm{MetA}}(\eta + \mu^{\mathrm{g}})/\mu^{\mathrm{g}} = 2.79 \cdot 10^{-3}$, where we used Eq. (C.11).

Compound parameters

The above parameters together determine the essential parameters of the system, a_1, a_2, a_3 and $\tilde{\eta}$ that are summarized in Table C.4.

C.2 Methods

C.2.1 Strains

All strains used in this study are derived from wild type *E. coli* K-12 strain NCM3722 [30]. The titratable $P_{LTet-O1}$-*metA* was assembled with PCR-amplified *km-rrn*BT-$P_{LTet-O1}$ using pKD13-*rrn*BT:$P_{LTet-O1}$ plasmid as the template and PCR-amplified *metA* gene using the *IntS* site flanking primers by the Gibson Assembly method. The resultant *km:rrn*BT:$P_{LTet-O1}$-*metA* was electroporated and recombined into the *IntS* site of a strain that already contains $P_{LTet-O1}$-*tetR* at the *ycad* site [43, 225]. The correct construct was selected with Kanamycin+ plates and confirmed by sequencing. The construct was further subjected to the knockout of the original *metA* gene with P1 transduction and named YCE76. The elimination of the kanamycin resistance cassette was done with pCP20 plasmid. Knock-outs of *luxS* and *metA* were transfered from JW2662 and JW3973 to NCM3722 strain via P1 transduction. Amino acid substitutions I229Y and LYD in strains JW3973-I229Y (ΔMetA) and JW3973-LYD (ΔMetA), respectively [98], were transferred to NCM3722 ΔMetA to yield strains YCE55 (NCM3722 $metA^{\mathrm{I229Y}}$) and YCE57 (NCM3722 $metA^{\mathrm{LYD}}$).

C.2.2 Culture medium

The culture medium used was based on N^-C^- minimal medium, containing K_2SO_4 (1 g), $K_2HPO_4 \cdot 3H_2O$ (17.7 g), KH_2PO_4 (4.7 g), $MgSO_4 \cdot 7H_2O$ (0.1 g) and NaCl (2.5 g) per liter. The medium was supplemented with 20 mM NH_4Cl, as nitrogen source, and 5 or 10 mM glycerol, as the sole carbon source. When needed, ampicillin and/or exogenous methionine were added to the culture. The working concentration of ampicillin used was 100 µg/ml and the stock solution was stored at -20°C. The working concentration of methionine normally used was 0.067 mM and the stock solutions were stored at 4°C. We also tested cell regrowth with different concentrations of methionine within the range 6.7 mM - $6.7 \cdot 10^{-5}$ mM. We found that the lag time before cell regrowth was completely abolished only by a methionine concentration of 0.067 mM. Lower concentrations were not enough to promote growth, while higher concentrations probably created methionine in excess, causing the production of too much cysteine, that is toxic for bacteria and increases the lag before regrowth [226]. In the case of the *metA* titratable strain YCE76, chlortetracycline (cTc) was used as inducer (0-24 ng/ml). All chemicals were purchased from Carl Roth, Karlsruhe, Germany.

C.2.3 Growth and starvation protocol

Cells were taken from a -80°C glycerol stock, streaked out on a LB agar plate and incubated around 12 hours at 37°C. Then a single colony was picked and grown in batch culture. For temperatures up to 39°C, cells were grown first on LB at the desired temperature (seed culture). Before reaching starvation, they were diluted and inoculated into pre-warmed minimal medium with glycerol (pre-culture). Cells grew in the pre-culture for several doublings to ensure exponential growth and were then diluted and inoculated into pre-warmed glycerol-minimal medium (experimental culture). Inoculation into the latter was chosen such that cells performed at least three additional doublings in the experimental culture before growth was measured. For high temperatures (above 39°C), the seed culture medium used was glycerol minimal medium with 1% LB in order to help the transition of the cells into the pre-culture. For small culture volumes, 5 ml of culture were grown in 20 mm x 150 mm glass test tubes (Fisher Scientific, Hampton, NH, USA) with disposable, polypropylene Kim-Kap closures (Kimble Chase, Vineland, NJ, USA). Larger volumes, 25, 50 and 100 ml were grown in 125, 250 and 500 ml baffled Erlenmeyer flasks

(Carl Roth, Karlsruhe, Germany), respectively, and Kim-Kap closures. All cultures were grown in a shaking water bath (WSB-30, Witeg, Wertheim, Germany) with water bath preservative (Akasolv, Akadia, Mannheim, Germany). After glycerol depletion, cell survival was quantified with viability measurements by plating on LB agar and counting the colony forming units (CFU) after an incubation period of 12 hours at 37°C. Samples were diluted in fresh N^-C^- minimal medium without carbon substrate and spread on LB agar using Rattler Plating Beads (Zymo Research, Irvine, CA, USA). LB agar was supplemented with 25 µg/ml 2,3,5-triphenyltetrazolium chloride to stain colonies and increase contrast for automated colony counting (Scan 1200, Interscience, Saint-Nom-la-Bretche, France) of 100-200 colonies per petri dish (92 x 16 mm, Sarstedt, Nümbrecht, Germany).

C.2.4 Protocol to induce population-wide dormancy at high temperatures

Bacteria were first grown in minimal medium supplemented with glycerol as a carbon substrate as described in Section C.2.3. After carbon depletion, cultures were starved for a certain time to allow depletion of MetA by degradation in the absence of de-novo synthesis. Then, the cultures were diluted into fresh medium with new glycerol and cells were allowed to recover with or without addition of exogenous methionine. Depending on the starvation time prior to dilution, the dilution factor used and the presence or absence of exogenous methionine, different lag times before regrowth were observed by optical density measurements (OD_{600}). In the experiments performed to test the growth-dormancy model, cultures were also diluted into their own supernatant, the supernatant of other cultures or medium from a starved culture where cells were previously killed with UV-light.

C.2.5 Quantification of the lag time

The lag time after glycerol re-addition was extracted from optical density measurements and corrected for the loss of viability during the period of starvation. Growth was modeled as $OD_{600} = A + Be^{\mu t}$, which, for long times, converges to $OD_{600} \approx Be^{\mu t} = (A + B)e^{\mu}(t - T_{\mathrm{lag}})$, with lag time T_{lag}. We extracted growth rate μ and the growing fraction of cells, B, from the time derivative of optical density $dOD_{600}/dt = \mu Be^{\mu t}$, using a fit across the recovery regime where the time derivative increases exponentially. The lag time $T_{\mathrm{lag}} = -\mu^{-1}\ln(B/(A + B))$ can then be calculated from the extracted parameters. Lastly, because optical density measurements do not distinguish between living and dead cells in the culture, we corrected the lag time estimation by subtracting the number of dead cells N_{d} from the initial number $N(0) = A + B$. This gives a correction factor $-\mu^{-1}\ln(N(0)/N_{\mathrm{d}})$. For 5 h starvation at 45°C, about one third of the cells perish. Thus, with growth rate 0.45 h^{-1} at 45°C, this yields a correction factor of 0.9 h. In Chapter 4, all lag times are corrected for perished cells.

C.2.6 Live/dead stain

Established commercial BacLight LIVE/DEAD (Thermo Fisher Scientific Inc., Waltham, Massachusetts, USA) staining was used when cells were microscopically imaged, according to manufacturing specifications.

C.2.7 Time-lapse microscopy

Microscopy was performed using agar pads in glass-bottom dishes. Agar pads contained medium identical to the culture medium, N^-C^-, supplemented with 20 mM NH_4Cl, 20 mM of glycerol and 2% agar-agar (Carl Roth, Karlsruhe, Germany). Cells were diluted and pipetted on the

pre-warmed agar pad. After the surface of the agar pad had dried, the agar pad was flipped on the glass window of a pre-warmed glass bottom dish (35 mm dish with 20 mm bottom well (In Vitro Scientific, USA). The glass bottom dishes were sealed with parafilm to reduce evaporation.

Time-lapse microscopy was performed using a Nikon Ti-E microscope with the Nikon Imaging Software NIS Elements 4.40 (Nikon, Tokyo, Japan). A phase contrast Plan Apo 100x oil objective was used, with numerical aperture of 1.45, a refractive index of 1.515 (Nikon, Tokyo, Japan) and a Andor Zyla VSC-02357 camera (Zyla-5.5, Andor, Belfast, Northern Ireland) with a binning of 1x1, a readout rate of 200 MHz and an exposure time of 200 ms. Conversion gain was set on 1/3 Dual gain and the spurious noise filter was activated. The calibration from length units to pixel was defined as 0.07 µm/px. Measurements were performed with activated perfect focus system and a PriorScan III drive stage. Temperature control was set by the Okolab Cage Incubation System and confirmed with a manual temperature measurements. Cell growth was monitored for 24 hours with continuous acquisition of phase-contrast and fluorescence images every 30 min at the desired temperature, e.g. 45°C.

C.2.8 Antibiotic treatment and survival quantification

To measure survival upon antibiotic treatment, cells were first grown in minimal medium with glycerol, as described in Section C.2.3. A first sample of the culture was extracted during exponential growth ($OD_{600} \sim 0.3 - 0.4$) and supplemented with ampicillin and glycerol with or without methionine. A second sample of the culture was extracted after 5 hours of starvation upon glycerol depletion, diluted 8 fold and supplemented with ampicillin and glycerol with or without methionine. Viability was then measured over time by plate counting, as described in Section C.2.3.

C.2.9 Heat shocks and survival quantification

Heat shocks were performed by transferring batch cultures (5 ml culture volume in a 20 mm x 150 mm borosilicate glass tube, Fisher Scientific, NH, USA) from one water bath to another (WSB-30, Witeg, Wertheim, Germany). Water baths were pre-set and equilibrated at the desired temperatures. To measure survival upon heat shocks, cells were first grown in minimal medium with glycerol, as described in Section C.2.3. A first sample of the culture was extracted during exponential growth ($OD_{600} \sim 0.3 - 0.4$), supplemented again with glycerol to avoid glycerol exhaustion and shifted to 50°C. A second sample of the culture was extracted after 3 hours of starvation upon glycerol depletion and shifted to 50°C. Viability was then measured over time by plate counting, as described in Section C.2.3.

C.2.10 Numerical analysis of the model

The numerical solution in Fig. 4.5 was obtained by numerically integrating Eq. (4.2) and Eq. (4.3) using the nonstiff differential equation solver *ode45* in Matlab (Mathworks, Natick, MA, USA). Initial conditions were $c_{\mathrm{met}}(0) = 0$ and $\phi_{\mathrm{MetA}}(0)$ ranging from $2 \cdot 10^{-5}$ to $2 \cdot 10^{-4}$. The parameters used in the calculations were $a_1 = 4.06$ 1/M, $a_3 = 148$ 1/M^2, $\chi_{\mathrm{MetA}} = 2.79 \cdot 10^{-3}$, $K_{\mathrm{M}} = 10^{-5}$ M, in accordance with estimates of Table C.2 and Table C.4.

The stability diagrams in Fig. 4.5D-E were calculated by solving Eq. (C.12) for the variable c_{met} using the *solve* function in Matlab (Mathworks, Natick, MA, USA) and varying different parameters. We shaded the regions according to the number of solutions at c^*_{met} concentrations higher or equal to zero. One zero solution, $c^*_{\mathrm{met}} = 0$, was denoted "dormancy region". Two zeros

solution, $c^{*,1}_{\mathrm{met}} = 0$ and $c^{*,2}_{\mathrm{met}} > 0$, was denoted "growth region". Three zeros solution was denoted "bistable region". In plot Fig. 4.5D, we computed c_{met} for different pairs of values of η and a_2, thereby plotting the solutions on the parameter space η-$j_{\mathrm{d}} = a_2 h g(c_{\mathrm{met}})$. In plot Fig. 4.5E, we computed again c_{met} for different pairs of values of η and j_{in}, thereby plotting the solutions on the parameter space η-j_{in}. In this case, as methionine influx is included, one solution at $c^{*}_{\mathrm{met}} > 0$ means that cells can grow on external methionine. This region was shaded "grey to white" to symbolize the growth rate dependence on the methionine influx. The other parameters used in the calculations were fixed at the values: $a_1 = 4.06$ 1/M, $a_3 = 148$ 1/M^2, $\chi_{\mathrm{MetA}} = 2.79 \cdot 10^{-3}$, $K_{\mathrm{M}} = 10^{-5}$ M, in accordance with estimates of Table C.3 and Table C.4.

C.2.11 Statistical analysis

Each lag time is the average of three independent experiments and its value is reported with one standard deviation.
Measurements of cell survival against antibiotic treatment were performed twice for each temperature and their values are reported with one standard deviation.
Survival measurements upon temperature shift from 37, 40, 42 and 45°C to 50°C were performed at least twice and are reported with one standard deviation.

C.3 Supplementary Figures

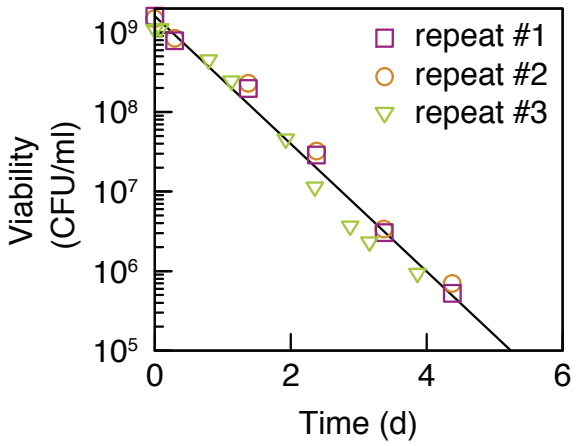

Figure C.1: Survival kinetics of wild-type cells starved at 45°C. Cell are grown in glycerol minimal medium at 45°C. The starvation following glycerol depletion leads to an exponential decay of bacterial viability, measured in colony forming units (CFU) per ml. Colors correspond to three independent experiments. The death rate $\gamma = (1.80 \pm 0.05)$ d^{-1} (slope of the black line, value reported with one standard deviation) is the average value of fits to the three independent experiments shown.

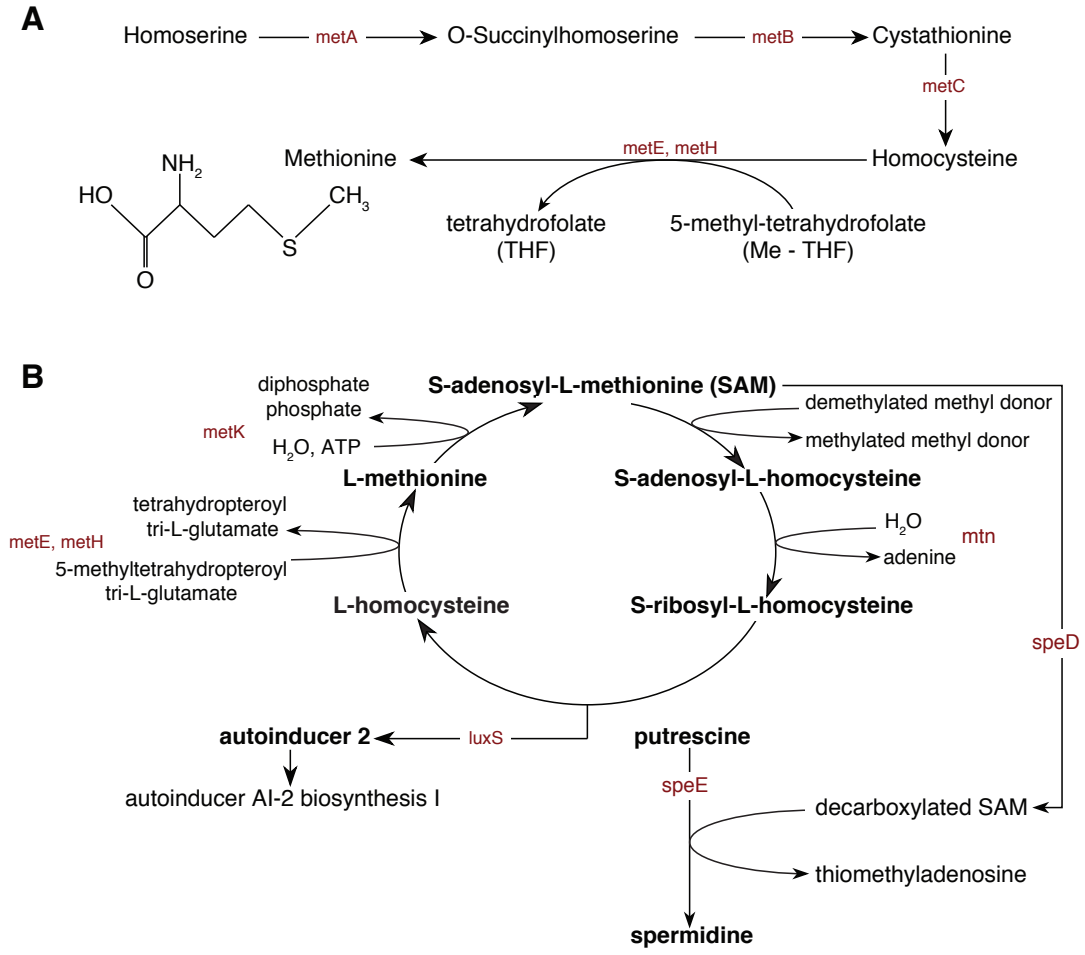

Figure C.2: L-methionine biosynthetic pathway and SAM cycle in *E. coli* K-12. (A) Methionine biosynthesis. The genes encoding the enzymes that catalyze each step are indicated in red: *metA* codes for homoserine O-succinyltransferase, *metB* for cystathionine γ-synthase, *metC* for cystathionine β-lyase, *metH* or *metE* for methionine synthase. The chemical structure of L-methionine is also reported. It contains an α-amino group (in the NH_3^+ form under biological conditions), an α-carboxylic acid group (in the $-COO$ form under biological conditions) and an S-methyl thioether side chain. **(B) S-adenosyl-L-methionine cycle I**. Methionine conversion into SAM, the major methyl donor in the cell. As in panel A, the genes encoding the enzymes that catalyze each step are indicated in red. Methionine is activated by condensation with ATP to form S-adenosyl-L-methionine (AdoMet or SAM). The synthesis of AdoMet is catalyzed by methionine adenosyltransferase, the *metK* gene product. Then, SAM donates its methyl group and it is converted to S-adenosyl-L-homocysteine (SAH). SAH is first hydrolyzed to S-ribosyl-L-homocysteine by 5'-methylthioadenosine, followed by conversion to L-homocysteine by S-ribosylhomocysteine lyase. The cycle continues with the methylation of L-homocysteine to L-methionine using a methyl group from a methylated folate. Finally, the cycle is completed with the regeneration of SAM by methionine adenosyltransferase. Within the cycle, there is always a fraction of methionine that is not recycled. This happens because SAM and S-rybosil-L-homocysteine are also used for two important functions. SAM is used to produce polyamines, such as spermidine, and S-rybosil-L homocysteine is involved in the synthesis of the autoinducer AI-2, catalyzed by the enzyme LuxS. Polyamines are polycations involved in many biological processes including binding to nucleic-acids, stabilizing membranes and stimulation of enzymes essentials for growth. They are also often used in responses to stress such as heat stress [203]. In this case, the enzyme SAM decarboxylase (from gene *speD*) converts SAM into decarboxylated SAM, which acts as a cofactor for spermidine biosynthesis. Then, spermidine synthase (from gene *speE*) converts putrescine to spermidine in the presence of decarboxylated SAM. The autoinducer AI-2 is an *E. coli* signalling molecule and could be used for cell-cell communication ("quorum sensing), allowing bacterial populations to coordinate gene expression as a function of cell density. Its biosynthesis is catalyzed by the enzyme S-ribosylhomocysteine lyase, from the gene *luxS*, which uses cleavage of S-ribosylhomocysteine. The image is based on information acquired from [202] and [227].

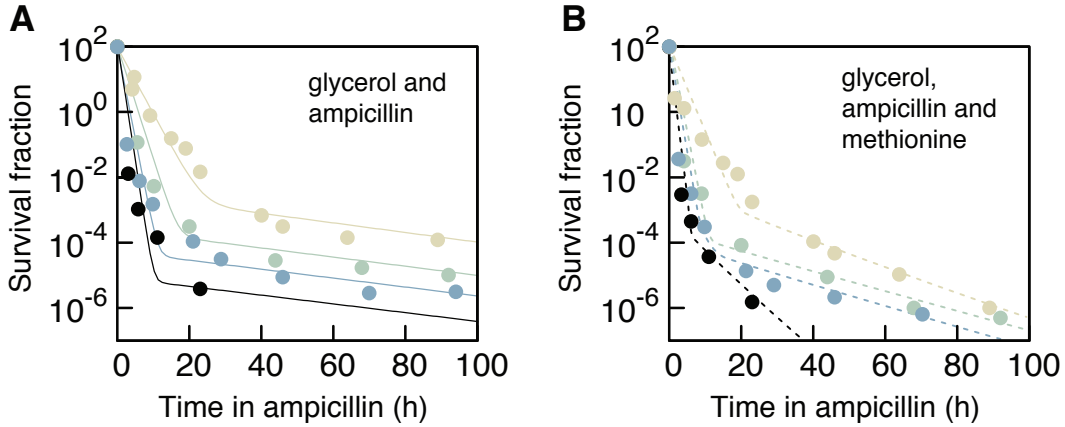

Figure C.3: Antibiotic persistence of exponentially growing wild-type cells. **(A)** Survival fraction of cells grown in minimal medium with glycerol at 37°C (black), 40°C (blue), 42°C (green), 45°C (yellow) and treated with ampicillin while exponentially growing (see Section C.2.8). As for starved cells in Fig. 4.7, for each temperature, there exists a biphasic survival kinetics, sign of the presence of persister cells. The fraction of persisters increases with temperature, also if the fraction of survivors is 10% of the survival fraction when cells are previously starved (see Fig. 4.7). **(B)** Survival fraction upon ampicillin and methionine treatment of cells while exponentially growing in minimal medium with glycerol. Colours correspond to the same temperatures of panel A. As for previously starved cells (Fig. 4.7), methionine abolishes 99% of the persisters. Lines in panels A (continuous) and B (dashed) indicate the bi-phasic fits $N = N_1 e^{-\gamma_1 t} + N_2 e^{-\gamma_2 t}$ where N is the cell viability and $N_1 + N_2 = 1$. γ_1 indicates the rate of viability decrease in the first phase, while γ_2 is the rate of viability decrease in the second phase.

C.4 Supplementary Tables

Temperature	Growth rate, -met (1/h)	Growth rate, +met (1/h)
25	0.30	0.33
27	0.38	0.42
29	0.48	0.53
31	0.54	0.60
33	0.60	0.69
35	0.65	0.78
37	0.70	0.86
39	0.75	0.95
40	0.78	0.97
41	0.75	0.96
42	0.71	0.95
43	0.62	0.81
44	0.54	0.72
45	0.45	0.62
46	0	0.49
47	0	0.14
48	0	0

Table C.1: Growth rates of wild-type cells at different temperatures, with and without methionine. Each value is the average of three independent repeats with a standard deviation of ~ 0.01.

Name	Symbol	Value	Unit	Reference	Comment
Growth rate	μ^g	0.45	1/h	This work.	*E. coli* K-12, *E. coli* K-12, 45°C, MM with glycerol
MetA copy number	N_{MetA}	1711	-	[207]	*E. coli* K-12, 37°C, MM with glucose
Avogadro constant	N_{A}	$6.02 \cdot 10^{23}$	1/mol	-	-
Typical free methionine concentration	c^g_{met}	$1.5 \cdot 10^{-4}$	M	[224]	*E. coli* B/r, 37°C, MM with glucose
Protein dry mass of *E. coli* concentration	M	$165 \cdot 10^{-15}$	g	[93]	*E. coli* B/r, 37°C, MM with glucose
Volume of *E. coli*	V	$1.3 \cdot 10^{-15}$	l	[93]	*E. coli* B/r, 37°C, MM with glucose
MetA decay rate	η	37°C: 1.1, 45°C: 1.6	1/h	[98]	*E. coli* JW3973, MM. with glucose
MetA molar mass	m_{MetA}	$3.56 \cdot 10^4$	g/mol	-	-
Spermidine concentration per cell	n_{spe}	$1.10 \cdot 10^6$	1/cell	[93]	*E. coli* B/r, 37°C, MM with glucose
Methionine affinity constant	K_{M}	10	μM	Estimated in this work.	-

Table C.2: Physiological parameters. Physiological parameters of the growth-dormancy model derived from measurements of this work and from the literature or estimated in this work. MM refers to minimal medium (see Section C.2.2).

Name	Symbol	Value	Unit	Calculation	Comment
Rate constant of methionine dependent growth	k_{p}	$3 \cdot 10^3$	$1/(\mathrm{M} \cdot \mathrm{h})$	$k_{\mathrm{p}} = \mu^g c_{\mathrm{met}}^{g^{-1}}$	Converts internal methionine concentration into growth.
Methionine concentration (in proteins)	$c_{\mathrm{met}}^{\mathrm{pro}}$	$2.75 \cdot 10^{-2}$	M	$c_{\mathrm{met}}^{\mathrm{pro}} = 3.23\% \frac{M}{V}/149$	3.23% is the fraction of the protein mass that is methionine and 149 g/mol is the molar mass of methionine. Both parameters are from Table C.5.
Spermidine concentration	c_{spe}	$1.41 \cdot 10^{-3}$	M	$c_{\mathrm{spe}} = n_{\mathrm{spe}} N_{\mathrm{A}}/V$	Per spermidine one methionine is used.
Active MetA mass fraction	ϕ_{MetA}^g	$6.13 \cdot 10^{-4}$	-	$\phi_{\mathrm{MetA}} = \frac{N_{\mathrm{MetA}} m_{\mathrm{MetA}}}{M N_{\mathrm{A}}}$	Does not include misfolded or degraded MetA.
MetA synthesis fraction	χ_{MetA}	$2.79 \cdot 10^{-3}$	-	$\chi_{\mathrm{MetA}} = \phi_{\mathrm{MetA}}^g \frac{\eta + \mu^g}{\mu^g}$	At 45°C.
Methionine production rate by MetA	h	20.3	M/h	$h = \frac{(c_{\mathrm{met}}^{\mathrm{pro}} + c_{\mathrm{met}}^g)\mu^g}{\phi_{\mathrm{MetA}}^g}$	-
Strength of the methionine drain	k_{d}	$6.3 \cdot 10^{-4}$	M/h	$k_{\mathrm{d}} = c_{\mathrm{spe}} \mu$	-

Table C.3: Model parameters. Derived estimates for parameters of the growth-dormancy model used to illustrate Fig. 4.5 in Chapter 4.

Name	Symbol	Value	Unit	Calculation	Comment
Rescaled protein synthesis	a_1	4.06	1/M	$k_{\mathrm{p}} c_{\mathrm{met}}^{\mathrm{pro}} h^{-1}$	-
Rescaled methionine drain	a_2	$3.1 \cdot 10^{-5}$	-	$k_{\mathrm{d}} h^{-1}$	-
Rescaled dilution term	a_3	148	$1/\mathrm{M}^2$	$k_{\mathrm{p}} h^{-1}$	-
Rescaled MetA decay rate	$\tilde{\eta}$	$37°\mathrm{C} : 0.37 \cdot 10^{-3}$ $45°\mathrm{C} : 0.53 \cdot 10^{-3}$	M	ηk_{p}^{-1}	Temperature dependent.

Table C.4: Compound parameters. Rescaled parameters used in the growth-dormancy model.

Amino acid	Occurrence rate	Mass(g/mol)	Relative mass
Glycine	7.34%	75.07	4.28%
Glutamate	5.75%	147.13	6.58%
Aspartate	5.14%	133.1	5.32%
Valine	7.09%	117.15	6.45%
Alanine	9.51%	89.09	6.58%
Arginine	5.54%	174.2	7.49%
Lysine	4.40%	146.19	4.99%
Aspargine	3.94%	132.12	4.04%
Methionine	2.79%	149.21	3.23%
Isoleucine	5.99%	131.18	6.10%
Threonine	5.39%	119.12	4.98%
Tryptophan	1.54%	204.23	2.44%
Cysteine	1.17%	121.15	1.10%
Tyrosine	2.87%	181.19	4.04%
Phenylalanine	3.91%	165.19	5.02%
Serine	5.81%	105.09	4.74%
Glutamine	4.44%	146.15	5.04%
Histidine	2.27%	155.16	2.73%
Leucine	10.67%	131.18	10.87%
Proline	4.45%	115.13	3.98%

Table C.5: Aminoacid occurrence rates and relative mass for *E. coli* K-12. Aminoacid frequency and relative abundance of aminoacids, in percent of total protein mass, estimated based on the codon frequency of *E. coli* from the Codon Usage Database [228].

Bibliography

[1] D. L. Hartl and D. E. Dykhuizen. The population genetics of *Escherichia coli*. Annual Review of Genetics 18, 31-68 (1984).

[2] A. Leimbach, J. Hacker, U. Dobrindt. *E. coli* as an all-rounder: the thin line between commensalism and pathogenicity. Current Topics in Microbiology and Immunology 358, 3-32 (2013).

[3] T. Escherich. The intestinal bacteria of the neonate and breast-fed infant. 1884. Review of Infectious Disease 10, 1220-1225 (1988).

[4] Z. D. Blount. The unexhausted potential of *E. coli*. Elife 25 (2015).

[5] F. H. Crick, L. Barnett, S. Brenner, R. J. Watts-Tobin. General nature of the genetic code for proteins. Nature 192, 1227-1232 (1961).

[6] M. Nirenberg, P. Leder, M. Bernfield, R. Brimacombe, J. Trupin, F. Rottman, C. O'Neal. RNA codewords and protein synthesis, VII. On the general nature of the RNA code. Biochemistry 53, 1161-1168 (1965).

[7] H.F. Judson. The Eighth Day of Creation. (Cold Spring Harbor Laboratory Press, 1996).

[8] L. K. Poulsen, F. Lan, C. S. Kristensen, P. Hobolth, S. Molin and K. A. Krogfelt, Spatial distribution of *Escherichia coli* in the mouse large intestine inferred from rRNA in situ hybridization. Infection and immunity 62, 5191-5194 (1994).

[9] C. U. Rang, T. R. Licht, T. Midtvedt, P. L. Conway, L. Chao, K. A. Krogfelt, P. S. Cohen and S. Molin. Estimation of growth rates of *Escherichia coli* bj4 in streptomycintreated and previously germfree mice by in situ rRNA hybridization. Clinical and diagnostic laboratory immunology 6, 434-436 (1999).

[10] J. Cremer, I. Segota, C. Y. Yang, M. Arnoldini, J. T. Sauls, Z. Zhang, E. Gutierrez, A. Groisman and T. Hwa. Effect of flow and peristaltic mixing on bacterial growth in a gut-like channel. Proceedings of the National Academy of Sciences 113, 11414-11419 (2016).

[11] J. D. van Elsas, A.V. Semenov, R. Costa, J. T. Trevors. Survival of *Escherichia coli* in the environment: fundamental and public health aspects. The ISME Journal 5, 173-183 (2011).

[12] H. Fukushima, K. Hoshina, and M. Gomyoda, Long-term survival of shiga toxinproducing *escherichia coli* o26, o111, and o157 in bovine feces. Applied and Environmental Microbiology 65, 5177-5181 (1999).

[13] S. E. Finkel. Long-term survival during stationary phase: evolution and the GASP phenotype. Nature Reviews Microbiology 4, 113-120 (2006).

[14] K. Gupta, T. M. Hooton, K. G. Naber, B. Wullt, R. Colgan, L. G. Miller, G. J. Moran, L. E. Nicolle, R. Raz, A. J. Schaeffer et al. International clinical practice guidelines for the treatment of acute uncomplicated cystitis and pyelonephritis in women: a 2010 update by the infectious diseases society of America and the European society for microbiology and infectious diseases. Clinical infectious diseases 52 (2011).

[15] T. A. Russo and J. R. Johnson. Medical and economic impact of extraintestinal infections due to *escherichia coli*: focus on an increasingly important endemic problem. Microbes and Infection 5, 449-456 (2003).

[16] J. B. Kaper, J. P. Nataro and H. L. Mobley. Pathogenic *escherichia coli*. Nature Reviews Microbiology 2, 123-140 (2004).

[17] J. C. Arthur, E. Perez-Chanona, M. Mühlbauer, S. Tomkovich, J. M. Uronis, F. Ting-Jia, B. J. Bampbell, T. Abujamel, B. Dogan, A. B. Rogers et al. Intestinal inflammation targets cancer-inducing activity of the microbiota. Science 338, 120-123 (2012).

[18] I. R. Lehman, M. J. Bessman, E. S. Simms, A. Kornberg. Enzymatic synthesis of deoxyribonucleic acid. I. Preparation of substrates and partial purification of an enzyme from *Escherichia coli*. Journal of Biological Chemistry 233, 163-170 (1958).

[19] A. Stevens. Incorporation of the adenine ribonucleotide into RNA by cell fractions from *E. coli*. Biochemical and Biophysical Research Communications 3, 92-96 (1960).

[20] E. L. Ellis and M. Delbrück. The growth of bacteriophage. Journal of General Physiology 22, 365-384 (1939).

[21] F. Jacob, D. Perrin, C. Sanchez, J. Monod. Lopéron: groupe de génes á expression coordonnée par un opérateur (The operon: a group of genes whose expression is coordinated by an operator). Comptes Rendus Hebdomadaires Des Séances De lAcadémie Des Sciences 250, 1727-1729 (1960).

[22] R. M. Harshey and T. Matsuyama. Dimorphic transition in *Escherichia coli* and *Salmonella typhimurium*: surfaceinduced differentiation into hyperflagellate swarmer cells. Proceedings of the National Academy of Sciences 91, 8631-8635 (1994).

[23] Y. Hu and A. R. Coates. Transposon mutagenesis identifies genes which control antimicrobial drug tolerance in stationary-phase *Escherichia coli*. FEMS Microbiology Letters 243, 117-124 (2005).

[24] M. Kamionka. Engineering of therapeutic proteins production in *Escherichia coli*. Current Pharmaceutical Biotechnology 12, 268-274 (2011).

[25] S. E. Luria and M. Delbrück. Mutations of bacteria from virus sensitivity to virus resistance. Genetics 28, 491-511 (1943).

[26] M. J. Wiser, N. Ribeck, R. E. Lenski. Long-term dynamics of adaptation in asexual populations. Science 342, 1364-1367 (2013).

[27] R. E. Lenski. Experimental studies of pleiotropy and epistasis in *Escherichia coli*. I. Variation in competitive fitness among mutants resistant to virus T4. Evolution 42, 425-432 (1988).

[28] S. Cohen, A. Chang, H. Boyer and R. Helling. Construction of biologically functional bacterial plasmids in vitro. Proceedings of the National Academy of Sciences 70, 3240-3244 (1973).

[29] F. R. Blattner, G. Plunkett, C. A. Bloch, N. T. Perna, V. Burland, M. Riley, J. Collado-Vides, J. D. Glasner, C. K. Rode and G. F. Mayhew, The complete genome sequence of *escherichia coli* K-12. Science 277, 1453-1462 (1997).

[30] E. Soupene, W. C. van Heeswijk, J. Plumbridge, V. Stewart, D. Bertenthal, H. Lee, G. Prasad, O. Paliy, P. Charernnoppakul, S. Kustu. Physiological studies of *Escherichia coli* strain MG1655: growth defects and apparent cross-regulation of gene expression. Journal of Bacteriology 185, 5611-5626 (2003).

[31] S. D. Brown and J. Suckjoon. Complete Genome Sequence of *Escherichia coli* NCM3722. Genome Announcements 3 (2015).

[32] M. T. Madigan, J. M. Martinko, K. S. Bender, D. H. Buckley and D. A. Stahl. Brock biology of microorganisms. Fourteenth edition. (Boston: Pearson, 2014).

[33] J. Monod. The Growth of Bacterial Cultures. Annual Review of Microbiology 3, 371-394 (1949).

[34] R. Kolter, D. A. Siegele. The stationary phase of the bacterial life cycle. Annual Review of Microbiology 47, 855-874 (1993).

[35] M. Schaechter, O. Maaløe, N. O. Kjeldgaard. Dependency on Medium and Temperature of Cell Size and Chemical Composition during Balanced Growth of *Salmonella typhimurium*. Journal of General Microbiology 19, 592-606 (1958).

[36] A. Hershey. Factors limiting bacterial growth: IV. The age of the parent culture and the rate of growth of transplants of *Escherichia coli*. Journal of Bacteriology 37, 285 (1939).

[37] A. Campbell. Synchronization of cell division. Bacteriological Reviews 21, 263-272 (1957).

[38] S. A. Janke, P. Fortnagel, R. Bergmann. Microbiological turbidimetry using standard photometers. Biospektrum 6, 501-502 (1999).

[39] R. M. Maier, I. L. Pepper and C. P. Gerba. Environmental Microbiology. (Academic Press, 2009).

[40] M. Scott, S. Klumpp, E.M. Mateescu and T. Hwa. Emergence of robust growth laws from optimal regulation of ribosome synthesis. Molecular Systems Biology 10 (2014).

[41] M. Scott, C. W. Gunderson, E. M. Mateescu, Z. Zhang, T. Hwa. Interdependence of Cell Growth and Gene Expression: Origins and Consequences. Science 330, 1099-1102 (2010).

[42] H. Bremer and P. P. Dennis, Modulation of chemical composition and other parameters of the cell at different exponential growth rates. 1553-1569, Washington, DC: Am Soc Microbiol, 2nd ed. (1996).

[43] S. Klumpp, Z. Zhang and T. Hwa. Growth rate-dependent global effects on gene expression in bacteria. Cell 139, 1366-1375 (2009).

[44] C. You, H. Okano, S. Hui, Z. Zhang, M. Kim, C. W. Gunderson, Y. P. Wang, P. Lenz, D. Yan, and T. Hwa. Coordination of bacterial proteome with metabolism by cyclic AMP signalling. Nature 500, 301-306 (2013).

[45] S. Hui, J. M. Silverman, S. S. Chen, D. W. Erickson, M. Basan, J. Wang, T. Hwa and J. R. Williamson. Quantiative proteomic analysis reveals a simple strategy of global resource allocation in bacteria. Molecular Systems Biology 11 (2015).

[46] D. W. Erickson, S. J. Schink, V. Patsalo, J. R. Williamson, U. Gerland and T. Hwa. A global resource allocation strategy governs growth transition kinetics of *Escherichia coli*. Nature 551, 119-123 (2017).

[47] R. E. Lenski, M. R. Rose, S. C. Simpson and S. C. Tadler. Long-Term Experimental Evolution in *Escherichia coli*. I. Adaptation and Divergence During 2000 Generations. The American Naturalist 138, 1315-1341 (1991).

[48] J. M. Wiser, N. Ribeck, E. R. Lenski. Long-Term Dynamics of Adaptation in Asexual Populations, Science 342, 1364-1367 (2013).

[49] S. J. Pirt, The Maintenance Energy of Bacteria in Growing Cultures. Proceedings of the Royal Society of London B 163, 224-231 (1965).

[50] A. H. Stouthamer, C. W. Bettenhausen. Utilization of energy for growth and maintenance in continuous and batch cultures of microorganisms. Biochimica et Biophysica Acta 301, 53-70 (1973).

[51] H. A. Orr, Fitness and its role in evolutionary genetics. Nature Reviews Genetics 10, 531-539 (2009).

[52] M. Eames and T. Kortemme. Cost-benefit tradeoffs in engineered lac operons. Science 336, 911-915 (2012).

[53] E. Dekel and U. Alon. Optimality and evolutionary tuning of the expression level of a protein. Nature 436, 588592 (2005).

[54] D. A. Drummond, J. D. Bloom, C. Adami, C. O. Wilke, F. H. Arnold. Why highly expressed proteins evolve slowly. Proceedings of the National Academy of Sciences 102, 14338 (2005).

[55] D. A. Drummond, C. O. Wilke. Mistranslation-induced protein misfolding as a dominant constraint on coding-sequence evolution. Cell 134, 341 (2008).

[56] O. Gefen, O. Fridman, I. Ronin, N. Q. Balaban. Direct observation of single stationary-phase bacteria reveals a surprisingly long period of constant protein production activity. Proceedings of the National Academy of Sciences 111, 556-561 (2014).

[57] A. Phaiboun, Y. Zhang, B. Park, M. Kim. Survival Kinetics of Starving Bacteria Is Biphasic and Density-Dependent. PLOS Computational Biology 11 (2015).

[58] T. M. Hoehler and B. B. Jørgensen. Microbial life under extreme energy limitation. Nature Reviews Microbiology 11, 83-94 (2013).

[59] M. Bergkessel, D. W. Basta, D. K. Newman. The physiology of growth arrest: uniting molecular and environmental microbiology. Nature Reviews Microbiology 14, 549-562 (2016).

[60] J. A. Imlay, The molecular mechanisms and physiological consequences of oxidative stress: lessons from a model bacterium. Nature Reviews Microbiology 11, 443-454 (2013).

[61] W. P. Williams. Cold induced lipid phase transitions. Philosophical Transactions of the Royal Society B 326, 555-570 (1990).

[62] R. H. Vreeland, W. D. Rosenzweig, D. W. Powers. Isolation of a 250 million-year-old halotolerant bacterium from a primary salt crystal. Nature 407, 897-900 (2000).

[63] P. Setlow. I will survive: DNA protection in bacterial spores. Trends in Microbiology 15, 172-180 (2007).

[64] F. J. Ryan. Spontaneous mutation in non-dividing bacteria. Genetics 40 (1955).

[65] S. E. Finkel and R. Kolter. Evolution of microbial diversity during prolonged starvation. Proceedings of the National Academy of Sciences 96, 4023-4027 (1999).

[66] A. Harrison. The response of Bacterium lactis aerogenes when held at growth temperature in the absence of nutriment: an analysis of survival curves. Proceedings of the Royal Society B Bio 152, 418-428 (1960).

[67] J. R. Postgate, J. R. Hunter. The Survival of Starved Bacteria. Journal of General Microbiology 29, 233-263 (1962).

[68] W. A. Moats. Kinetics of Thermal Death of Bacteria. Journal of Bacteriology 105, 165-171 (1971).

[69] O. N. Peled, A. Salvadori, U. N. Peled and D. K. Kidby. Death of Microbial Cells: Rate Constant Calculations. Journal of Bacteriology 129, 1648-1650 (1976).

[70] K. Kumada, K. Koike and K. Fujiwara. The Survival of Bacteria under Starvation Conditions: a Mathematical Expression of Microbial Death. Journal of General Microbiology 131, 2309-2312 (1985).

[71] C. A. Reeve, A. T. Bockman, A. Matin. Role of protein degradation in the survival of carbon-starved *Escherichia coli* and *Salmonella typhimurium*. Journal of Bacteriology 157, 758-763 (1984).

[72] C. A. Reeve, P. S. Amy, A. Matin. Role of protein synthesis in the survival of carbon-starved *Escherichia coli* K-12. Journal of Bacteriology 160, 1041-1046 (1984).

[73] R. Lange, R. Hengge-Aronis. Identification of a central regulator of stationary-phase gene expression in *Escherichia coli*. Molecular Microbiology 5, 49-59 (1991).

[74] D. S. Kim, S. Thomas, H. S. Fogler. Effects of pH and Trace Minerals on Long-Term Starvation of *Leuconostoc mesenteroides*. Applied and Environmental Microbiology 66, 976-981 (2000).

[75] R. Hengge-Aronis. Survival of hunger and stress: The role of *rpoS* in early stationary phase gene regulation in *E. coli*. Cell 72, 165-168 (1993).

[76] R. Hengge-Aronis. Back to log phase: σ^S as a global regulator in the osmotic control of gene expression in *Escherichia coli*. Molecular Microbiology 21, 887-893 (1996).

[77] S. Dukan and T. Nyström. Oxidative Stress Defense and Deterioration of Growth-arrested *Escherichia coli* Cells. Journal of Biological Chemistry 274, 26027-26032 (1999).

[78] M. M. Zambrano, D. A. Siegele, M. Almiron, A. Tormo, R. Kolter. Microbial Competition: *Escherichia coli* Mutants That Take Over Stationary Phase Cultures. Science 259 (1993).

[79] R. Hengge. Stationary phase gene regulation in *Escherichia coli*. Chapter 5.6.3. in EcoSal Escherichia coli and Salmonella: Cellular and Molecular Biology. (ASM Press, Washington, DC, 2011).

[80] C. L. Patten, M. G. KirchhoF, M. R. Schertzberg, R.A. Morton, H.E. Schellhorn. Microarray analysis of RpoS-mediated gene expression in *Escherichia coli* K-12. Molecular Genetics and Genomics 272, 580-91 (2004).

[81] A. G. Franchini, J. Ihssen and T. Egli. Effect of Global Regulators RpoS and Cyclic-AMP/CRP on the Catabolome and Transcriptome of *Escherichia coli* K12 during Carbon- and Energy-Limited Growth. PLoS ONE 10 (2015).

[82] A. Maciag, C. Peano, A. Pietrelli, T. Egli, G. De Bellis, P. Landini. In vitro transcription profiling of the σS subunit of bacterial RNA polymerase: re-definition of the σS regulon and identification of σS-specific promoter sequence elements. Nucleic Acids Research 39, 5338-55 (2011).

[83] H. Merrikh, A. E. Ferrazzoli, A. Bougdour, A. Olivier-Mason and S. T. Lovett. A dna damage response in *escherichia coli* involving the alternative sigma factor Rpos. Proceedings of the National Academy of Sciences 106, 611-616 (2009).

[84] C. Peano, J. Wolf, J. Demol, E. Rossi, L. Petiti, G. De Bellis, J. Geiselmann, T. Egli, S. Lacour, and P. Landini. Characterization of the Escherichia coli σS core regulon by Chromatin Immunoprecipitation-sequencing (ChIP-seq) analysis. Scientific Reports 5 (2015).

[85] V. W. Soo and T. K. Wood. Antitoxin MqsA represses curli formation through the master biofilm regulator CsgD. Scientific Reports 3 (2013).

[86] J. Ihssen and T. Egli. Specific growth rate and not cell density controls the general stress response in *Escherichia coli*. Microbiology 150, 1637-1648 (2004).

[87] J. Ihssen and T. Egli. Global physiological analysis of carbon and energy limited growing *Escherichia coli* confirms a high degree of catabolic flexibility and preparedness for mixed substrate utilization. Environmental Microbiology 7, 1568-1581 (2005).

[88] A. Teich, S. Meyer, H. Y. Lin, L. Andersson, S. O. Enfors and P. Neubauer. Growth rate related concentration changes of the starvation response regulators σ^S and ppGpp in glucose limited fed batch and continuous cultures of *Escherichia coli*. Biotechnology Progress 15, 123-129 (1999).

[89] A. Schmidt, K. Kochanowski, S. Vedelaar, E. Ahrne, B. Volkmer, L. Callipo, K. Knoops, M. Bauer, R. Aebersold and M. Heinemann. The quantitative and condition-dependent *Escherichia coli* proteome. Nature Biotechnology 34, 104-110 (2016).

[90] P. van Bodegom. Microbial Maintenance: A Critical Review on Its Quantification. Microbial Ecology 53, 513-523 (2007).

[91] M. Schaechter, J. L. Ingraham, F. C. Neidhardt. Microbe. (ASM Press, 2006).

[92] E. A. Mordukhova, H. S. Lee and J. G Pan. Improved Thermostability and Acetic Acid Tolerance of *Escherichia coli* via Directed Evolution of Homoserine o-Succinyltransferase. Applied and Environmental Microbiology 74, 7660-7668 (2008).

[93] F. C. Neidhardt, J. Ingraham, K. B. Low, B. Magasanik, M. Schaechter and H. E. Umbarger. *Escherichia coli* and *Salmonella typhimurium*, Cellular and Molecular Biology 1 & 2. (Microbiology, Washington, D.C., 1987).

[94] E. Gur, D. Biran, E. Gazit and E. Z. Ron. In vivo aggregation of a single enzyme limits growth of *Escherichia coli* at elevated temperatures. Molecular Microbiology 46, 1391-1397 (2002).

[95] D. Biran, E. Gur, L. Gollan and E. Z. Ron. Control of methionine biosynthesis in Escherichia coli by proteolysis. Molecular Microbiology 37, 1436-1443 (2000).

[96] E. Z. Ron and B. D. Davis. Growth Rate of *Escherichia coli* at Elevated Temperatures: Limitation by Methionine. Journal of Bacteriology 107, 391-396 (1971).

[97] E. Z. Ron and M. Shani. Growth Rate of *Escherichia coli* at Elevated Temperatures: Reversible Inhibition of Homoserine Trans-Succinylase. Journal of Bacteriology 107, 397-400 (1971).

[98] E. A. Mordukhova, D. Kim and J. Pan. Stabilized homoserine o-succinyltransferases (MetA) or L-methionine partially recovers the growth defect in *Escherichia coli* lacking ATP-dependent proteases or the DnaK chaperone. BMC Microbiology 13 (2013).

[99] E. Z. Ron. Growth rate of *Enterobacteriaceae* at elevated temperatures: limitation by methionine. Journal of Bacteriology 124 (1975).

[100] A. Wyman, E. Shelton and H. Paulus. Regulation of homoserine transacetylase in whole cells of *Bacillus polymyxa*. Journal of Biological Chemistry 250, 3904-3908 (1975).

[101] C. Katz, A. Rasouly, E. Gur, Y. Shenhar, D. Biran, E.Z. Ron. Temperature-dependent proteolysis as a control element in *Escherichia coli* metabolism. Research in Microbiology 160, 684-686 (2009).

[102] M. Fauvart, V. N. De Groote and J. Michiels. Role of persister cells in chronic infections: clinical relevance and perspectives on anti-persister therapies. Journal of Medical Microbiology 60, 699-709 (2011).

[103] I. Levin-Reisman, I. Ronin, O. Gefen, I. Braniss, N. Shoresh and N. Balaban. Antibiotic tolerance facilitates the evolution of resistance. Science 355, 826-830 (2017).

[104] N. Q. Balaban. Definitions and guidelines for research on antibiotic persistence. Nature Reviews Microbiology 17, 441-448 (2019).

[105] J. Bigger. Treatment of staphylococcal infections with penicillin by intermittent sterilization. Lancet 244, 497-500 (1944).

[106] N.Q. Balaban, J. Merrin, R. Chait, L. Kowalik and S. Leibler. Bacterial persistence as a phenotypic switch. Science 305, 1622-1625 (2004).

[107] S. Helaine and E. Kugelberg. Bacterial persisters: formation, eradication, and experimental systems. Trends in Microbiology 22, 417-424 (2014).

[108] S. Amato, C. H. Fazen, C. Henry, W. W. K. Mok, M. A. Orman, E. L. Sandvik, K. G. Volzing and M. P. Brynildsen. The role of metabolism in bacterial persistence. Frontiers in Microbiology 5, 70 (2014).

[109] E. A. Mordukhova, J. G. Pan. Stabilization of Homoserine-O-Succinyltransferase (MetA) Decreases the Frequency of Persisters in *Escherichia coli* under Stressful Conditions. PLoS ONE 9 (2014).

[110] S. Helaine, A. M. Cheverton, K. G. Watson, L. M. Faure, S. A. Matthews, D. W. Holden. Internalization of *Salmonella* by macrophages induces formation of non replicating persisters. Science 343, 204-208 (2014).

[111] T. Dörr, M. Vulic and K. Lewis. Ciprofloxacin causes persister formation by inducing the TisB toxin in *Escherichia coli*. PLOS Biology 8 (2010).

[112] R. A. Fisher, B. Gollan and S. Helaine. Persistent bacterial infections and persister cells. Nature Reviews Microbiology 15, 453-464 (2017).

[113] H. S. Moyed and K. P. Bertrand. *hipA*, a newly recognized gene of *Escherichia coli* K-12 that affects frequency of persistence after inhibition of murein synthesis. Journal of Bacteriology 155, 768-775 (1983).

[114] K. Gerdes, S. K. Christensen and A. Lobner-Olesen. Prokaryotic toxin-antitoxin stress response loci. Nature Reviews Microbiology 3, 371-382 (2005).

[115] E. Rotem, A. Loinger, I. Ronin, I. Levin-Reisman, C. Gabay, N. Shoresh, O. Biham and N. Q. Balaban. Regulation of phenotypic variability by a threshold-based mechanism underlies bacterial persistence. Proceedings of the National Academy of Sciences 107, 12541-12546 (2010).

[116] S. Hansen, K. Lewis and M. Vulic. Role of global regulators and nucleotide metabolism in antibiotic tolerance in *Escherichia coli*. Antimicrobial Agents and Chemotherapy 52, 2718-2726 (2008).

[117] K. Lewis. Riddle of biofilm resistance. Antimicrobial Agents and Chemotherapy 45, 999-1007 (2001).

[118] M. D. Lafleur, Q. Qi, K. Lewis. Patients with long-term oral carriage harbor high persister mutants of *Candida albicans*. Antimicrobial Agents and Chemotherapy 54, 39-44 (2010).

[119] L. R. Mulcahy, J. L. Burns, S. Lory, K. Lewis. Emergence of *Pseudomonas aeruginosa* strains producing high levels of persister cells in patients with cystic fibrosis. Journal of Bacteriology 192, 6191-6199 (2010).

[120] M. A. Schumacher, P. Balani, J. Min, N. B. Chinnam, S. Hansen, M. Vulić, K. Lewis and R. G. Brennan. HipBA-promoter structures reveal the basis of heritable multidrug tolerance. Nature 524, 59-64 (2015).

[121] P. Kaiser, R. R. Regoes, T. Dolowschiak, S.Y. Wotzka, J. Lengefeld, E. Slack, A. J. Grant, M. Ackermann, W-D. Hardt. Cecum lymphonod dendritic cells harbor slow-drowing bacteria phenotypically tolerant to antibiotic treatment. PLOS Biology 12 (2014).

[122] X. Z. Li, H. Nikaido. Efflux-mediated drug resistance in bacteria. Drugs 69, 1555-1623 (2009).

[123] K. N. Adams, K. Takaki, L. E. Connolly, H. Wiedenhoft, K. Winglee, O. Humbert, P. H. Edelstein, C. L. Cosma, L. Ramakrishnan. Drug tolerance in replicating *Mycobacteria* mediated by a macrophage-induced efflux mechanism. Cell 145, 39-53 (2011).

[124] Y. Pu, Z. Zhao, Y. Li, J. Zou, Q. Ma, Y. Zhao, Y. Ke, Y. Zhu, H. Chen, M. A. B. Baker, H. Ge, Y. Sun, X.S. Xie, F. Bai. Enhanced efflux activity facilitates drug tolerance in dormant bacterial cells. Molecular Cell 62, 284-294 (2016).

[125] N. R. Cohen, M. A. Lobritz, J. J. Collins. Microbial persistence and the road to drug resistance. Cell Host Microbe 13, 632-642 (2013).

[126] E. Gullberg, S. Cao, O. G. Berg, C. Ilbäck, L. Sandegren, D. Hughes, D. I. Andersson. Selection of resistant bacteria at very low antibiotic concentrations. PLOS Pathogens 7, 1-9 (2011).

[127] B. Van den Bergh, M. Fauvart, J. Michiels. Formation, physiology, ecology, evolution and clinical importance of bacterial persisters. FEMS Microbiology Reviews 41, 219-251 (2017).

[128] J. G. Hurdle, A. J. ONeill, I. Chopra, R. E. Lee. Targeting bacterial membrane function: an underexploited mechanism for treating persistent infections. Nature Reviews Microbiology 9, 62-75 (2011).

[129] V. Braun, C. Bös, M. Braun, H. Killmann. Outer membrane channels and active transporters for the uptake of antibiotics? Journal of Infectious Diseases 183 (2001).

[130] J. R. Morones-Ramirez, J. A. Winkler, C. S. Spina, J. J. Collins. Silver enhances antibiotic activity against Gram negative bacteria. Science Translational Medicine 5 (2013).

[131] J. S. Kim, P. Heo, T. J. Yang, K. S. Lee, D. H. Cho, B. T. Kim, J. H. Suh, H. J. Lim, D. Shin, S. K. Kim, D. H. Kweon. Selective killing of bacterial persisters by a single chemical compound without affecting normal antibiotic-sensitive cells. Antimicrobial Agents and Chemotherapy 55, 5380-5383 (2011).

[132] O. Fridman, A. Goldberg, I. Ronin, N. Shoresh and N. Balaban. Optimization of lag time underlies antibiotic tolerance in evolved bacterial populations. Nature 418 (2014).

[133] V. Chubukov and U. Sauer. Environmental dependence of stationary-phase metabolism in *bacillus subtilis* and *escherichia coli*. Applied and Environmental Microbiology 80, 2901-2909 (2014).

[134] A. Battesti, N. Majdalani, and S. Gottesman. The Rpos-mediated general stress response in *Escherichia Coli*. Annual Review of Microbiology 65, 189-213 (2011).

[135] E. I. Garvie, The growth of *escherichia coli* in buffer substrate and distilled water. Journal of Bacteriology, 69, 393-398 (1955).

[136] W. Kollath. Vitaminahnliche substanzen in ihrer wirkung auf das wachstum der in influenzabazillen. Zentr. Bakt. Parasitenk., Abt.I., Orig., 93, 506-519 (1924).

[137] E. A. Steinhaus and J. M. Birkeland. Studies on the life and death of bacteria: I. the senescent phase in aging cultures and the probable mechanisms involved. Journal of Bacteriology, 38, 249-261 (1939).

[138] C. Mason, G. Hamer, and J. D. Bryers. The death and lysis of microorganisms in environmental processes. FEMS Microbiology Letters, 39, 373-401 (1986).

[139] A. L. Koch. Death of bacteria in growing culture. Journal of Bacteriology 77, 623-629 (1959).

[140] F. J. Ryan. Bacterial Mutation in a Stationary Phase and the Question of Cell Turnover. Journal of General Microbiology 21, 530-549 (1959).

[141] M. M. Klosinska, C. A. Crutchfield, P. H. Bradley, J. D. Rabinowitz and J. R. Broach. Yeast cells can access distinct quiescent states. Genes & Development 25, 336-349 (2011).

[142] L. Wang and M. J. Wise. Glycogen with short average chain length enhances bacterial durability. Naturwissenschaften 98, 719-729 (2011).

[143] M. Basan, S. Hui, H. Okano, Z. Zhang, Y. Shen, J. R. Williamson, T. Hwa. Overflow metabolism in *Escherichia coli* results from efficient proteome allocation. Nature 528, 99-104 (2015).

[144] F. C. Neidhardt, J. L. Ingraham and M. Schaechter. Physiology of the bacterial cell: a molecular approach. (Sinauer associates, Sunderland, MA, 1990).

[145] A. J. Wolfe. The acetate switch. Microbiology and Molecular Biology Reviews 69, 12-50 (2005).

[146] M. De Mey, S. De Maeseneire, W. Soetaert and E. Vandamme. Minimizing acetate formation in *E. coli* fermentations. Journal of Industrial Microbiology and Biotechnology 34, 689-700 (2007).

[147] R. T. Voegele, G. D. Sweet, W. Boos. Glycerol kinase of *Escherichia coli* is activated by interaction with the glycerol facilitator. Journal of Bacteriology 175, 1087-1094 (1993).

[148] E. R. Zinser and R. Kolter. *Escherichia coli* evolution during stationary phase. Research in Microbiology 155, 328-336 (2004).

[149] N. O. Kjeldgaard, O. Maaløe and M. Schaechter. The transition between different physiological states during balanced growth of *salmonella typhimurium*. Journal of General Microbiology 19, 607-616 (1958).

[150] C. Kaleta, S. Schäuble, U. Rinas, S. Schuster. Metabolic costs of amino acid and protein production in *Escherichia coli*. Biotechnology Journal 8, 1105-1114 (2013).

[151] J. Mandelstam and H. Halvorson. Turnover of protein and nucleic acid in soluble and ribosome fractions of non-growing *escherichia coli*. Biochimica et Biophysica Acta 40, 43-49 (1960).

[152] O. Maaløe. Regulation of the protein-synthesizing machinery-ribosomes, trna, factors and so on. Biological regulation and development, 487-542. (Springer, 1979).

[153] J. R. Houser, C. Barnhart, D. R. Boutz, S. M. Carroll, A. Dasgupta, J. K. Michener et al. Controlled Measurement and Comparative Analysis of Cellular Components in *E. coli* Reveals Broad Regulatory Changes in Response to Glucose Starvation. PLOS Computational Biology 11 (2015).

[154] D. L. Nelson and M. M. Cox. Lehninger principles of biochemistry. (Worth Publishers, New York, 2000).

[155] S. R. De Groot and P. Mazur. Non-Equilibrium Thermodynamics. (Dover Publications, New York, 1985).

[156] H. Link, T. Fuhrer, L. Gerosa, N. Zamboni and U. Sauer. Real-time metabolome profiling of the metabolic switch between starvation and growth. Nature Methods 12, 1091-7 (2015).

[157] L. M. Chevin. On measuring selection in experimental evolution. Biology Letters 7, 210-213 (2011).

[158] J. F. Crow and M. Kimura. An introduction to population genetics theory. (Harper and Row, New York, 1970).

[159] D. E. Rozen, P. Nadge, J. Arjan de Visser, R. E. Lenski and D. Schneider. Death and cannibalism in a seasonal environment facilitate bacterial coexistence. Ecology Letters 12, 34-44 (2009).

[160] M. Ghoul and S. Mitri. The Ecology and Evolution of Microbial Competition. Trends in Microbiology 24, 833-845 (2006).

[161] L. Notley and T. Ferenci. Induction of RpoS-dependent functions in glucose-limited continuous culture: what level of nutrient limitation induces the stationary phase of *Escherichia coli*? Journal of Bacteriology 178, 1465-1468 (1996).

[162] R. Hengge-Aronis and D. Fischer, Identification and molecular analysis of *glgS*, a novel growth phase-regulated and *rpoS*-dependent gene involved in glycogen synthesis in *Escherichia coli*. Molecular Microbiology 6, 1877-1886 (1992).

[163] D. W. Ribbons and E. A. Dawes. Environmental and growth conditions affecting the endogenous metabolism of bacteria. Annals of the New York Academy of Sciences 102, 564-586 (1963).

[164] T. Fung, N. Kwong, T. van der Zwan and M. Wu. Residual Glycogen Metabolism in *Escherichia coli* is Specific to the Limiting Macronutrient and Varies During Stationary Phase. Journal of Experimental Microbiology and Immunology 17, 83-87 (2013).

[165] M. Lynch and G. K. Marinov. The bioenergetic costs of a gene. Proceedings of the National Academy of Sciences 112, 15690-15695 (2015).

[166] T. Ferenci. Hungry bacteria - definition and properties of a nutritional state. Environmental Microbiology 3, 605-611 (2001).

[167] W. Chesbro. The domains of slow bacterial growth. Canadian Journal of Microbiology 34, 427-435 (1988).

[168] J. R. Postgate and J. R. Hunter. The Survival of Starved Bacteria. Journal of General Microbiology 29, 233-263 (1962).

[169] R. E. Strange. Bacterial Glycogen and Survival. Nature 220, 606-607 (1968).

[170] D. A. Gray, G. Dugar, P. Gamba, H. Strahl, M. J. Jonker and L. W. Hamoen. Extreme slow growth as alternative strategy to survive deep starvation in bacteria. Nature Communications 10 (2019).

[171] D. W. Pettigrew, W. Z. Liu, C. Holmes, N. D. Meadow and S. Roseman. A single amino acid change in *Escherichia coli* glycerol kinase abolishes glucose control of glycerol utilization in vivo. Journal of Bacteriology 178, 2846-52 (1996).

[172] E. Barth, K. V. Gora, K. M. Gebendorfer, F. Settele, U. Jacob and J. Winter. Interplay of cellular cAMP levels, σ^S activity and oxidative stress resistance in *Escherichia coli*. Microbiology 155, 1680-1689 (2009).

[173] R. J. Parkes, B. A. Cragg, J. C. Fry, R. A. Herbert, J. W. T. Wimpenny, J. A. Allen and M. Whitfield. Bacterial biomass and activity in deep sediment. Layers from the Peru Margin [and Discussion]. Philosophical Transactions of the Royal Society of London. Series A, Mathematical and Physical Sciences 331, 139-153 (1990).

[174] B. A. Lomstein, A. T. Langerhuus, S. D'Hondt, B. B. Jørgensen, A. J. Spivack. Endospore abundance, microbial growth and necromass turnover in deep sub-seafloor sediment. Nature 484, 101-104 (2012).

[175] S. D'Hondt, S. Rutherford and A. J. Spivack. Metabolic activity of subsurface life in deep-sea sediments. Science 295, 2067-2070 (2002).

[176] J. T. Lennon and S.E. Jones. Microbial seed banks: the ecological and evolutionary implications of dormancy. Nature Reviews Microbiology 119, 119-130 (2011).

[177] W. Beyeler, P. L. Rogers and A. Fiechter. A simple technique for the direct determination of maintenance energy coefficient: an example with *Zymomonas mobilis*. Applied Microbiology and Biotechnology 19, 277-280 (1984).

[178] J. B. Russell and G. M. Cook. Energetics of Bacterial Growth: Balance of Anabolic and Catabolic Reactions. Microbiological Reviews, 59, 48-62 (1995).

[179] A. L. Koch. The adaptive responses of *Escherichia coli* to a feast and famine existence. Advances in Microbial Physiology 6, 147-217 (1971).

[180] J.C. Li, T. Liu, Y. Wang, A. P. Mehta and P.G. Schultz. Enhancing protein stability with genetically encoded non-canonical amino acids. Journal of the American Chemical Society 140, 15997-16000 (2018).

[181] M. Mori, S. Schink, D. Erickson, U. Gerland and T. Hwa, Quantifying the benefit of a proteome reserve in fluctuating environments. Nature Communications 8 (2017).

[182] E. M. Windels, J. E. Michiels, M. Fauvart, T. Wenseleers, B. Van den Berg, J. Michiels. Bacterial persistence promotes the evolution of antibiotic resistance by increasing survival and mutation rates. The ISME Journal 13, 1239-1251 (2019).

[183] R. Trastoy, T. Manso, L. Fernndez-Garcia, L. Blasco, A. Ambroa, M. L. Prez del Molino, G. Bou, R. Garca-Contreras, T.K. Wood, M. Tomas. Mechanisms of bacterial tolerance and persistence in the gastrointestinal and respiratory environments. Clinical Microbiology Reviews 31 (2018).

[184] G. Hobby. Observations on the mechanism of action of penicillin. Proceedings of the Society for Experimental Biology and Medicine 50, 281-285 (1942).

[185] B. W. Kwan, J. A. Valenta, M. J. Benedik, T. K. Wood. Arrested protein synthesis increases persister-like cell formation. Antimicrobial Agents and Chemotherapy 57, 1468-1473 (2013).

[186] J. S. Kim and T. K. Wood. Tolerant, growing cells from nutrient shifts are not persister cells. mBio 8 (2017).

[187] D. Shah, Z. Zhang, A. Khodursky, N. Kaldalu, K. Kurg, K. Lewis. Persisters: a distinct physiological state of *E. coli*. BMC Microbiology 6 (2006).

[188] N. Vazquez-Laslop, H. Lee and A. A. Neyfakh. Increased persistence in *Escherichia coli* caused by controlled expression of toxins or other unrelated proteins. Journal of Bacteriology 188, 3494-3497 (2006).

[189] I. Keren, D. Shah, A. Spoering, N. Kaldalu and K. Lewis. Specialized persister cells and the mechanism of multidrug tolerance in *Escherichia coli*. Journal of Bacteriology 186, 8172-8180 (2004).

[190] B. M. Ahmer. Cell-to-cell signalling in *Escherichia coli* and *Salmonella enterica*. Molecular Microbiology 52, 933-945 (2004).

[191] A. Jõers, N. Kaldalu and T. Tenson. The Frequency of Persisters in *Escherichia coli* Reflects the Kinetics of Awakening from Dormancy. Journal of Bacteriology 192, 3379-84 (2010).

[192] A. Gutierrez, S. Jain, P. Bhargava, M. Hamblin, M. A. Lobritz, J. J. Collins. Understanding and sensitizing density-dependent persistence to quinolone antibiotics. Molecular Cell 68, 1147-1154 (2017).

[193] K. Cardoso, R. F. Gandra, E. S. Wisniewski, C. A. Osaku, M. K. Kadowaki, V. Felipach-Neto, L. F. Haus, R. Rde C. Simão. DnaK and GroEL are induced in response to antibiotic and heat shock in *Acinetobacter baumannii*. Journal of Medical Microbiology 59, 1061-1068 (2010).

[194] D. R. MacFadden, S. F. McGough, D. Fisman, M. Santillana and J. S. Brownstein. Antibiotic resistance increases with local temperature. Nature Climate Change 8 (2018).

[195] K. Murakami, T. Ono, D. Viducic, S. Kayama, M. Mori, K. Hirota, K. Nemoto, Y. Miyake. Role of *rpoS* gene of *Pseudomonas aeruginosa* in antibiotic tolerance. FEMS Microbiology Letters 242, 161-167 (2005).

[196] C. Rugarli et al. Medicina interna sistematica. 7th Edition. (Edra Masson, 2015).

[197] M. X. Byndloss and R.M. Tsolis. Chronic bacterial pathogens: mechanisms of persistence. Microbiology Spectrum 4 (2016).

[198] W. Mc Dermott. Microbial persistence. Yale Journal of Biology and Medicine 30, 257-291 (1958).

[199] I. U. Mysorekar and S. J. Hultgren. Mechanisms of uropathogenic *Escherichia coli* persistence and eradication from the urinary tract. Proceedings of the National Academy of Sciences 103, 14170-14175 (2006).

[200] S. Barat, B. Steeb, A. Maz, D. Bumann. Extensive in vivo resilience of persistent *Salmonella*. Plos One 7 (2012).

[201] D. Biran, N. Brot, H. Weissbach and E. Z. Ron. Heat Shock-Dependent Transcriptional Activation of the *metA* Gene of *Escherichia coli*. Journal of Bacteriology 177, 1374-1379 (1995).

[202] E. R. Hondorp and R. G. Matthews. Methionine. EcoSal Plus 3.6.1.7 (2013).

[203] P. Shah and E. Swiatlo. A multifaceted role for polyamines in bacterial pathogens. Molecular Microbiology 68, 4-16 (2008).

[204] J. A. Megerle, G. Fritz, U. Gerland, K. Jung, J. O. Rädler. Timing and dynamics of single cell gene expression in the arabinose utilization system. Biophysical Journal 95, 2103-2115 (2008).

[205] N. Friedman, L. Cai and X. S. Xie. Linking stochastic dynamics to population distribution: An analytical framework of gene expression. Physical Review Letters 97 (2006).

[206] Y. Taniguchi, P. J. Choi, G. W. Li, H. Chen, M. Babu, J. Hearn, A. Emili, X. S. Xie. Quantifying *E. coli* Proteome and Transcriptome with Single-Molecule Sensitivity in Single Cells. Science 329 (2010).

[207] G. W. Li, D. Burkhardt, C. Gross, J. S. Weissman. Quantifying absolute protein synthesis rates reveals principles underlying allocation of cellular resources. Cell 157, 624-635 (2014).

[208] J. W. Veening, W. K. Smits and O. P. Kuipers. Bistability, Epigenetics and Bet-Hedging in Bacteria. Annual Review of Microbiology 62, 193-210 (2008).

[209] A. Gardner, S. A. West, A. S. Griffin. Is Bacterial Persistence a Social Trait? PLoS ONE 2 (2007).

[210] I. G. Jong, P. Haccou and O. P. Kuipers. Bet hedging or not? A guide to proper classification of microbial survival strategies. Bioessays 33, 215-223 (2011).

[211] P. L. Graumann. Different genetic programmes within identical bacteria under identical conditions: the phenomenon of bistability greatly modifies our view on bacterial populations. Molecular Microbiology 61, 560-563 (2006).

[212] S. V. Avery. Microbial cell individuality and the underlying sources of heterogeneity. Nature Reviews Microbiology 4, 577-587 (2006).

[213] D. Dubnau, R. Losick. Bistability in bacteria. Molecular Microbiology 61, 564-572 (2006).

[214] S. S. Evans, E. A. Repasky and D. T. Fisher. Fever and the thermal regulation of immunity: the immune system feels the heat. Nature Reviews Immunology 15, 335-349 (2015).

[215] N. G. Cogan, H. Rath, N. Kommerein, S. N. Stumpp and M. Stiesch. Theoretical and experimental evidence for eliminating persister bacteria by manipulating killing timing. FEMS Microbiology Letters 363 (2016).

[216] D. P. Gnanadhas, M. Elango, A. Datey, D. Chakravortty. Chronic lung infection by *Pseudomonas aeruginosa* biofilm is cured by L-Methionine in combination with antibiotic therapy. Scientific Reports 5 (2015).

[217] P. J. Garlick. Toxicity of Methionine in Humans. The Journal of Nutrition 136, 1722S-1725S (2006).

[218] E. Soupene, W. C. van Heeswijk, J. Plumbridge, V. Stewart, D. Bertenthal, H. Lee, G. Prasad, O. Paliy, P. Charernnoppakul and S. Kustu. Physiological Studies of *Escherichia coli* Strain MG1655: Growth Defects and Apparent Cross-Regulation of Gene Expression. Journal of Bacteriology 185, 5611-5626 (2003).

[219] L. N. Csonka, T. P. Ikeda, S. A. Fletcher and S. Kustu. The accumulation of glutamate is necessary for optimal growth of *Salmonella typhimurium* in media of high osmolality but not induction of the proU operon. Journal of Bacteriology 176, 6324-6333 (1994).

[220] S. Benthin, J. Nielsen and J. Villadsen. A simple and reliable method for the determination of cellular rna content. Biotechnology Techniques 5, 39-42 (1991).

[221] J. H. Miller. Experiments in molecular genetics. (CSHL Press, New York, 1972).

[222] S. Taheri-Araghi, S. D. Brown, J. T. Sauls, D. B. McIntosh and S. Jun. Cell-size control and homeostasis in bacteria. Current Biology 25, 385-391 (2015).

[223] S. H. Strogatz. Nonlinear Dynamics and Chaos: with Applications to Physics, Biology, Chemistry and Engineering. (Boulder, CO: Westview Press, a member of the Perseus Books Group, 2015).

[224] B. D. Bennett, E. H. Kimball, M. Gao, R. Osterhout, S. J. Van Dien, J. D. Rabinowitz. Absolute metabolite concentrations and implied enzyme active site occupancy in *Escherichia coli*. Nature Chemical Biology 5, 593-599 (2009).

[225] K. A. Datsenko and B. L. Wanner. One-step inactivation of chromosomal genes in Escherichia coli K-12 using PCR products. Proceedings of the National Academy of Sciences 97, 6640-6645 (2000).

[226] M. De Felice, M. Levinthal, M. Iaccarino and J. Guardiola. Growth inhibition as a consequence of antagonism between related amino acids: effect of valine in Escherichia coli K-12. Microbiol.Rev. 43, 42-58 (1979).

[227] I. M. Keseler, A. Mackie, A. Santos-Zavaleta, R. Billington, C. Bonavides-Martínez, R. Caspi, C. Fulcher, S. Gama-Castro, A. Kothari, M. Krummenacker et al. The EcoCyc database: reflecting new knowledge about *Escherichia coli* K-12. Nucleic Acids Research 45, D543-D550 (2017).

[228] D. A. Benson, M. Cavanaugh, K. Clark, I. Karsch-Mizrachi, D. J. Lipman, J. Ostell, E. W. Sayers. Nucleic Acids Research 41, D36-D42 (2013).

Acknowledgements

This PhD has been one of the hardest challenges of my life, which has made me grow professionally and as a person. This life-changing experience would have never been possible without the support and the mentoring of many special people.
First of all, I would like to thank my supervisor, Prof. Dr. Ulrich Gerland, for giving me the opportunity to do my thesis with him and the freedom to explore and investigate new phenomena. In particular, thank you for approving and supporting my attendance to many inspiring conferences and scientific meetings all over the world. Thank you also for introducing me to the exciting world of quantitative biology and the laboratories. I would have otherwise never discovered either my skills of accuracy and meticulousness in experimental work, or my passion for it. Furthermore, the responsibility you gave me of managing the laboratory in the last two years has crucially advanced my personal and scientific development.
I would also like to thank Prof. Dr. Petra Schwille and Prof. Dr. Erwin Frey, for their comments and useful discussion about the projects and for their suggestions about time management and future life plans.
Many thanks to the QBM Graduate School of the LMU and to all of its members, especially Mara and Filiz, who have supported and accompanied me throughout these years.
I then dedicate a special thanks to Dr. Severin Josef Schink. My words will never adequately express my gratitude to you. Thank you for guiding me through my discovery of quantitative biology, training me in the laboratory and making me acquiring a deep sense of critical thinking. I am proud to have shared with you the first years of the establishment of our TUM laboratory. It was so much effort, but also a lot of satisfaction. And thank you for giving me the opportunity to work with you in Harvard. That was one of the most exciting and inspiring moments of my life. Also, thanks to Annick for our walks and chats together there.
Related to this, many thanks also to Prof. Dr. Markus Basan, for allowing me to work in his group in Harvard. The scientific discussions with you were a great source of inspiration and guided me towards the right direction of our project.
I would also like to express my gratitude to Constantin, Dina, Mariel and Yvonne, for having contributed with passion to my PhD research projects.
A special thought to all the members of my research group. Some are still here, some others have left, but they all contributed to making my life at work and outside easier and enjoyable. Above all, Nanni, because you are not only a very helpful colleague, but a good friend. Your calm and positivity have always managed to raise my spirits, especially when the experiments in the laboratory were unsuccessful. Florian, because from the moment you carried my luggage in the middle of the countryside, while barely knowing me, you have always been my guardian angel in the group, helping me through every day difficulties. Vladimir, for your enjoyable wine tasting times. Linda, for your cakes, which often count more than words. Michael, for having shared anxieties, joys and deadlines of this PhD. Patrick, for our deep conversations about the way we do research and the life problems.
Thanks to my laboratory team and to my students, especially Hamid, Zara, Felix and Michael,

because teaching is always a source of learning, also for ourselves, and watching your achievements has been a great satisfaction.
Thanks to Prof. Dr. Kirsten Jung and her laboratory team for teaching me the molecular biology techniques.
Thanks to Laura Darabas, for having carefully followed all my bureaucratic procedures with professionalism and precision and for helping me in the economic management of the laboratory.
Thanks to the laboratory technicians, for offering their help and resources for setting up our TUM laboratory and helping me repair devices, and to Dr. Dominik Maslak for teaching me to work best with the bioreactors.
I would also like to thank Dr. Adriano Barra and Dr. Elena Agliari, for encouraging me to undertake this journey five years ago and, above all, for helping me overcome the discouragement of the first year.
Thanks to Riccardo, for the time spent with me discussing theoretical models and his psychological support.
Thanks to all the wonderful people I met in Munich. Moving to a foreign city alone without speaking the language was not easy. You all, those who before and those who after, have made every single moment of my daily life lighter and joyful.
Among the many, Nicola. You are one of my best friends. You shared with me every sad and happy moment of these years and you always had the right word to say at the right time. Marilú, of whom I have a great esteem both professionally and as a friend. Thank you for helping me deal with my complicated emotional moments and waiting for my right decisions. Saba, my best roommate ever, who I often miss when I go back home in the evening. Andrea, for our first months in Munich spent together, for our runs along the river, our dinners, holidays and chats. Elena, for her wise advice and her example of practicality and concreteness in facing both life and human relationships. And behind her, Silvia, Andrea and all the members of the Palombella Group, for all the moments shared together. Sara, who always reminds me what the important values in life are. Claudio, for his particular humor that has made me laugh at the end of many days. Helmut and Edda, for having watched over me in these years in Munich.
Thanks to all my old friends, who never left me and continue to cheer me on in life. Thank you for giving me the strength to go on, every time I said I couldn't make it.
Thanks to my big family, that often believes in me more than I do and is at the same time a springboard for my dreams and a lightning rod in my difficult moments.
Last, but most certainly not least, my love, Rudi, for this wonderful last year together. Your mental and psychological support in writing this thesis was indispensable and made my life more peaceful and happier than ever before.